

APPLIED RADIOLOGY®

THE JOURNAL OF PRACTICAL MEDICAL IMAGING AND MANAGEMENT

September–October 2020
Vol. 49, No. 5

EDITORIAL

Rising into Fall

SA-CME CREDIT

Pregnancy-associated Breast Cancer and Other Breast Disease: A Radiologic Review

A Ong, SC Harvey, LA Mullen, Johns Hopkins University School of Medicine, Baltimore, MD

Imaging Cystic Head and Neck Lesions, Part 1

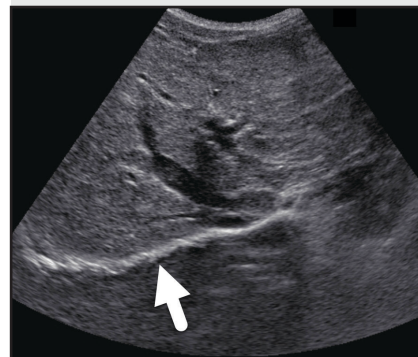
BW Wright, RH Wiggins III, University of Utah, Salt Lake City, UT

Improving Body Imaging Throughput in the Midst of COVID-19

JV Thomas, KK Porter, SA Woodard, A Singhal, MB Frazier, DE Morgan, CL Canon, University of Alabama at Birmingham, Birmingham, AL

Eye on AI: The Power of Triage (CADt) in Breast Imaging

L Watanabe, USC Keck School of Medicine, Los Angeles, CA, and CureMetrix Inc, San Diego, CA



Pediatric Radiological Case

Cystic Fibrosis Liver Disease

WWW.APPLIEDRADIOLOGY.COM

Magnetic Resonance Imaging (MRI) Is an Important Diagnostic Tool for Breast Cancer Detection

The American Society of Breast Surgeons recommends considering supplemental imaging (breast MRI or ultrasound) in addition to annual mammography in women with increased breast density (C and D density)* (beginning at age 40)¹

* Class C or 3 density = heterogeneously dense; Class D or 4 density = extremely dense

Patients for which the American College of Radiology recommends annual screening breast MRI as a supplement to mammography include:²

- Women with ≥20% lifetime risk of breast cancer (beginning at age 30)[†]
- Women with personal history of breast cancer and dense breasts
- Women diagnosed with breast cancer under the age of 50
- Women with a known BRCA mutation (beginning at age 30)[†]

[†] Annual MRI (without mammography) is recommended in these patients starting between ages 25–30

Indication

Gadavist® (gadobutrol) injection is a gadolinium-based contrast agent indicated for use with magnetic resonance imaging (MRI) to assess the presence and extent of malignant breast disease in adult patients.

Important Safety Information

WARNING: NEPHROGENIC SYSTEMIC FIBROSIS (NSF)

Gadolinium-based contrast agents (GBCAs) increase the risk for NSF among patients with impaired elimination of the drugs. Avoid use of GBCAs in these patients unless the diagnostic information is essential and not available with non-contrasted MRI or other modalities. NSF may result in fatal or debilitating fibrosis affecting the skin, muscle and internal organs.

- The risk of NSF appears highest among patients with:
 - Chronic, severe kidney disease (GFR <30 mL/min/1.73m²), or
 - Acute kidney injury
- Screen patients for acute kidney injury and other conditions that may reduce renal function. For patients at risk for chronically reduced renal function (for example, age >60 years, hypertension or diabetes), estimate the glomerular filtration rate (GFR) through laboratory testing.
- For patients at highest risk for NSF, do not exceed the recommended GADAVIST dose and allow a sufficient period of time for elimination of the drug from the body prior to any re-administration.

Contraindication and Important Information about Hypersensitivity Reactions: Gadavist® is contraindicated in patients with history of severe hypersensitivity reactions to Gadavist®. Anaphylactic and other hypersensitivity reactions with cardiovascular, respiratory, or cutaneous manifestations, ranging from mild to severe, including death, have uncommonly occurred following Gadavist® administration. Before Gadavist® administration, assess all patients for any history of a reaction to contrast media, bronchial asthma and/or allergic disorders. These patients may have an increased risk for a hypersensitivity reaction to Gadavist®.

Please see brief summary on adjacent pages.





Gadavist® (gadobutrol) Injection Is the First and Only Gadolinium-based Contrast Agent Approved for Breast MRI

➤ Visit [Gadavist.com](https://gadavist.com) or schedule time with a Bayer in Radiology representative to learn more

Important Safety Information (continued)

Gadolinium Retention: Gadolinium is retained for months or years in several organs. Linear GBCAs cause more retention than macrocyclic GBCAs. At equivalent doses, retention varies among the linear agents. Retention is lowest and similar among the macrocyclic GBCAs. Consequences of gadolinium retention in the brain have not been established, but they have been established in the skin and other organs in patients with impaired renal function. While clinical consequences of gadolinium retention have not been established in patients with normal renal function, certain patients might be at higher risk. These include patients requiring multiple lifetime doses, pregnant and pediatric patients, and patients with inflammatory conditions. Consider the retention characteristics of the agent and minimize repetitive GBCA studies, when possible.

Acute Kidney Injury: In patients with chronic renal impairment, acute kidney injury sometimes requiring dialysis has been observed with the use of GBCAs. Do not exceed the recommended dose; the risk of acute kidney injury may increase with higher than recommended doses.

Extravasation and Injection Site Reactions: Ensure catheter and venous patency before the injection of Gadavist®. Extravasation into tissues during Gadavist® administration may result in moderate irritation.

Overestimation of Extent of Malignant Disease in MRI of the Breast: Gadavist® MRI of the breast overestimated the histologically confirmed extent of malignancy in the diseased breast in up to 50% of the patients.

Adverse Reactions: The most frequent ($\geq 0.5\%$) adverse reactions associated with Gadavist® in clinical studies were headache (1.7%), nausea (1.2%) and dizziness (0.5%).

Please see brief summary on adjacent pages.

References: 1. Consensus Statement on Screening Mammography. The American Society of Breast Surgeons website. <https://www.breastsurgeons.org/docs/statements/Position-Statement-on-Screening-Mammography.pdf>. Accessed June 9, 2020. 2. Breast Cancer Screening in Women at Higher-Than-Average Risk: Recommendations From the ACR. American College of Radiology website. [https://www.jacr.org/article/S1546-1440\(17\)31524-7/fulltext](https://www.jacr.org/article/S1546-1440(17)31524-7/fulltext). Accessed June 9, 2020.

Bayer, the Bayer Cross, and Gadavist are trademarks owned by and/or registered to Bayer in the U.S. and/or other countries. Other trademarks and company names mentioned herein are properties of their respective owners and are used herein solely for informational purposes. No relationship or endorsement should be inferred or implied.

© 2020 Bayer. This material may not be reproduced, displayed, modified or distributed without the express prior written consent of Bayer.
Printed in the USA. PP-GADA-US-0353-1 August 2020

Gadavist®
(gadobutrol) injection
1 mmol/mL

GADAVIST (gadobutrol) injection, for intravenous use
Initial U.S. Approval: 2011

BRIEF SUMMARY OF PRESCRIBING INFORMATION
CONSULT PACKAGE INSERT FOR FULL PRESCRIBING INFORMATION

WARNING: NEPHROGENIC SYSTEMIC FIBROSIS (NSF)

Gadolinium-based contrast agents (GBCAs) increase the risk for NSF among patients with impaired elimination of the drugs. Avoid use of GBCAs in these patients unless the diagnostic information is essential and not available with non-contrast MRI or other modalities. NSF may result in fatal or debilitating fibrosis affecting the skin, muscle and internal organs.

- The risk for NSF appears highest among patients with:
 - Chronic, severe kidney disease ($\text{GFR} < 30 \text{ mL/min/1.73m}^2$), or
 - Acute kidney injury.
- Screen patients for acute kidney injury and other conditions that may reduce renal function. For patients at risk for chronically reduced renal function (for example, age > 60 years, hypertension or diabetes), estimate the glomerular filtration rate (GFR) through laboratory testing.
- For patients at highest risk for NSF, do not exceed the recommended Gadavist dose and allow a sufficient period of time for elimination of the drug from the body prior to any re-administration [see *Warnings and Precautions* (5.1)].

1 INDICATIONS AND USAGE

1.1 Magnetic Resonance Imaging (MRI) of the Central Nervous System (CNS)

Gadavist is indicated for use with magnetic resonance imaging (MRI) in adult and pediatric patients, including term neonates, to detect and visualize areas with disrupted blood brain barrier and/or abnormal vascularity of the central nervous system.

1.2 MRI of the Breast

Gadavist is indicated for use with MRI in adult patients to assess the presence and extent of malignant breast disease.

1.3 Magnetic Resonance Angiography (MRA)

Gadavist is indicated for use in magnetic resonance angiography (MRA) in adult and pediatric patients, including term neonates, to evaluate known or suspected supra-aortic or renal artery disease.

1.4 Cardiac MRI

Gadavist is indicated for use in cardiac MRI (CMRI) to assess myocardial perfusion (stress, rest) and late gadolinium enhancement in adult patients with known or suspected coronary artery disease (CAD).

4 CONTRAINDICATIONS

Gadavist is contraindicated in patients with history of severe hypersensitivity reactions to Gadavist.

5 WARNINGS AND PRECAUTIONS

5.1 Nephrogenic Systemic Fibrosis

Gadolinium-based contrast agents (GBCAs) increase the risk for nephrogenic systemic fibrosis (NSF) among patients with impaired elimination of the drugs. Avoid use of GBCAs among these patients unless the diagnostic information is essential and not available with non-contrast MRI or other modalities. The GBCA-associated NSF risk appears highest for patients with chronic, severe kidney disease ($\text{GFR} < 30 \text{ mL/min/1.73m}^2$) as well as patients with acute kidney injury. The risk appears lower for patients with chronic, moderate kidney disease ($\text{GFR} 30$ to $59 \text{ mL/min/1.73m}^2$) and little, if any, for patients with chronic, mild kidney disease ($\text{GFR} 60$ to $89 \text{ mL/min/1.73m}^2$). NSF may result in fatal or debilitating fibrosis affecting the skin, muscle and internal organs. Report any diagnosis of NSF following Gadavist administration to Bayer Healthcare (1-888-842-2937) or FDA (1-800-FDA-1088 or www.fda.gov/medwatch).

Screen patients for acute kidney injury and other conditions that may reduce renal function. Features of acute kidney injury consist of rapid (over hours to days) and usually reversible decrease in kidney function, commonly in the setting of surgery, severe infection, injury or drug-induced kidney toxicity. Serum creatinine levels and estimated GFR may not reliably assess renal function in the setting of acute kidney injury. For patients at risk for chronically reduced renal function (for example, age > 60 years, diabetes mellitus or chronic hypertension), estimate the GFR through laboratory testing.

Among the factors that may increase the risk for NSF are repeated or higher than recommended doses of a GBCA and degree of renal impairment at the time of exposure. Record the specific GBCA and the dose administered to a patient. For patients at highest risk for NSF, do not exceed the recommended Gadavist dose and allow a sufficient period of time for elimination of the drug prior to re-administration. For patients receiving hemodialysis, consider the prompt initiation of hemodialysis following the administration of a GBCA in order to enhance the contrast agent's elimination [see *Use in Specific Populations* (8.6) and *Clinical Pharmacology* (12.3)]. The usefulness of hemodialysis in the prevention of NSF is unknown [see *Clinical Pharmacology* (12.3)].

5.2 Hypersensitivity Reactions

Anaphylactic and other hypersensitivity reactions with cardiovascular, respiratory or cutaneous manifestations, ranging from mild to severe, including death, have uncommonly occurred following Gadavist administration [see *Adverse Reactions* (6)].

- Before Gadavist administration, assess all patients for any history of a reaction to contrast media, bronchial asthma and/or allergic disorders. These patients may have an increased risk for a hypersensitivity reaction to Gadavist.
- Administer Gadavist only in situations where trained personnel and therapies are promptly available for the treatment of hypersensitivity reactions, including personnel trained in resuscitation.

Most hypersensitivity reactions to Gadavist have occurred within half an hour after administration. Delayed reactions can occur up to several days after administration. Observe patients for signs and symptoms of hypersensitivity reactions during and following Gadavist administration.

5.3 Gadolinium Retention

Gadolinium is retained for months or years in several organs. The highest concentrations (nanomoles per gram of tissue) have been identified in the bone, followed by other organs (for example, brain, skin, kidney, liver, and spleen). The duration of retention also varies by tissue and is longest in bone. Linear GBCAs cause more retention than macrocyclic GBCAs. At equivalent doses, gadolinium retention varies among the linear agents with Omniscan (gadodiamide) and Optimark (gadoversetamide) causing greater retention than other linear agents [Eovist (gadoxetate disodium), Magnevist (gadopentetate dimeglumine), MultiHance (gadobenate dimeglumine)]. Retention is lowest and similar among the macrocyclic GBCAs [Dotarem (gadoterate meglumine), Gadavist (gadobutrol), ProHance (gadoteridol)].

Consequences of gadolinium retention in the brain have not been established. Pathologic and clinical consequences of GBCA administration and retention in skin and other organs have been established in patients with impaired renal function [see *Warnings and Precautions* (5.1)]. There are rare reports of pathologic skin changes in patients with normal renal function. Adverse events involving multiple organ systems have been reported in patients with normal renal function without an established causal link to gadolinium retention [see *Adverse Reactions* (6.2)].

While clinical consequences of gadolinium retention have not been established in patients with normal renal function, certain patients might be at higher risk. These include patients requiring multiple lifetime doses, pregnant and pediatric patients, and patients with inflammatory conditions. Consider the retention characteristics of the agent when choosing a GBCA for these patients. Minimize repetitive GBCA imaging studies particularly closely spaced studies, when possible.

5.4 Acute Kidney Injury

In patients with chronic renal impairment, acute kidney injury sometimes requiring dialysis has been observed with the use of some GBCAs. Do not exceed the recommended dose; the risk of acute kidney injury may increase with higher than recommended doses.

5.5 Extravasation and Injection Site Reactions

Ensure catheter and venous patency before the injection of Gadavist. Extravasation into tissues during Gadavist administration may result in moderate irritation [see *Nonclinical Toxicology* (13.2)].

5.6 Overestimation of Extent of Malignant Disease in MRI of the Breast

Gadavist MRI of the breast overestimated the histologically confirmed extent of malignancy in the diseased breast in up to 50% of the patients [see *Clinical Studies* (14.2)].

5.7 Low Sensitivity for Significant Arterial Stenosis

The performance of Gadavist MRA for detecting arterial segments with significant stenosis (>50% renal, >70% supra-aortic) has not been shown to exceed 55%. Therefore, a negative MRA study alone should not be used to rule out significant stenosis [see *Clinical Studies* (14.3)].

6 ADVERSE REACTIONS

The following serious adverse reactions are discussed elsewhere in labeling:

- Nephrogenic Systemic Fibrosis (NSF) [see *Boxed Warning and Warnings and Precautions* (5.1)].
- Hypersensitivity reactions [see *Contraindications* (4) and *Warnings and Precautions* (5.2)].

6.1 Clinical Trials Experience

Because clinical trials are conducted under widely varying conditions, adverse reaction rates observed in the clinical trials of a drug cannot be directly compared to rates in the clinical trials of another drug and may not reflect the rates observed in clinical practice.

The adverse reactions described in this section reflect Gadavist exposure in 7,713 subjects (including 184 pediatric patients, ages 0 to 17 years) with the majority receiving the recommended dose. Approximately 52% of the subjects were male and the ethnic distribution was 62% Caucasian, 28% Asian, 5%

Hispanic, 2.5% Black, and 2.5% patients of other ethnic groups. The average age was 56 years (range from 1 week to 93 years).

Overall, approximately 4% of subjects reported one or more adverse reactions during a follow-up period that ranged from 24 hours to 7 days after Gadavist administration.

Adverse reactions associated with the use of Gadavist were usually mild to moderate in severity and transient in nature.

Table 2 lists adverse reactions that occurred in $\geq 0.1\%$ subjects who received Gadavist.

Table 2: Adverse Reactions

| Reaction | Rate (%) n=7713 |
|---|--------------------|
| Headache | 1.7 |
| Nausea | 1.2 |
| Dizziness | 0.5 |
| Dysgeusia | 0.4 |
| Feeling Hot | 0.4 |
| Injection site reactions | 0.4 |
| Vomiting | 0.4 |
| Rash (includes generalized, macular, papular, pruritic) | 0.3 |
| Erythema | 0.2 |
| Paresthesia | 0.2 |
| Pruritus (includes generalized) | 0.2 |
| Dyspnea | 0.1 |
| Urticaria | 0.1 |

Adverse reactions that occurred with a frequency of $< 0.1\%$ in subjects who received Gadavist include: hypersensitivity/anaphylactic reaction, loss of consciousness, convulsion, parosmia, tachycardia, palpitation, dry mouth, malaise and feeling cold.

6.2 Postmarketing Experience

The following additional adverse reactions have been reported during postmarketing use of Gadavist. Because these reactions are reported voluntarily from a population of uncertain size, it is not possible to reliably estimate their frequency or establish a causal relationship to drug exposure.

- Cardiac arrest
- Nephrogenic Systemic Fibrosis (NSF)
- Hypersensitivity reactions (anaphylactic shock, circulatory collapse, respiratory arrest, pulmonary edema, bronchospasm, cyanosis, oropharyngeal swelling, laryngeal edema, blood pressure increased, chest pain, angioedema, conjunctivitis, hyperhidrosis, cough, sneezing, burning sensation, and pallor) [see *Warnings and Precautions* (5.2)].
- General Disorders and Administration Site Conditions: Adverse events with variable onset and duration have been reported after GBCA administration [see *Warnings and Precautions* (5.3)]. These include fatigue, asthenia, pain syndromes, and heterogeneous clusters of symptoms in the neurological, cutaneous, and musculoskeletal systems.
- Skin: Gadolinium associated plaques

8 USE IN SPECIFIC POPULATIONS

8.1 Pregnancy

Risk Summary

GBCAs cross the placenta and result in fetal exposure and gadolinium retention. The human data on the association between GBCAs and adverse fetal outcomes are limited and inconclusive (see *Data*). In animal reproduction studies, although teratogenicity was not observed, embryolethality was observed in monkeys, rabbits and rats receiving intravenous gadobutrol during organogenesis at doses 8 times and above the recommended human dose. Retardation of embryonal development was observed in rabbits and rats receiving intravenous gadobutrol during organogenesis at doses 8 and 12 times, respectively, the recommended human dose (see *Data*). Because of the potential risks of gadolinium to the fetus, use Gadavist only if imaging is essential during pregnancy and cannot be delayed.

The estimated background risk of major birth defects and miscarriage for the indicated population is unknown. In the U.S. general population, the estimated background risk of major birth defects and miscarriage in clinically recognized pregnancies is 2 to 4% and is 15 to 20%, respectively.

Data

Human Data

Contrast enhancement is visualized in the placenta and fetal tissues after maternal GBCA administration.

Cohort studies and case reports on exposure to GBCAs during pregnancy have not reported a clear association between GBCAs and adverse effects in the exposed neonates. However, a retrospective cohort study, comparing pregnant

women who had a GBCA MRI to pregnant women who did not have an MRI, reported a higher occurrence of stillbirths and neonatal deaths in the group receiving GBCA MRI. Limitations of this study include a lack of comparison with non-contrast MRI and lack of information about the maternal indication for MRI. Overall, these data preclude a reliable evaluation of the potential risk of adverse fetal outcomes with the use of GBCAs in pregnancy.

Animal Data

Gadolinium Retention

GBCAs administered to pregnant non-human primates (0.1 mmol/kg on gestational days 85 and 135) result in measurable gadolinium concentration in the offspring in bone, brain, skin, liver, kidney, and spleen for at least 7 months. GBCAs administered to pregnant mice (2 mmol/kg daily on gestational days 16 through 19) result in measurable gadolinium concentrations in the pups in bone, brain, kidney, liver, blood, muscle, and spleen at one month postnatal age.

Reproductive Toxicology

Embryolethality was observed when gadobutrol was administered intravenously to monkeys during organogenesis at doses 8 times the recommended single human dose (based on body surface area); gadobutrol was not maternally toxic or teratogenic at this dose. Embryolethality and retardation of embryonal development also occurred in pregnant rats receiving maternally toxic doses of gadobutrol (≥ 7.5 mmol/kg body weight; equivalent to 12 times the human dose based on body surface area) and in pregnant rabbits (≥ 2.5 mmol/kg body weight; equivalent to 8 times the recommended human dose based on body surface area). In rabbits, this finding occurred without evidence of pronounced maternal toxicity and with minimal placental transfer (0.01% of the administered dose detected in the fetuses).

Because pregnant animals received repeated daily doses of Gadavist, their overall exposure was significantly higher than that achieved with the standard single dose administered to humans.

8.2 Lactation

Risk Summary

There are no data on the presence of gadobutrol in human milk, the effects on the breastfed infant, or the effects on milk production. However, published lactation data on other GBCAs indicate that 0.01 to 0.04% of the maternal gadolinium dose is present in breast milk and there is limited GBCA gastrointestinal absorption in the breast-fed infant. Gadobutrol is present in rat milk (see *Data*). The developmental and health benefits of breastfeeding should be considered along with the mother's clinical need for Gadavist and any potential adverse effects on the breastfed infant from Gadavist or from the underlying maternal condition.

Data

In lactating rats receiving 0.5 mmol/kg of intravenous [^{153}Gd]-gadobutrol, 0.01% of the total administered radioactivity was transferred to the pup via maternal milk within 3 hours after administration, and the gastrointestinal absorption is poor (approximately 5% of the dose orally administered was excreted in the urine).

8.4 Pediatric Use

The safety and effectiveness of Gadavist have been established in pediatric patients, including term neonates, for use with MRI to detect and visualize areas with disrupted blood brain barrier and/or abnormal vascularity of the central nervous system and for use in MRA to evaluate known or suspected supra-aortic or renal artery disease. Use of Gadavist in these indications is supported by adequate and well-controlled studies in adults and supportive imaging data in two studies in 135 patients 2 to less than 18 years of age and 44 patients less than 2 years of age with CNS and non-CNS lesions, and pharmacokinetic data in 130 patients 2 to less than 18 years of age and 43 patients less than 2 years of age, including term neonates [see *Clinical Pharmacology* (12.3) and *Clinical Studies* (14.1)]. The frequency, type, and severity of adverse reactions in pediatric patients were similar to adverse reactions in adults [see *Adverse Reactions* (6.1)]. No dose adjustment according to age is necessary in pediatric patients [see *Dosage and Administration* (2.1), *Clinical Pharmacology* (12.3), and *Clinical Studies* (14.1)]. The safety and effectiveness of Gadavist have not been established in preterm neonates for any indication or in pediatric patients of any age for use with MRI to assess the presence and extent of malignant breast disease, or for use in CMRI to assess myocardial perfusion (stress, rest) and late gadolinium enhancement in patients with known or suspected coronary artery disease (CAD).

NSF Risk

No case of NSF associated with Gadavist or any other GBCA has been identified in pediatric patients ages 6 years and younger. Pharmacokinetic studies suggest that clearance of Gadavist is similar in pediatric patients and adults, including pediatric patients age younger than 2 years. No increased risk factor for NSF has been identified in juvenile animal studies of gadobutrol. Normal estimated GFR (eGFR) is around 30 mL/min/1.73m² at birth and increases to mature levels around 1 year of age, reflecting growth in both glomerular function and relative body surface area. Clinical studies in pediatric patients younger than 1 year of age have been conducted in patients with the following

minimum eGFR: 31 mL/min/1.73m² (age 2 to 7 days), 38 mL/min/1.73m² (age 8 to 28 days), 62 mL/min/1.73m² (age 1 to 6 months), and 83 mL/min/1.73m² (age 6 to 12 months).

Juvenile Animal Data

Single and repeat-dose toxicity studies in neonatal and juvenile rats did not reveal findings suggestive of a specific risk for use in pediatric patients including term neonates and infants.

8.5 Geriatric Use

In clinical studies of Gadavist, 1,377 patients were 65 years of age and over, while 104 patients were 80 years of age and over. No overall differences in safety or effectiveness were observed between these subjects and younger subjects, and other reported clinical experience has not identified differences in responses between the elderly and younger patients. In general, use of Gadavist in elderly patients should be cautious, reflecting the greater frequency of impaired renal function and concomitant disease or other drug therapy. No dose adjustment according to age is necessary in this population.

8.6 Renal Impairment

Prior to administration of Gadavist, screen all patients for renal dysfunction by obtaining a history and/or laboratory tests [see *Warnings and Precautions* (5.1)]. No dosage adjustment is recommended for patients with renal impairment.

Gadavist can be removed from the body by hemodialysis [see *Warnings and Precautions* (5.1) and *Clinical Pharmacology* (12.3)].

10 OVERDOSAGE

The maximum dose of Gadavist tested in healthy volunteers, 1.5 mL/kg body weight (1.5 mmol/kg; 15 times the recommended dose), was tolerated in a manner similar to lower doses. Gadavist can be removed by hemodialysis [see *Use in Specific Populations* (8.6) and *Clinical Pharmacology* (12.3)].

13 NONCLINICAL TOXICOLOGY

13.1 Carcinogenesis, Mutagenesis, Impairment of Fertility

No carcinogenicity studies of gadobutrol have been conducted.

Gadobutrol was not mutagenic in *in vitro* reverse mutation tests in bacteria, in the HGPRT (hypoxanthine-guanine phosphoribosyl transferase) test using cultured Chinese hamster V79 cells, or in chromosome aberration tests in human peripheral blood lymphocytes, and was negative in an *in vivo* micronucleus test in mice after intravenous injection of 0.5 mmol/kg.

Gadobutrol had no effect on fertility and general reproductive performance of male and female rats when given in doses 12.2 times the human equivalent dose (based on body surface area).

13.2 Animal Toxicology and/or Pharmacology

Local intolerance reactions, including moderate irritation associated with infiltration of inflammatory cells was observed after paravenous administration to rabbits, suggesting the possibility of occurrence of local irritation if the contrast medium leaks around veins in a clinical setting [see *Warnings and Precautions* (5.5)].

17 PATIENT COUNSELING INFORMATION

- Advise the patient to read the FDA-approved patient labeling (Medication Guide).

Nephrogenic Systemic Fibrosis

Instruct patients to inform their physician if they:

- Have a history of kidney disease and/or liver disease, or
- Have recently received a GBCA

GBCAs increase the risk of NSF among patients with impaired elimination of drugs. To counsel patients at risk of NSF:

- Describe the clinical manifestation of NSF
- Describe procedures to screen for the detection of renal impairment

Instruct the patients to contact their physician if they develop signs or symptoms of NSF following Gadavist administration, such as burning, itching, swelling, scaling, hardening and tightening of the skin; red or dark patches on the skin; stiffness in joints with trouble moving, bending or straightening the arms, hands, legs or feet; pain in the hip bones or ribs; or muscle weakness.

Common Adverse Reactions

Inform patients that they may experience:

- Reactions along the venous injection site, such as mild and transient burning or pain or feeling of warmth or coldness at the injection site
- Side effects of headache, nausea, abnormal taste and feeling hot

General Precautions

Gadolinium Retention

- Advise patients that gadolinium is retained for months or years in brain, bone, skin, and other organs in patients with normal renal function. The clinical consequences of retention are unknown. Retention depends on multiple factors and is greater following administration of linear GBCAs than following administration of macrocyclic GBCAs. [see *Warnings and Precautions* (5.3)].

Instruct patients receiving Gadavist to inform their physician if they:

- Are pregnant or breastfeeding
- Have a history of allergic reaction to contrast media, bronchial asthma or allergic respiratory disorder

© 2011, Bayer HealthCare Pharmaceuticals Inc. All rights reserved.

Manufactured for:



Bayer HealthCare

Bayer HealthCare Pharmaceuticals Inc.

Whippany, NJ 07981

Manufactured in Germany

6905905BS

APPLIED RADIOLOGY®

THE JOURNAL OF PRACTICAL MEDICAL IMAGING AND MANAGEMENT

Anderson Publishing, Ltd., 180 Glenside Avenue, Scotch Plains, NJ 07076

Tel: 908-301-1995 Fax: 908-301-1997 Email: info@appliedradiology.com

| | | | | | |
|------------------|---------------------|-----------------|-------------------|----------------------|----------------------|
| PRESIDENT & CEO | O Oliver Anderson | GROUP PUBLISHER | Kieran N Anderson | ASSOCIATE PUBLISHER | Cristine Funke RT(R) |
| EXECUTIVE EDITOR | Joseph F Jalkiewicz | ART/PRODUCTION | Barbara A Shopiro | CIRCULATION DIRECTOR | Cindy Cardinal |

EDITORIAL ADVISORY BOARD

EDITOR-IN-CHIEF

Erin Simon Schwartz, MD, FACP
Perelman School of Medicine,
University of Pennsylvania
The Children's Hospital of Philadelphia
Philadelphia, PA

EDITORS EMERITI

Theodore E Keats, MD
Stuart E Mirvis, MD, FACP

ADVOCACY/ GOVERNMENTAL AFFAIRS

Associate Editor
David Youmans, MD, FACP
Princeton Radiology Associates
Princeton, NJ

Seth Hardy, MD, MBA, FACP
Penn State Health Milton S Hershey
Medical Center
Hershey, PA

Ryan K Lee, MD, MBA
Einstein Healthcare Network
Philadelphia, PA

ARTIFICIAL INTELLIGENCE

Associate Editor
Lawrence N Tanenbaum, MD, FACP
RadNet, Inc.
New York, NY

Sonia Gupta, MD
Beth Israel Deaconess Medical Center
Harvard Medical School
Boston, MA

BODY IMAGING

Kristin K Porter, MD, PhD
The Kirklin Clinic of UAB Hospital
Birmingham, AL

Elliot K Fishman, MD
Johns Hopkins Hospital
Baltimore, MD

BREAST IMAGING

Phan T Huynh, MD
Baylor St Luke's Medical Center
Houston, TX

CARDIOPULMONARY IMAGING

Associate Editor
Charles S White, MD
University of Maryland School of Medicine
Baltimore, MD

Jeanne B Ackman, MD
Massachusetts General Hospital
Boston, MA

Saurabh Jha, MBBS, MRCS, MS
Perelman School of Medicine
University of Pennsylvania
Philadelphia, PA

EMERGENCY RADIOLOGY

Associate Editor
Melissa Davis, MD, MBA
Department of Radiology and Imaging
Emory University
Atlanta, GA

ENTERPRISE IMAGING

Rasu Shrestha, MD, MBA
Atrium Health
Charlotte, NC

Eliot Siegel, MD
VA Maryland Healthcare System
University of Maryland School of Medicine
Baltimore, MD

INTERVENTIONAL RADIOLOGY

Jeffrey C Hellinger, MD, MBA
Lenox Hill Radiology
New York, NY

Minhaj S Khaja, MD, MBA
University of Virginia Health System
Charlottesville, VA

MEDICAL INDUSTRY

Ronald B Schilling, PhD
RBS Consulting Group
Los Altos Hills, CA

MEDICOLEGAL ISSUES

Michael M Raskin, MD, MPH, JD
University Medical Center
Tamarac, FL

MUSCULOSKELETAL IMAGING

Jamshid Tehranzadeh, MD
University of California Medical Center
Orange, CA

NEURORADIOLOGY

Wende N Gibbs, MD.
Mayo Clinic
Phoenix, AZ

Blake A Johnson, MD, FACP
Center for Diagnostic Imaging
Minneapolis, MN

C Douglas Phillips, MD, FACP
Weill Cornell Medical College/
New York-Presbyterian Hospital
New York, NY

NUCLEAR MEDICINE

Wengen Chen, MD, PhD
University of Maryland Medical Center
Baltimore, MD

K Elizabeth Hawk, MS, MD, PhD
Stanford University School of Medicine
Radiology Partners
Los Angeles, CA

PEDIATRIC RADIOLOGY

Associate Editor
Alexander Towbin, MD
Cincinnati Children's Hospital Medical Center
Cincinnati, OH

Michael L Francavilla, MD
Perelman School of Medicine,
University of Pennsylvania
The Children's Hospital of Philadelphia
Philadelphia, PA

Marilyn J Siegel, MD, FACP
Washington University School of Medicine
Mallinckrodt Institute of Radiology
St. Louis, MO

RADIOLOGICAL CASES

Associate Editor
Jennifer Cranny, MD
Denver Health
Denver, CO

Thomas Lee Pope, Jr, MD, FACP
Envision Healthcare
Denver, CO

ULTRASOUND

John P McGahan, MD
University of California
Davis, CA

©2020 Anderson Publishing, Ltd. All rights reserved. Reproduction in whole or part without written permission is strictly prohibited. USPS: 0943-180

APPLIED RADIOLOGY

THE JOURNAL OF PRACTICAL MEDICAL IMAGING AND MANAGEMENT

SA-CME

10 Pregnancy-associated Breast Cancer and Other Breast Disease: A Radiologic Review

This article and SA-CME activity illustrates the expected changes to the breast during pregnancy and lactation, and describes the appropriate diagnostic approach to evaluating pregnancy-associated breast complaints.

Andrew Ong, MD; Susan C. Harvey, MD;
Lisa A. Mullen, MD

18 Imaging Cystic Head and Neck Lesions, Part 1

Part 1 of this article series presents an overview of cystic lesions in the oral cavity, pharynx, masticator space, and parotid space.

Brad Wright, MD; Richard H. Wiggins III, MD, CIIP, FSIIM

26 Pediatric Cephaloceles: A Multimodality Review

Although imaging is vital for characterizing cephaloceles, little appears in the radiology literature on this complex topic. This review illustrates the four major types of cephaloceles using a multimodality approach with prenatal and postnatal correlation.

Marijan Pejic, MD; Kyle Luecke, MD; Avner Meoded, MD; Jerry Tuite, MD; Javier Quintana, MD; Jennifer Neville Kucera, MD, MS

33 Improving Body Imaging Throughput in the Midst of COVID-19

We discuss our experience using fast MRI body imaging protocols in combination with strategic use of free-standing facilities to safely reduce our patient backlog and manage our MR imaging load.

John V Thomas, MD; Kristin K Porter, MD, PhD;
Stefanie A Woodard, DO; Aparna Singhal, MD;
Mason B Frazier, MD; Desiree E Morgan, MD;
Cheri L Canon, MD, FACR, FFAWR

Applied Radiology (ISSN 0160-9963, USPS 943180) is published in print 6 times a year, January, March, May, July, September, and November, by Anderson Publishing Ltd at 180 Glenside Ave., Scotch Plains NJ 07076. Periodicals postage paid at Scotch Plains, NJ and additional mailing offices. Free subscriptions for US-based qualified radiology professionals. Subscriptions for the US and its territories and possessions: \$115 per year, \$225 for two years. Foreign and Canadian subscriptions \$215 for one year payable in US funds, international money orders, or by credit card only. Postmaster: Please send address changes to Applied Radiology, PO Box 317, Lincolnshire, IL 60069-0317 (847-564-5942) or email AppliedRadiology@Omeda.com.

DEPARTMENTS

8 Editorial: Rising into Fall

Erin Simon Schwartz, MD, FACR

36 Eye on AI: The Power of Triage (CADt) in Breast Imaging

Lisa Watanabe, MD

40 Radiology Matters: The Future is Bright for Collaboration Between AI and Breast Imagers

Mary Beth Massat

44 Pediatric Radiological Case: Cystic Fibrosis Liver Disease

David Chung, MD; Joseph J Palermo, MD;
Richard Towbin, MD; Alexander J Towbin, MD

47 Radiological Case: Hemangiopericytoma of the Third Ventricle

Shreeja Kadakia, BS; Khuram Kazmi, MD

49 Radiological Case: GIST of the Duodenum and Proximal Jejunum with an Ampullary Neuroendocrine Tumor

Mohammed Mirza, MD; Joshua Boulter;
Alula Tesfay, MD

52 Radiological Case: Dorsal Thoracic Arachnoid Web and Spinal Cord Compression

Tiffany Y So, MBBS, BMedSci, MMed (Radiology),
FRANZCR; Kateryna Burlak, MBBS;
William A MacLaurin, MBBS, FRANZCR

56 Wet Read: Ode to a Beeper

C. Douglas Phillips, MD, FACR

Bonus Case AR Online

Intraosseous Lipoma of the Sacrum

Scott P Patterson, MD; Dina Patterson, MD;
Shaka M Walker, MD

APPLIEDRADIOLOGY.COM

Built to perform.

BASED ON INSIGHTS THAT IMPACT PATIENT CARE



We all know that screening is the best way to detect breast cancer earlier and digital breast tomosynthesis (DBT) improves image quality for better detection. But now it's time to get smarter about it.

ASPIRE Cristalle with DBT is built with insight into image quality, operational excellence, and a better patient experience.

ASPIRE *Cristalle*
with Digital Breast Tomosynthesis

SUPERIOR DIAGNOSTIC ACCURACY — superior (lower) recall rates for non-cancer cases

LESS STRESSFUL EXAM — patented Comfort Paddle gently adapts to the breast's curves for noticeably improved comfort

LOW DOSE — achieve exceptional images with gentle dose for every breast type.

SEE MORE OF THE INSIGHTS that helped create one of the world's most precise and comfortable mammography systems at **cristalle.fujimed.com**



*As a radiology
community
we can all
benefit from
the experience
of others.*

Rising into Fall

Erin Simon Schwartz, MD, FACR

Autumn. Back to school time. Yet this school year will be an unusual combination of in-person and virtual learning for many — including those embarking on medical careers and those starting their radiology training.

In a typical year, the radiology trainees who started in July would be settling into the rhythm of their programs and starting to feel like part of a team by now, having enjoyed summer gatherings to get to know their new colleagues and their families.

But this is a year unlike any other.

Sadly, it has become unsafe and, in many places, illegal to have large parties. It is also not clearly safe to sit shoulder to shoulder at workstations. And with many people working from home or utilizing other alternative arrangements, there is a need to optimize virtual education while also creating that sense of community and belonging so vital for us all. Can this need be met through video chat services and other technologies? How has your program adapted to ensure your trainees receive sufficient instruction and practical experience? Have you developed novel uses for existing technologies, or new technologies that others can use?

As a radiology community we can all benefit from the experience of others. I know I am searching for tools to facilitate remote teaching, and we would love to know how you are navigating these important topics during this prolonged uncertain and challenging time. Let's discuss on Twitter. Please follow us and share your thoughts @Applied_Rad.

Please Welcome our New Board Members

As most of you are aware, my predecessor, Stuart E Mirvis, MD, FACR, was a world-renowned Emergency and Trauma Radiology expert. Dr Mirvis developed and led the Section of Trauma and Emergency Radiology for the R Adams Cowley Shock Trauma Center at the University of Maryland in Baltimore, MD. His retirement left us with a need to recruit experts in the growing area of Emergency Radiology.

I am delighted to announce the formation of a new section, Emergency Radiology, under the direction of our newest Editorial Advisory Board member and Associate Editor, Melissa A Davis, MD, MBA. Dr Davis is an Assistant Professor and the Medical Director of Quality in the Department of Radiology and Imaging, Emory University, Atlanta, GA. She brings a wealth of expertise in this rapidly growing subspecialty. We are looking forward to her help in growing our coverage of this important field with emergency and trauma imaging content.

We are also thrilled to welcome two additional new board members:

Michael L Francavilla, MD, Pediatric Radiology, Children's Hospital of Philadelphia and Perelman School of Medicine, University of Pennsylvania, Philadelphia, PA;

Minhaj S Khaja, MD, MBA, Interventional Radiology, University of Virginia Health System, Charlottesville, VA.

These are challenging times, but we are not going to let them stop us from rising to the challenge of bringing you all the best of medical imaging — in print and online.

Be well.

Dr Schwartz is the Editor-in-Chief of Applied Radiology. She is an Associate Professor of Radiology, Perelman School of Medicine, University of Pennsylvania, and a Pediatric Neuroradiologist at The Children's Hospital of Philadelphia. She can be reached at erin@appliedradiology.com.

SA-CME Information

Pregnancy-associated Breast Cancer and Other Breast Disease: A Radiologic Review

Description

Pregnancy associated breast cancer (PABC) is a subset of breast cancer that is typically diagnosed at more advanced stages and carries a worse prognosis. The physiological breast changes that occur during pregnancy and lactation can often make clinical and radiological evaluation difficult.

Ultrasound is the primary imaging modality in the evaluation of pregnancy associated breast lesions with high sensitivity and lack of radiation. Mammography is generally considered safe during pregnancy and lactation and may also be used to assess for PABC. Dynamic contrast enhanced breast MRI is not recommended during pregnancy; however, it may safely be performed in lactating women to evaluate extent of disease or for high risk screening.

This article reviews appropriate imaging evaluation of the pregnant or lactating woman, and showcases the imaging features of benign and malignant lesions occurring during pregnancy and lactation. Many benign lesions, including fibroadenoma and lactating adenoma, can mimic malignancy. New or growing solid masses occurring during pregnancy and lactation should be further evaluated with imaging and biopsy, to avoid a delay in a potential cancer diagnosis.

Learning Objectives

After completing this activity, the participant will be able to:

- Describe the physiological changes of the breast that occur during pregnancy and lactation and how these changes manifest on imaging.
- Recognize common benign entities that affect women during pregnancy and lactation.
- Differentiate the imaging characteristics of pregnancy associated breast cancer from benign lesions.

Accreditation/Designation Statement

The Institute for Advanced Medical Education is accredited by the Accreditation Council for Continuing Medical Education (ACCME) to provide continuing medical education for physicians.

The Institute for Advanced Medical Education designates this journal-based CME activity for a maximum of 1 AMA PRA Category 1 Credit™. Physicians should only claim credit commensurate with the extent of their participation in the activity. These credits qualify as SA-CME credits.

Authors

Andrew Ong, MD; Lisa A Mullen, MD, Division of Breast Imaging, Johns Hopkins University School of Medicine, Baltimore, MD. Susan C. Harvey, MD, Hologic, Inc.

Target Audience

- Radiologists
- Related Imaging Professionals

System Requirements

In order to complete this program, you must have a computer with a recently updated browser and a printer. For assistance accessing this course online or printing a certificate, email CustomerService@AppliedRadiology.org.

Instructions

This activity is designed to be completed within the designated time period. To successfully earn credit, participants must complete the activity during the valid credit period. To receive SA-CME credit, you must:

1. Review this article in its entirety.
2. Visit www.appliedradiology.org/SAM2.
3. Login to your account or create an account (new users).
4. Complete the posttest and review the discussion and references.
5. Complete the evaluation.
6. Print your certificate.

Estimated time for completion: **1 hour**

Date of release and review: **September 1, 2020**

Expiration date: **August 31, 2022**

Disclosures

No authors, faculty, or any individuals at IAME or *Applied Radiology* who had control over the content of this program have any relationships with commercial supporters. *Note: During the preparation of this article Dr Harvey was Chief, Division of Breast Imaging at Johns Hopkins and not yet an employee of Hologic.*

Pregnancy-associated Breast Cancer and Other Breast Disease: A Radiologic Review

Andrew Ong, MD; Lisa A Mullen, MD; Susan C. Harvey, MD

Breast cancer is the most common malignancy affecting women, accounting for 30% of all new cancer diagnoses in 2018. Despite its high incidence, breast cancer carries a favorable prognosis, with a 90% five-year survival rate for all stages combined.¹ Improvements in screening techniques with advancement in both patient and clinician education have been paramount in detecting breast cancer at earlier stages and dramatically reducing overall mortality and morbidity.^{2,3}

A subset of breast cancer cases, specifically during pregnancy, is usually diagnosed at more advanced stages and carries a worse prognosis.⁴⁻⁶ Mortality rates were shown to be nearly 50% higher for cases of pregnancy associated breast cancer (PABC) compared with non-PABC.⁷ A meta-analysis of 3268 cases showed that PABC had a significantly higher risk of death than non-PABC with hazard ratio of 1.44; 95% CR [1.27-1.63]; PABC was independently associated with higher

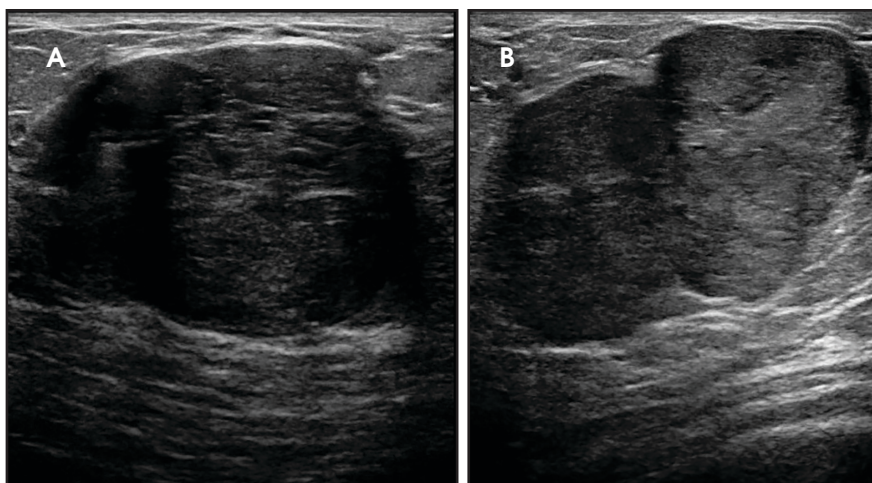


FIGURE 1. 28-year-old patient, 36 weeks pregnant, who presented with two palpable right breast lumps. Sonographic evaluation showed two separate hypoechoic masses in the right breast, (A) located at 11:00 and (B) located at 2:30. Biopsy proved both masses to be fibroadenomas.

mortality, particularly those diagnosed shortly postpartum.⁸

Fortunately, PABC is relatively uncommon with an approximate incidence of 1 in every 3,000 pregnancies, comprising only 3% of all breast cancer cases.^{9,10} However, a recent large US population-based study showed an uptrend in the overall incidence of PABC between 2001-2013, which has been postulated to largely result from women delaying childbearing until a later age.¹⁰

PABC is defined as breast cancer presenting during pregnancy or up to one year postpartum. Naturally, PABC has added repercussions and diagnostic urgency given that the disease process

and treatments will ultimately affect both the mother and fetus if diagnosed during pregnancy. Additionally, a myriad of physiological breast changes occur in response to the hormonal stimulation of pregnancy, which makes clinical and radiologic evaluation technically difficult.

Currently, there is a paucity of literature on PABC. Intrinsic challenges and lack of awareness have been postulated to contribute to the delay in diagnosis, which is a major factor in the overall poor prognosis.¹¹ Thus, it is critical to be aware of this diagnosis. The goal of this article is to illustrate the expected changes to the breast during pregnancy

Affiliations: Drs Ong and Mullen, Division of Breast Imaging, Johns Hopkins University School of Medicine, Baltimore, MD. Note: Dr Harvey is currently with Hologic, Inc. but when this article was written was with Johns Hopkins University School of Medicine, Baltimore, MD.

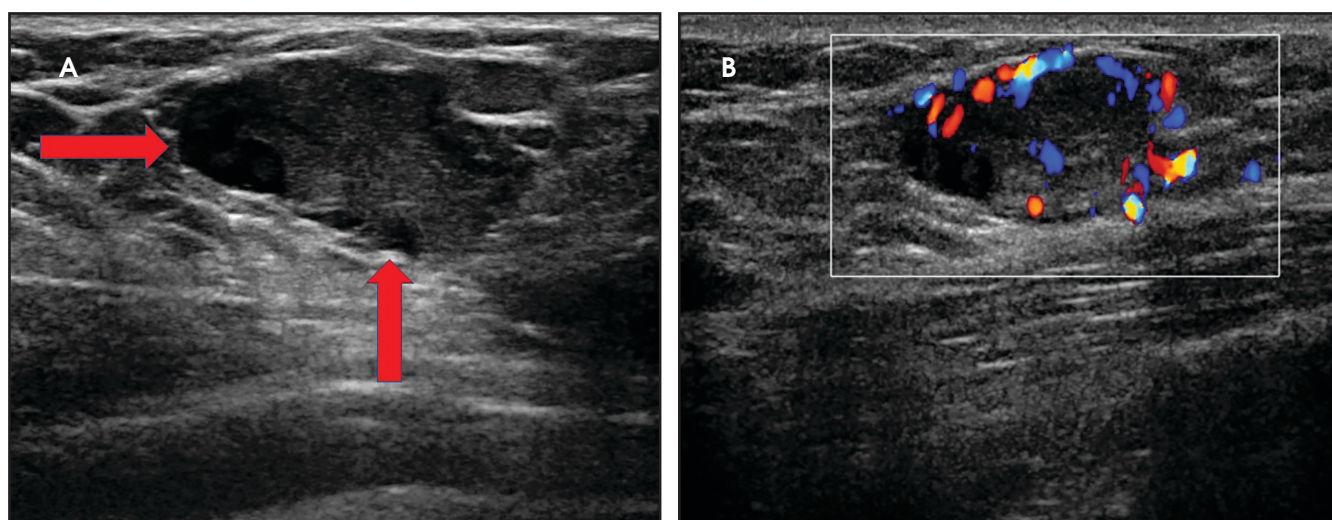


FIGURE 2. 27-year-old patient, 28 weeks pregnant, who presented with a palpable right breast lump. (A) Sonographic evaluation showed a hypoechoic mass with cystic areas (arrows). (B) Color Doppler images demonstrated marked internal vascularity. Biopsy proved the mass to be a lactating adenoma.

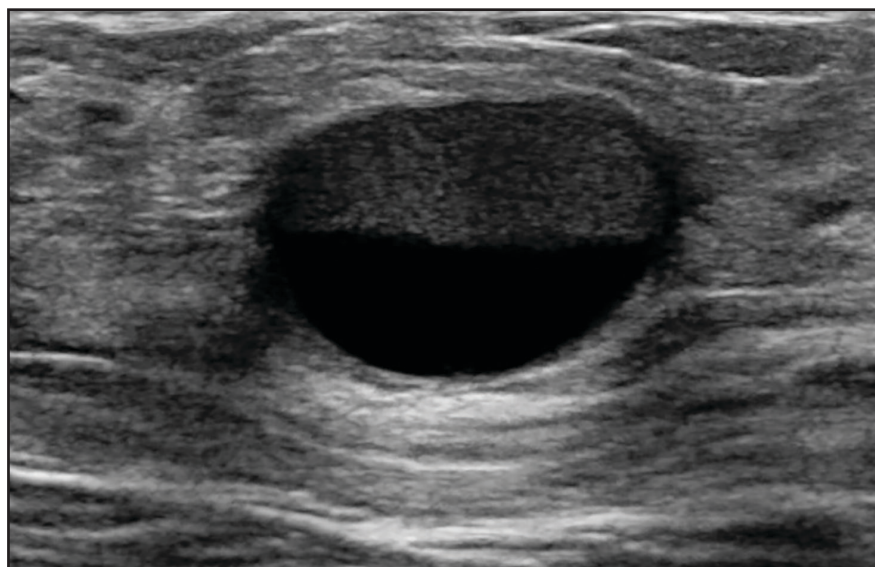


FIGURE 3. 29-year-old lactating patient, 10 months postpartum, who presented with a painless palpable right breast lump. Sonographic images showed a well-circumscribed cystic lesion with a fat-fluid level, consistent with a galactocele.

and lactation and the appropriate diagnostic approach when evaluating pregnancy associated breast complaints. Also, this work highlights key imaging characteristics that can help distinguish benign from malignant processes.

Physiological Changes

During pregnancy and lactation, the breast undergoes physiological changes that are driven by fluctuating levels of estrogen, progesterone, and prolactin. Increasing estrogen

levels secreted by the placenta induce growth of both the ductal system and surrounding stroma with large quantities of adipose tissue deposition and increased glandular vascularity. Simultaneously, increasing progesterone levels play a synergistic role with estrogen by causing further maturation of the breast lobules and alveoli with the secretory characteristics of the alveoli cells being developed.¹¹⁻¹³

Estrogen and progesterone, though essential for breast development during

pregnancy, cause inhibition of milk production. Concentrations of both these hormones significantly drop near the end of pregnancy and immediately after parturition, eliminating their inhibitory effects. On the other hand, secretion of prolactin by the pituitary gland steadily increases throughout pregnancy and, when unopposed by estrogen and progesterone, promotes the synthesis of milk. A few weeks postpartum, prolactin concentrations also return to basal levels; however, milk production is sustained by breast feeding, which induces intermittent spikes of marked prolactin secretion.

Clinically, these changes cause increasing firmness, volume, and nodularity to the breast which persists through lactation and makes physical examination progressively more problematic.^{11,14} This correlates with markedly increased fibroglandular breast parenchyma, which affects the appearance of the breast tissue on mammography, ultrasound, and MRI, and changes the overall sensitivity and utility of the various radiologic modalities.

Radiologic Evaluation

Most pregnant women fall below the recommended age for annual mammographic screening, with the median age at diagnosis of PABC being 33-34 years.^{4,5} Thus, imaging evaluation of

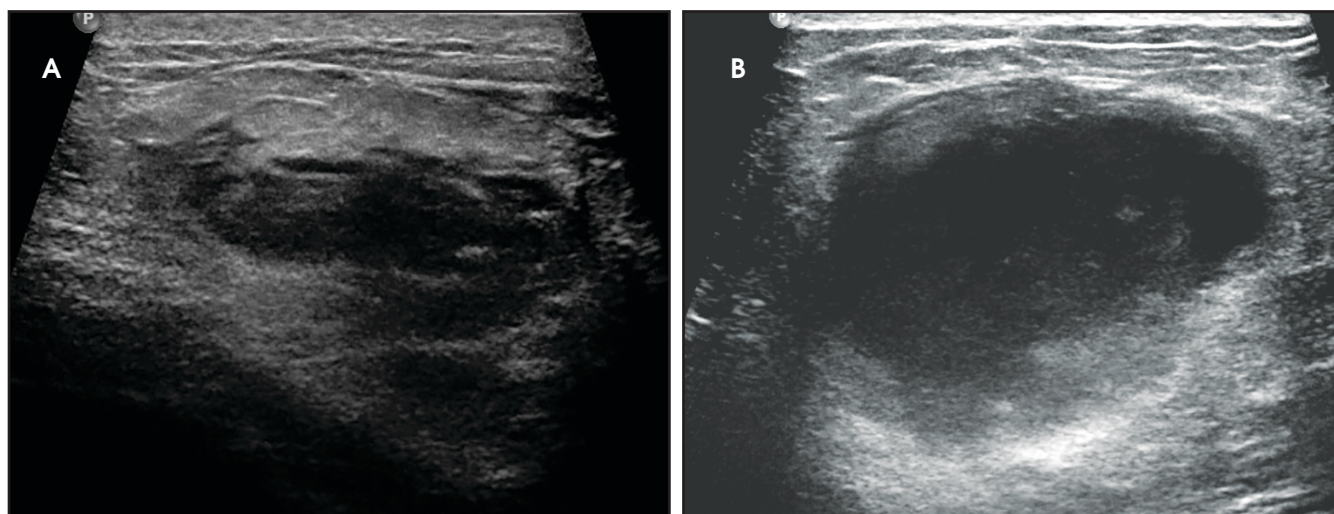


FIGURE 4. Puerperal mastitis with abscess in two different patients. (A) 34-year-old patient, several weeks postpartum, who had stopped breast feeding, and (B) 23-year-old patient who was 4 months postpartum and breast feeding. Both patients presented with a palpable lump. Ultrasound evaluation demonstrated a heterogeneous complex hypoechoic cystic mass in both cases. For patient A, biopsy of the mass was performed, with result of abscess, and culture of fluid aspirated from the mass grew *Staphylococcus aureus*. For patient B, biopsy of the mass yielded lactational/secretory changes with acute and chronic inflammation, and culture of fluid aspirated from the mass showed no growth, which may have been related to prior antibiotic treatment.

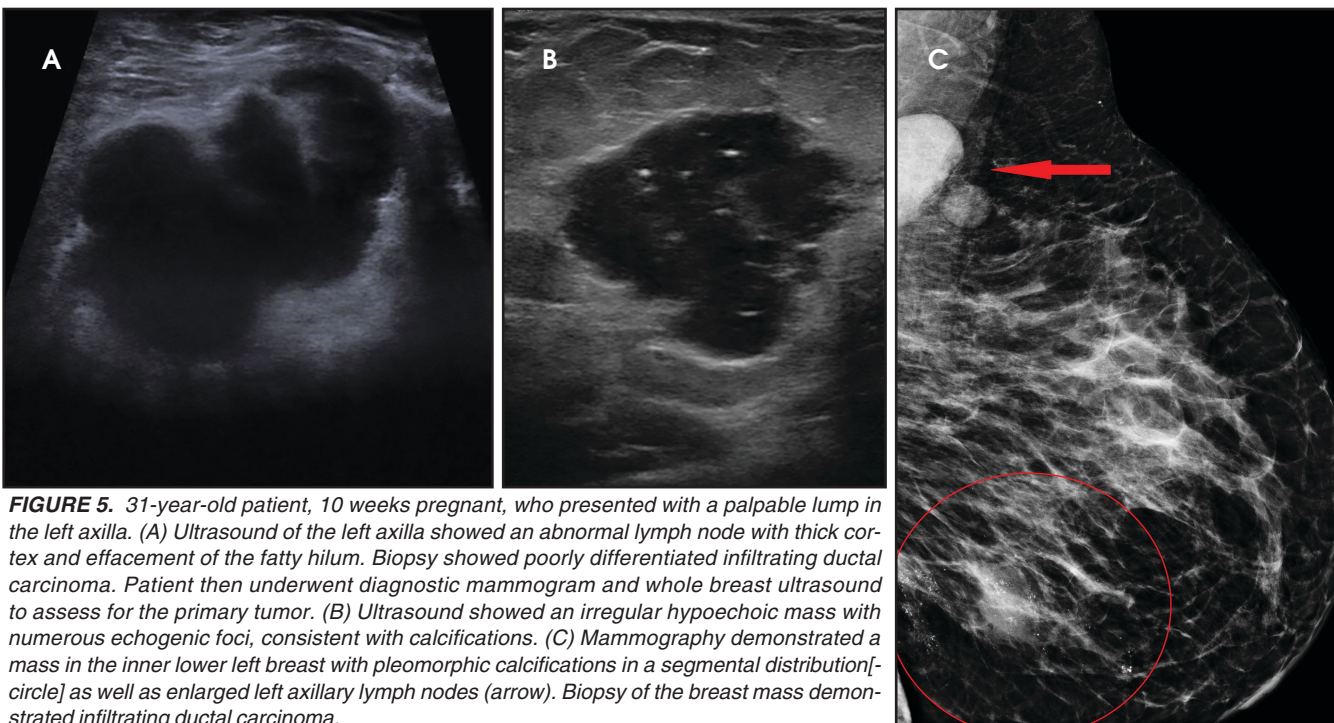


FIGURE 5. 31-year-old patient, 10 weeks pregnant, who presented with a palpable lump in the left axilla. (A) Ultrasound of the left axilla showed an abnormal lymph node with thick cortex and effacement of the fatty hilum. Biopsy showed poorly differentiated infiltrating ductal carcinoma. Patient then underwent diagnostic mammogram and whole breast ultrasound to assess for the primary tumor. (B) Ultrasound showed an irregular hypoechoic mass with numerous echogenic foci, consistent with calcifications. (C) Mammography demonstrated a mass in the inner lower left breast with pleomorphic calcifications in a segmental distribution [circle] as well as enlarged left axillary lymph nodes (arrow). Biopsy of the breast mass demonstrated infiltrating ductal carcinoma.

PABC is predominantly diagnostic in nature. Most patients present with a palpable breast lump that can easily be assessed with ultrasound (US). Furthermore, given the lack of radiation and high sensitivity of between 86.7%–100%, US is easily the test of choice.^{15,16}

Sonographically, the increase in the non-glandular fibrofatty tissue during pregnancy causes the breast parenchyma to appear diffusely more hypoechoic.^{16–18} During lactation, the breast parenchyma becomes diffusely echogenic due to proliferation of glandular components and production of

milk rich in fat. During this time, prominent ducts and increased vascularity can also be observed.^{14–18}

Mammography may also be used to assess for PABC with physiological changes manifesting as marked increase in parenchymal density and breast size.¹² However, owing to the

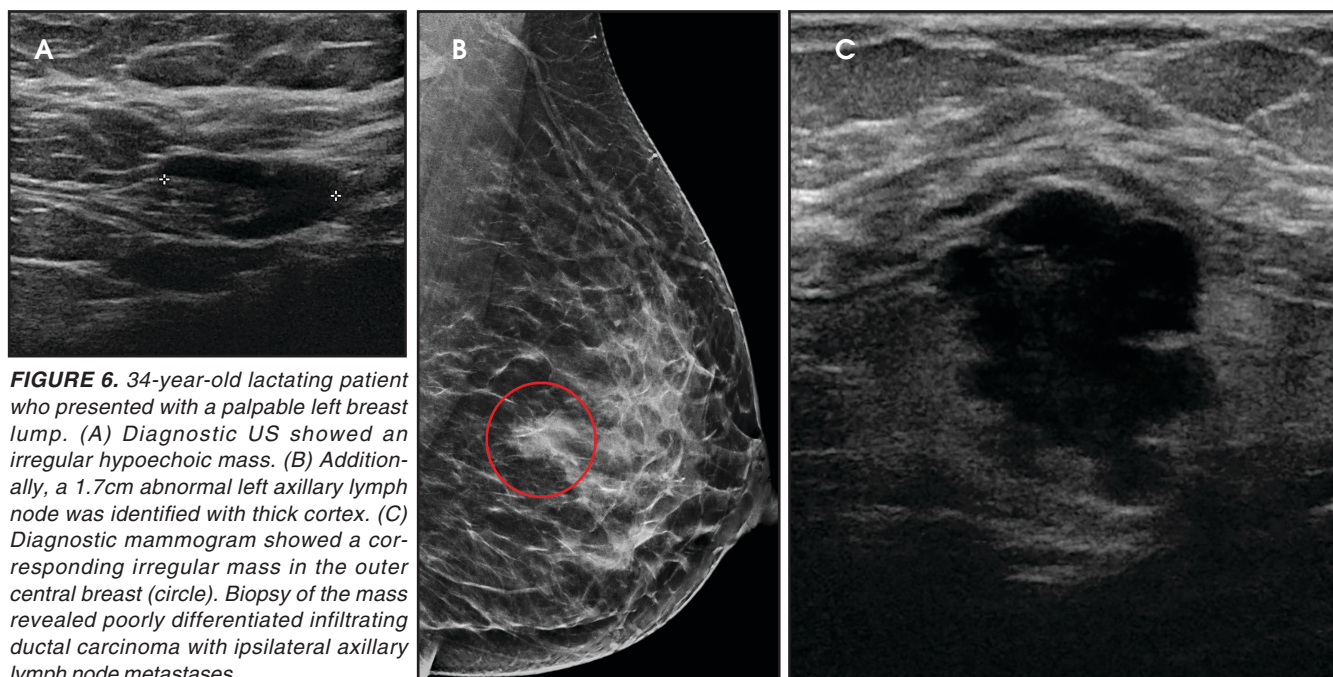


FIGURE 6. 34-year-old lactating patient who presented with a palpable left breast lump. (A) Diagnostic US showed an irregular hypoechoic mass. (B) Additionally, a 1.7cm abnormal left axillary lymph node was identified with thick cortex. (C) Diagnostic mammogram showed a corresponding irregular mass in the outer central breast (circle). Biopsy of the mass revealed poorly differentiated infiltrating ductal carcinoma with ipsilateral axillary lymph node metastases.

median age of women with PABC, mammography is typically recommended only if there is high suspicion for malignancy or to determine extent of disease.¹¹ This is because mammography is less sensitive compared to ultrasound with studies reporting sensitivities between 78-87% in the setting of PABC.^{6, 15, 19} For lactating women 40 and older, mammography is considered appropriate.

Mammography is generally considered safe during pregnancy and lactation.²⁰ It is important that radiologists be prepared to discuss radiation safety with patients and referring providers, who are often hesitant due to perceived risks. The fetus is most susceptible to radiation-induced malformations during the first trimester, believed to occur with exposure greater than 0.05 Gy of radiation. However, performing standard two-view mammography of each breast with abdominal shielding exposes the fetus to ~0.003-0.004 Gy, a minimal fetal radiation exposure. There is no proven carcinogenic effect of mammography in lactating women.^{11, 20}

Currently, dynamic contrast enhanced (DCE) breast MRI is not recommended during pregnancy. Based on the current

American College of Radiology (ACR) appropriateness guidelines, there is insufficient safety data for the fetus, and its diagnostic role has not been established. MRI is only recommended during pregnancy when the risk-benefit ratio is clearly defined by the disease process and predicted outcome.^{18, 20}

During lactation, DCE breast MRI may be safely performed to evaluate the extent of disease or for high-risk screening. Gadolinium is considered safe during lactation with very low concentrations found in the produced milk.²¹ The current ACR guidelines do not require patients to discontinue breast feeding, though patients may pump and discard breast milk for 24 hours after gadolinium administration to fully excrete the contrast and thus avoid any ingestion by the infant.^{20, 21}

Since breast MRI is not typically performed during pregnancy, the physiological changes observed on MRI are typically of lactating women. Like other modalities, the physiological changes are manifested as increased breast parenchymal. A few small-scale studies have shown rapid, moderate to marked increased background enhancement, which is postulated to be

secondary to increased perfusion. Additionally, there is diffusely increased T2 signal from milk production within the breast tissue.^{22, 23}

Previous reports have hypothesized that the increased background enhancement would limit the value of DCE breast MRI in pregnant and lactating patients; however, a small case series showed that it was able to accurately detect all breast cancers in five cases.²³ Also, in a recent retrospective study, preoperative MRI was shown to be 98% sensitive at detecting tumors. More importantly, in 28% of those cases, MRI changed surgical management by showing greater extent of disease or pathologically proven larger tumor burden compared to ultrasound and mammography.²⁴

Another recent small cohort study showed that noncontrast breast MRI using diffusion tensor imaging (DTI) could be used in adjunct with other modalities in detecting PABC, evaluating the symptomatic breast, and screening high risk women during pregnancy.²⁵ These studies show that MRI may be of value in the management of PABC despite current recommendations and further research to explore these roles is necessary.

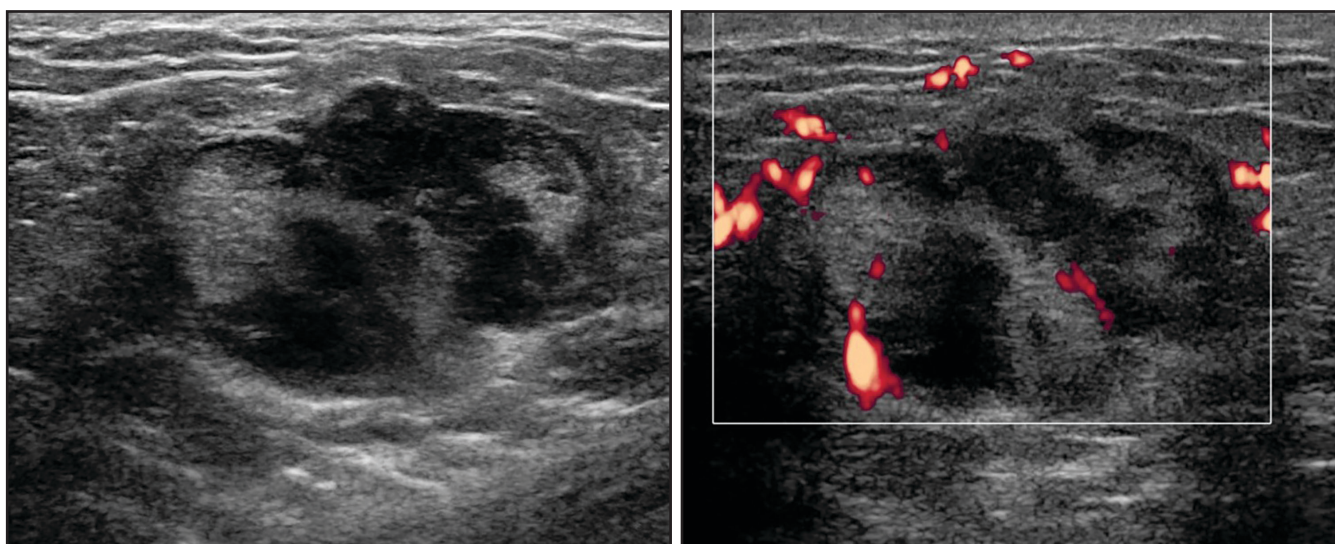


FIGURE 7. 33-year-old lactating patient, 1 month postpartum, who presented with a tender breast lump in the right breast. (A) US showed a heterogeneously hypoechoic mass with parallel orientation. (B) Power Doppler demonstrated peripheral and internal vascularity. Biopsy of the mass revealed diffuse large B-cell lymphoma.

Common Benign Disorders

As in non-pregnant young females, the most common benign tumors associated with pregnancy are fibroadenomas. It is postulated that the majority of fibroadenomas are present before pregnancy but become apparent as they grow with rising hormone levels. Clinically, these present as painless, palpable, and rubbery masses, and are often multiple and bilateral. Imaging findings are similar to those of non-pregnant patients: an oval, well-circumscribed hypoechoic mass. In the setting of pregnancy or lactation, for a growing fibroadenoma or a new solid-appearing mass, even with benign features, image-guided biopsy and pathologic correlation is recommended (Figure 1).^{11,13,14}

An uncommon benign entity that mainly occurs in the setting of pregnancy, typically in the 3rd trimester, is an infarcted fibroadenoma. The etiology is likely a rapidly growing fibroadenoma, secondary to increased hormones, that eventually outgrows its blood supply. This produces variable imaging patterns depending on the severity of infarction. These lesions can have heterogeneous echotexture, internal cystic spaces, and ill-defined or irregular borders, mimicking malignancy and often requiring pathological confirmation. Another form

of fibroadenoma that may mimic malignancy is a fibroadenoma with secretory hyperplasia or lactational changes. This is thought to be due to hormone sensitive epithelial cells within the fibroadenoma, which are stimulated and undergo growth of the ductal elements in a similar manner to normal mammary tissue related to increased hormone levels. Sonographically, these typically show heterogeneous echotexture with hyperechoic areas, dilated ducts, and intraleisional cysts. Secretory like calcifications may be seen on mammography.^{11,13,14}

Lactating adenomas comprise a fourth kind of benign tumor and are unique to pregnancy and lactation. They are often indistinguishable from fibroadenomas on imaging and pathologically. They usually present as palpable, solid, and mobile masses during the 3rd trimester or during lactation and can be multiple and bilateral. Their typical sonographic appearance is of a solid hypoechoic and oval, mass that is circumscribed and may have microlobulations (Figure 2A); color Doppler evaluation typically shows internal vascularity (Figure 2B). Posterior acoustic enhancement may be present secondary to intraleisional fluid. Like fibroadenomas, lactating adenomas may also infarct and be painful, causing the lesion

to have a heterogeneous appearance under imaging which can mimic malignancy.^{13,14,26}

Lactating women can also develop galactoceles, which are the most common benign breast masses in these patients. Galactoceles occur predominantly after cessation of breastfeeding, but they occasionally can occur during lactation and, rarely, in the 3rd trimester.¹³ They are caused by milk obstructing a duct, inducing dilation of the obstructed portion and forming a complex cystic lesion. Fluctuating amounts of internal degraded milk products and surrounding inflammatory changes cause variable imaging appearances. Typically, these are oval shaped, with variable echogenicity depending on fat content and age of the lesion; they may begin as anechoic and show increasing echogenicity as they age. Internal vascularity should never be seen, although surrounding hyperemia is common due to surrounding inflammatory changes. Occasionally, a fat-fluid level may be observed that is pathognomonic (Figure 3). The majority of galactoceles resolve spontaneously.^{11,13,14}

A fifth benign entity commonly seen during lactation but infrequently during pregnancy is puerperal mastitis. The mechanism of infection is disruption of

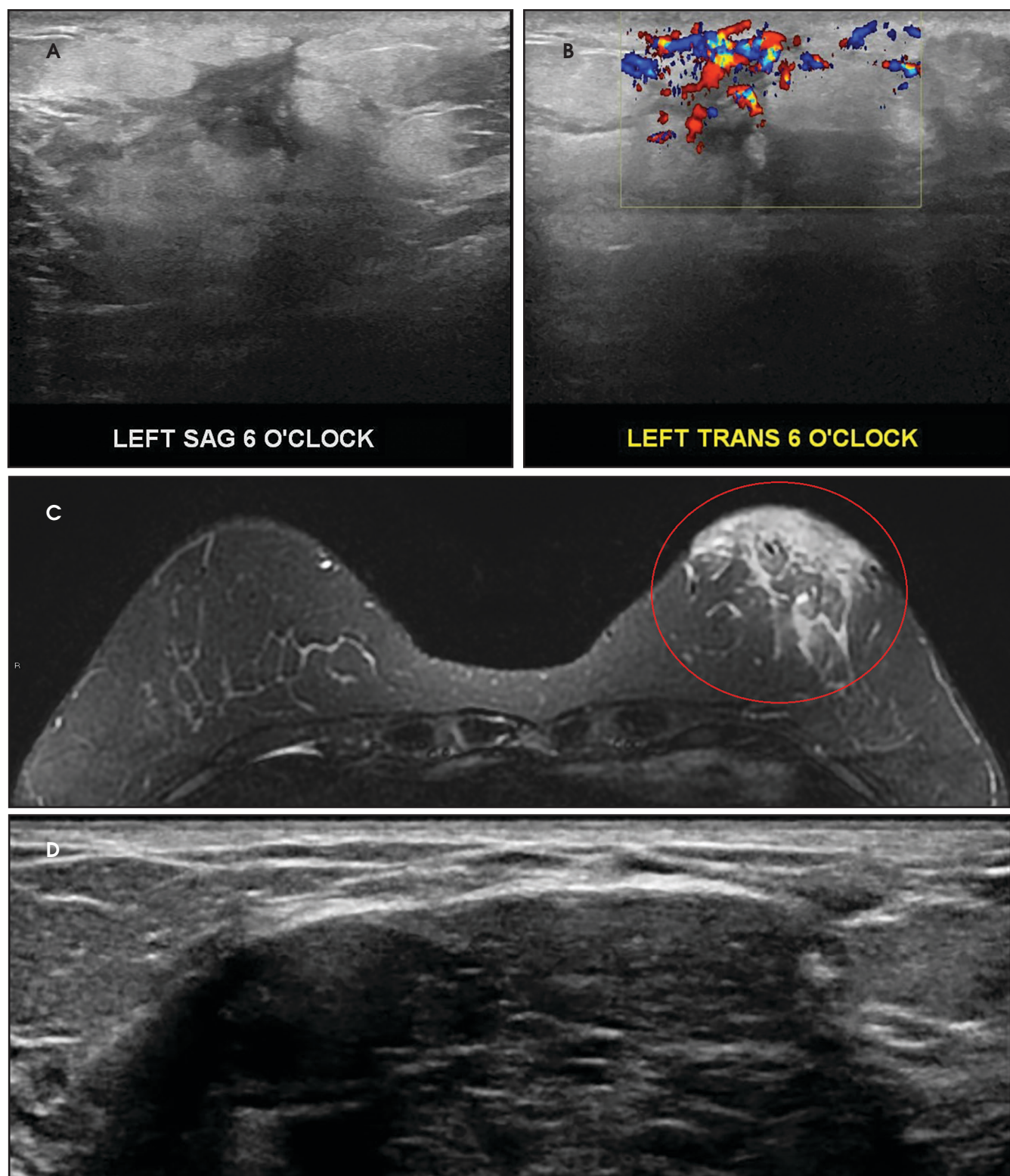


FIGURE 8. 29-year-old patient, 3 weeks postpartum, who presented with a palpable left breast mass with associated purple discoloration of the skin. (A) Ultrasound evaluation showed an irregular hypoechoic mass (B) with marked internal and surrounding vascularity on color Doppler. Punch biopsy of the involved skin showed angiosarcoma, and core biopsy of the breast mass showed low-grade angiosarcoma involving breast parenchyma. (C) STIR sequence MRI images showed skin thickening with hyperintense signal (circle). (D) Postcontrast MRI maximum intensity projection (MIP) image showed an enhancing mass with multiple large feeding vessels (circle).

the nipple epithelium and milk stasis, resulting in retrograde spread of bacteria, typically *Staphylococcus aureus* and *Streptococcus*. Patients clinically present with an erythematous, edematous, and painful breast. Diagnosis can be made based on clinical findings when uncomplicated, though imaging work-up may be necessary if there is poor response to antibiotics or concern of an underlying abscess. Ultrasound is the modality of choice, with sonographic findings of mastitis including skin thickening, decreased parenchymal echogenicity, and increased vascularity. An abscess will typically appear as a complex hypoechoic cystic mass with peripheral vascularity and posterior acoustic enhancement (Figure 4).^{14,16,18}

Treatment of puerperal mastitis consists of antibiotics and frequent breastfeeding or breast expression to limit milk stasis. Ultrasound-guided aspiration should be considered for drainage of an abscess to provide pain relief and to shorten illness duration. If the abscess persists or recurs, repeat drainage should be performed.^{7,14,18} In atypical or refractory cases, further work-up with mammography and US should be considered, owing to the overlap of radiologic and clinical findings of infection and inflammatory breast cancer. Image-guided core needle biopsy or skin-punch biopsy may be necessary if there is suspicious imaging or clinical features.^{14,18}

Pregnancy-associated Breast Cancer

Women with PABC typically present with a firm, painless, and palpable lump that is frequently non-mobile.^{15,26} Additional presentations include unilateral breast enlargement with skin thickening, nipple retraction, and nipple discharge.²⁷ As in non-pregnant patients, the most common breast cancer associated with pregnancy is invasive ductal carcinoma, with the pregnancy-associated malignancies having more aggressive histological features. Middleton et al showed that the most common histological subtype

in 39 cases of PABC was a high-grade tumor that was estrogen and progesterone negative with increased rates of lymphovascular invasion.²⁸

The imaging appearance of PABC is similar to that of non-gestational breast cancer. Nearly all cases of PABC present with the unifying sonographic finding of a mass.^{15,27} Ultrasound features that typically signify a malignant rather than a benign process include a hypoechoic mass that is taller than it is wide, with indistinct or spiculated borders. Enlarged axillary lymph nodes may also be present in the setting of lymph node metastases. (Figures 5, 6) It has been reported that PABC often shows large cystic components, and up to 63% of these malignancies display posterior acoustic enhancement – findings that are typically associated with benign lesions.^{15,23} Thus, it is imperative that biopsy be considered in the setting of a new solid mass found on ultrasound during pregnancy, even without suspicious features, to avoid delay in care.

Mammographically, the most common presentation of PABC is a mass with or without associated features, such as skin thickening, calcifications, and axillary lymphadenopathy, followed by calcifications without an associated mass (Figures 5,6). A less common presentation is skin thickening with generalized increased parenchymal density, typically seen in inflammatory breast cancer. This presentation can be confused with puerperal mastitis, which can lead to a delay in diagnosis.^{6,15,27}

The literature on MRI evaluation of PABC is sparse, as contrast-enhanced MRI is considered contraindicated in pregnancy; most published research focuses on postpartum and lactating women. Despite concern that increased background enhancement could reduce sensitivity, a recent study by Myers et al showed that contrast-enhanced MRI had a sensitivity of 98% in detecting malignancy. The most common MRI appearance was of an enhancing mass

with 62% of the PABC displaying an irregular shape and 66% having irregular margins.²⁴ In a recent prospective cohort by Nissan et al evaluating the feasibility of noncontrast MRI using DTI, PABC most often appeared as decreased diffusivity and maximal anisotropy values when compared to normal pregnant fibroglandular tissue.²⁵

Atypical Pregnancy-related Malignancies of the Breast

There are two distinct but uncommon types of primary lymphomas that affect the breast, both of which are especially rare during pregnancy and lactation. The first, Burkitt Lymphoma, is the less common of the two, presenting as diffuse bilateral breast enlargement that affects younger puerperal women. Classically, this type of breast lymphoma is categorized as the endemic or African type, which has been linked to the Epstein-Barr virus, though there are also sporadic cases. On imaging, this malignancy manifests as diffuse bilateral increase in parenchymal density corresponding to the infiltrative tumor process.^{11,29} The more common subtype, non-Hodgkin lymphoma of the breast, typically affects older women. These are usually unilateral with presentation and imaging features that are similar to those of breast carcinoma.²⁹ Although this lymphoma is not typically associated with pregnancy, there are a few confirmed cases in puerperal women (Figure 7).

Another rare entity that can affect puerperal women is primary breast angiosarcoma. This aggressive tumor occurs sporadically in younger women; 6-12% of these tumors are associated with pregnancy or lactation.³⁰ Clinically, they present as a painless, rapidly growing, and palpable mass, often accompanied by an adjacent bluish skin discoloration.^{30,31} The mammographic appearance is nonspecific, with the most common presenting feature being an ill-defined noncalcified mass or a focal asymmetry. Up to 33% of breast angiosarcomas are mammographically occult. Sonographically, these tumors display

varying echogenicity and may have circumscribed or ill-defined borders; on color Doppler, angiosarcomas typically display marked hypervascularity (Figure 8). On MRI, these tumors appear heterogeneous, displaying decreased signal intensity on T1 sequences and high signal on T2 sequences. Low-grade angiosarcomas typically show a persistent enhancement pattern on contrast-enhanced MRI, while high-grade tumors display rapid enhancement and wash-out, with large draining vessels possibly being visualized (Figure 8).³¹

Conclusion

PABC is a subset of breast cancer that carries a poor prognosis. During pregnancy, the breast undergoes many physiologic changes that make an imaging diagnosis challenging. Ultrasound is the primary imaging modality in the diagnostic work-up for PABC, though mammography and MRI may also play a role. Palpable masses presenting in pregnant or lactating women should undergo prompt imaging evaluation. New or growing solid masses should be further evaluated with biopsy to avoid delaying a potential cancer diagnosis.

REFERENCES

1. Siegel RL, Miller KD, Jemal A. Cancer statistics, 2018. *CA Cancer J Clin*. 2018; 68(1):7–30.
2. Cortesi L, Chiuri VE, Ruscelli S, et al. Prognosis of screen-detected breast cancers: results of a population-based study. *BMC Cancer*. 2006; 6:17.
3. Tabár L, Dean PB, Chen TH, et al. The incidence of fatal breast cancer measures the increased effectiveness of therapy in women participating in mammography screening. *Cancer*. 2019; 125(4):515–523.
4. Ring AE, Smith IE, Ellis PA. Breast cancer and pregnancy. *Ann Oncol*. 2005; 16:1855–1860.
5. Navrozoglou I, Vrekoussis T, Kontostolis E, et al. Breast cancer during pregnancy: a mini-review. *Eur J Surg Oncol*. 2008; 34:837–843.
6. Liberman L, Giess CS, Dershaw DD, et al. Imaging of pregnancy-associated breast cancer. *Radiology*. 1994; 191:245–248.
7. Johansson AL, Anderson TM, Hsieh CC, et al. Stage at diagnosis and mortality in women with pregnancy associated breast cancer (PABC). *Breast Cancer Res Treat*. 2013; 139(1):183–92.
8. Azim HA Jr, Santoro L, Russel-Edu W, et al. Prognosis of pregnancy-associated breast cancer: a meta-analysis of 30 studies. *Cancer Treat Rev*. 2012; 38(7):834–42.
9. Pavlidis N, Pentrouidakis G. The pregnant mother with breast cancer: diagnostic and therapeutic management. *Cancer Treat Rev*. 2005; 31:439–47.
10. Cottreau CM, Dashevsky L, Andrade SE, et al. Pregnancy-Associated Cancer: A U.S. Population-Based Study. *J Womens Health (Larchmt)*. 2019; 28(2):250–257.
11. Sabate JM, Clotet M, Torrubia S, et al. Radiologic evaluation of breast disorders related to pregnancy and lactation. *Radiographics*. 2007; 27(Suppl 1):S101–S124.
12. Hall JE, Guyton AC. *Guyton and Hall textbook of medical physiology*, 13th ed. Philadelphia, PA: Saunders/Elsevier, 2016.
13. Stavros AT. *Breast ultrasound*. Philadelphia, PA: Lippincott Williams & Wilkins, 2004.
14. Vashi R, Hooley R, Butler R, et al. Breast imaging of the pregnant and lactating patient: physiologic changes and common benign entities. *AJR Am J Roentgenol*. 2013; 200:329–336.
15. Ahn BY, Kim HH, Moon WK, et al. Pregnancy- and lactation-associated breast cancer: mammographic and sonographic findings. *J Ultrasound Med*. 2003; 22: 491–497.
16. Holanda AAR, Gonçalves AKS, Medeiros RD, et al. Ultrasound findings of the physiological changes and most common breast diseases during pregnancy and lactation. *Radiol Bras*. 2016; 49:389–396.
17. Ramsay DT, Kent JC, Hartmann RA, et al. Anatomy of the lactating human breast redefined with ultrasound imaging. *J Anat*. 2005; 206: 525–534.
18. Joshi S, Dialani V, Marotti J, et al. Breast disease in the pregnant and lactating patient: radiological-pathological correlation. *Insights Imaging*. 2013; 4:527–538.
19. Yang W, Dryden M, Gwyn K, et al. Imaging of breast cancer diagnosed and treated with chemotherapy during pregnancy. *Radiology*. 2006; 239:52–60.
20. diFlorio-Alexander RM, Slanetz PJ, Moy L, et al. ACR Appropriateness Criteria® Breast Imaging of Pregnant and Lactating Women. Available at <https://acsearch.acr.org/docs/3102382/Narrative/>. American College of Radiology. Accessed Date 2/4/2019.
21. Webb JA, Thomsen HS, Morcos SK. The use of iodinated and gadolinium contrast media during pregnancy and lactation. *Eur Radiol*. 2005; 15: 1234–1240.
22. Taleb AC, Slanetz PJ, Edmister WB, et al. The lactating breast: MRI findings and literature review. *Breast J*. 2003; 9:237–240.
23. Espinosa LA, Daniel BL, Vidarsson L, et al. The lactating breast: contrast-enhanced MR imaging of normal tissue and cancer. *Radiology*. 2005; 237:429–436.
24. Myers KS, Green LA, Lebron L, et al. Imaging appearance and clinical impact of preoperative breast MRI in pregnancy-associated breast cancer. *AJR Am J Roentgenol*. 2017; 209(3):W177–W183.
25. Nissan N, Furman-Haran E, Allweis T, et al. Noncontrast breast MRI during pregnancy using diffusion tensor imaging: a feasibility study. *J Magn Reson Imaging*. 2019; 49(2): 508–517.
26. Barco NI, Vidal MC, Fraile M, et al. Lactating adenoma of the breast. *J Hum Lact*. 2016; 32(3):559–62.
27. Vashi R, Hooley R, Butler R, et al. Breast imaging of the pregnant and lactating patient: imaging modalities and pregnancy-associated breast cancer. *AJR Am J Roentgenol*. 2013; 200(2):321–8.
28. Middleton LP, Amin M, Gwyn K, et al. Breast cancer in pregnant women: assessment of clinicopathologic and immunohistochemical features. *Cancer*. 2003; 98:1055–1060.
29. Bobrow LG, Richards MA, Happerfield LC, et al. Breast lymphomas: a clinicopathologic review. *Hum Pathol*. 1993; 24:274–278.
30. Pramanik R, Gogia A, Malik PS, Gogi R. Metastatic primary angiosarcoma of the breast: can we tame it the metronomic way. *Indian J Med Paediatr Oncol*. 2017; 38:228–31.
31. Glazebrook K.N., Magut M.J., Reynolds C. Angiosarcoma of the breast. *AJR Am J Roentgenol*. 2008; 190:533–538.

Cystic Lesions of the Head and Neck: Benign or Malignant?

Brad Wright, MD; Richard H Wiggins III, MD, CIIP, FSIIM

Editor's note: This is the first part of a two-part series. Part 2 will appear in the November/December 2020 issue of Applied Radiology.

Cystic lesions of the head and neck, ranging from benign and incidental cysts to life-threatening infections and malignancy, present a common and important diagnostic challenge.

Although some pathologies can present as trans-spatial masses, most cystic lesions are confined to well-defined anatomical spaces. A differential diagnosis can be sharpened by identifying the involved spaces and obtaining a good patient history (Table 1).

This series presents an overview of benign and malignant cystic lesions of the head and neck, emphasizing their appearance on CT and MRI. Part 1 focuses on lesions of the oral cavity, pharynx, masticator space, and parotid space. Part 2 will cover lesions of the carotid space and associated lymph nodes, as well as the retropharyngeal, prevertebral, and visceral spaces, and the supraclavicular fossa.

Lesions of the Oral Cavity

The oral cavity can be divided into 4 anatomical subunits: the oral mucosal surface (or space), the oral tongue, the sublingual space, and the submandibular

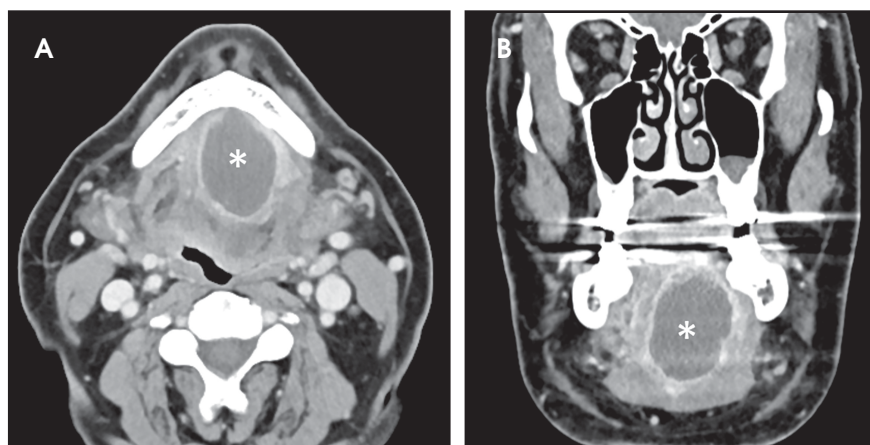


FIGURE 1. A lingual abscess in a 62-year-old with floor of the mouth swelling 2 weeks after an upper respiratory infection. Axial (A) and coronal (B) images from a contrast-enhanced CT (CECT) demonstrate a circumscribed rim-enhancing cystic lesion (white asterisks) centered in the root of the tongue.

space.¹ Lesions of the oral mucosal surface are readily examined by the clinician and generally not imaged unless a deep component is suspected.

In the oral tongue, the common cystic lesion is a lingual abscess. Similar to abscesses elsewhere in the body, a lingual abscess typically demonstrates a well-circumscribed margin, fluid attenuation on CT or fluid signal intensity on MRI, and peripheral enhancement (Figure 1).^{2,3} Risk factors include poor oral hygiene, penetrating trauma (eg, piercings), and an immunocompromised state.⁴

The sublingual space (SLS) lies superior to the mylohyoid muscle and

contains fat, the sublingual glands, the submandibular ducts, and neurovascular bundles. The submandibular space (SMS) lies inferior to the mylohyoid muscle and contains fat, the submandibular glands and lymph nodes, and the anterior bellies of the digastric muscles (Figure 2). Both spaces are shaped like a horseshoe, and they communicate at the posterior margin of the mylohyoid muscle.¹

The differential diagnoses for cystic lesions in the SLS and SMS are overlapping but not identical. Both spaces can become infected with an abscess. Epidermoid cysts are more common in the

Affiliation: University of Utah, Salt Lake City, UT. Disclosures: None

Table 1. Cystic lesions in the oral cavity and neck (excluding the teeth, bones, and CNS)

| Anatomical structure, space, or region | Differential diagnosis |
|--|---|
| Tongue | Abscess, thyroglossal duct cyst (base of tongue) |
| Sublingual space | Abscess, simple ranula, epidermoid cyst, submandibular duct obstruction |
| Submandibular space | Abscess, dermoid cyst, diving ranula, vascular malformation |
| Pharyngeal mucosal space | Abscess (palatine tonsil), Thornwaldt cyst, retention cyst |
| Parapharyngeal space | Abscess, vascular malformation |
| Masticator space | Abscess (odontogenic), vascular malformation |
| Near the mandibular angle | 2nd branchial cleft cyst, necrotic or suppurative lymph node, parotid tail lesion |
| Parotid space | Abscess, necrotic or suppurative lymph node, sialocele, 1st branchial cleft cyst, Sjögren syndrome, lymphoepithelial lesions, Warthin tumor, cystic BMT |
| Carotid space and adjacent nodes | Abscess, schwannoma, necrotic or suppurative node |
| Retropharyngeal space | Abscess, edema, necrotic or suppurative lymph node |
| Prevertebral space | Abscess (related to discitis), longus colli tendinitis |
| Visceral space | Abscess, thyroglossal duct cyst, colloid cyst in thyroid, anaplastic thyroid carcinoma, laryngocele, laryngeal retention cyst, esophageal diverticulum, tracheal diverticulum |
| Supraclavicular fossa | Necrotic left supraclavicular (Virchow) node, lymphocele |
| Trans-spatial or multifocal | Abscess, necrotic or suppurative lymph nodes, vascular malformation, thyroglossal duct cyst, branchial cleft cyst |

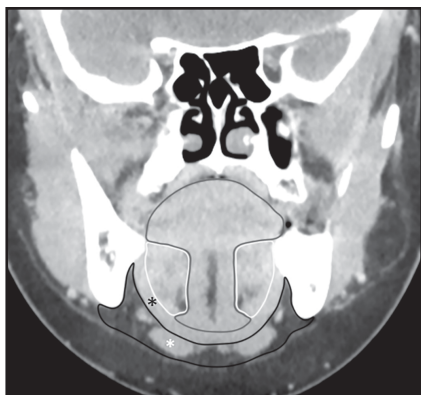


FIGURE 2. A coronal image from a CECT demonstrating the sublingual space (SLS) and submandibular space (SMS). The SLS (white outline) lies superior to the mylohyoid muscle (black asterisk) and adjacent to the intrinsic and extrinsic muscles of the tongue (gray outline). The SMS (black outline) lies inferior to the mylohyoid and contains fat, the anterior bellies of the digastric muscles (white asterisk), lymph nodes, and submandibular glands (not seen on this slice).

SLS, and dermoid cysts (with pathognomonic floating fat globules resembling a “sack of marbles”)⁵⁻⁷ are more common in the SMS.⁸ Submandibular duct obstruction occurs in the SLS, and may be caused by calculi, which can usually be

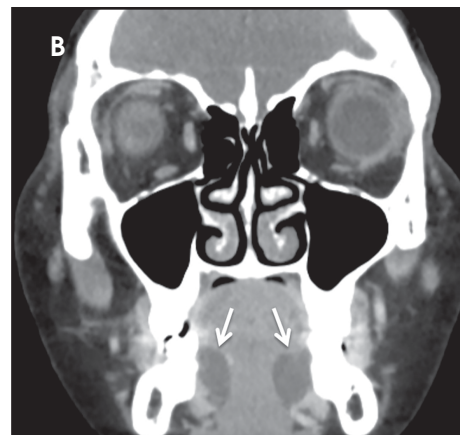
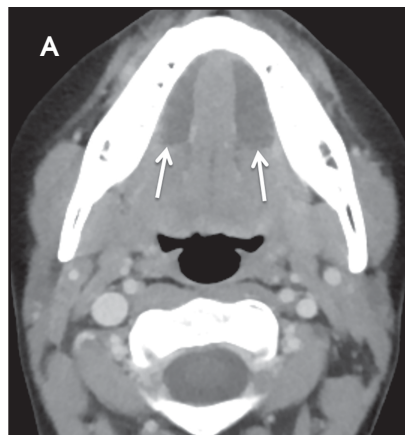


FIGURE 3. A simple ranula in a 24-year-old referred by their dentist for a floor of the mouth abnormality. Axial (A) and coronal (B) images from a CECT demonstrate a large horseshoe-shaped cystic lesion filling the bilateral sublingual spaces (white arrows). An epidermoid cyst could also have this appearance but is less common.

identified on CT,⁶ or by strictures, which are better evaluated with conventional or MR sialography.⁹

A ranula is a mucinous cyst confined to the SLS, resulting from obstruction or damage to the sublingual gland, or obstruction of the submandibular duct. Unless infected, a ranula is thin walled and unilocular, filling one or both sides of the SLS “horseshoe.” (Figure 3).^{1,8} An epidermoid cyst can mimic a ranula

but is less common. When the ranula extends into the SMS, most commonly via a defect in the mylohyoid muscle,¹⁰ it becomes a diving (or plunging) ranula, often leaving only a small residual collection (or “tail”) of fluid in the SLS that is helpful for diagnosis (Figure 4).^{8,11,12}

Vascular malformations can occur almost anywhere in the head and neck and are usually trans-spatial, but they often involve the SMS when they first present

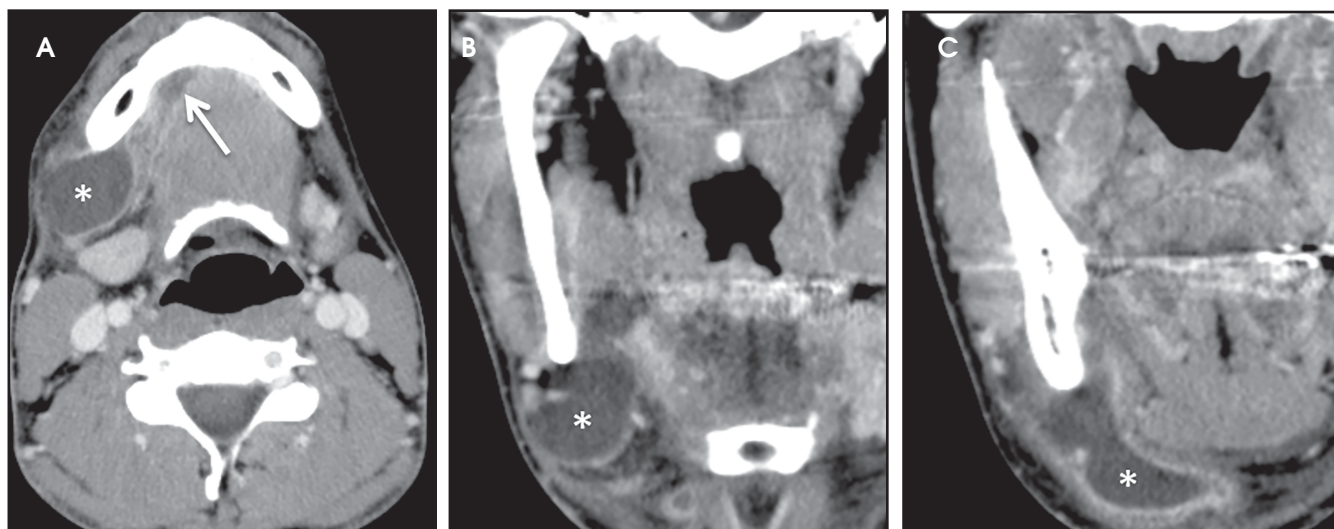


FIGURE 4. An infected diving (plunging) ranula in a 23-year-old with recurrent submandibular swelling. Axial (A) and coronal (B) images from a CECT demonstrate a rim-enhancing cystic lesion that is mostly in the right submandibular space (white asterisks), with a “tail” of residual fluid in the right sublingual space (white arrow).

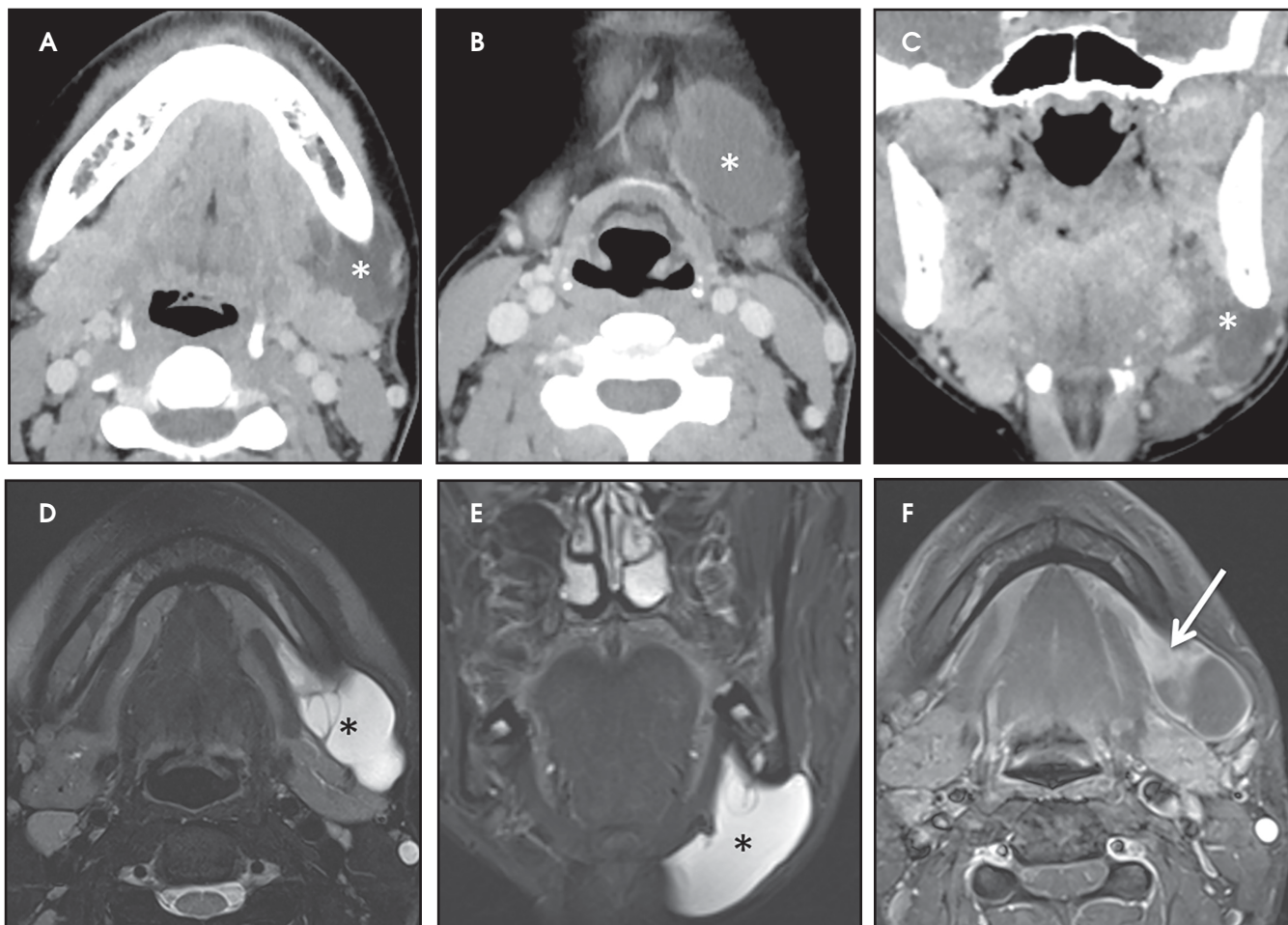


FIGURE 5. A lymphatic malformation in a 19-year-old with a slowly growing submandibular lump. Axial (A) and coronal (B) images from a CECT demonstrate a trans-spatial multilocular cystic lesion involving the left masticator, submandibular, and anterior cervical spaces (white asterisks). On further evaluation with MRI (C and D), the lesion is predominantly hyperintense with thin septations (black asterisk) on an axial T2-weighted image (C), with a small submandibular enhancing component (white arrow) on the axial T1-weighted image with contrast and fat saturation (D).

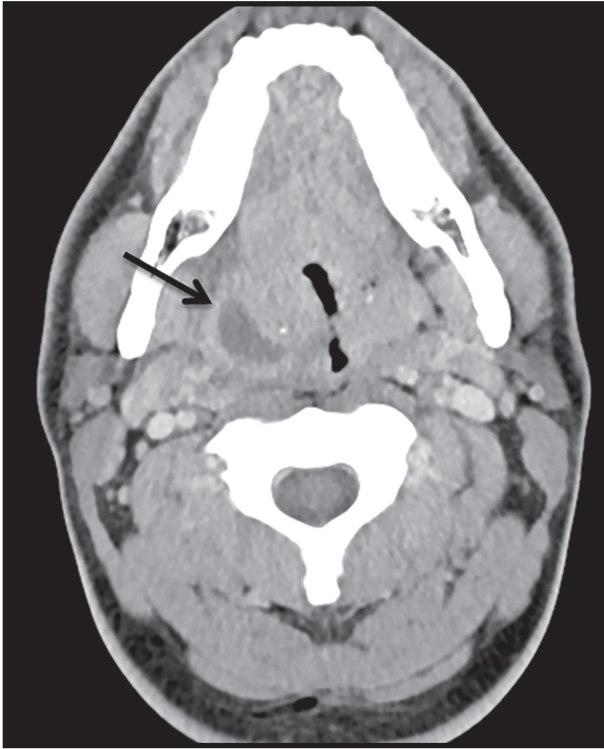


FIGURE 6. A peritonsillar abscess in a 35-year-old with fever and dysphagia. An axial image from a CECT demonstrates swelling of the right palatine tonsil with associated faintly rim-enhancing cystic lesion (black arrows) and effacement of the adjacent parapharyngeal fat.



FIGURE 7. An axial image from a CECT demonstrating the masticator space (black outline) and parotid space (white outline) on the right side. A prominent retromaxillary fat pad (white asterisk) lies just anterior to the masticator space. The parotid gland has a deep lobe (black arrow) and superficial lobe (white arrow).

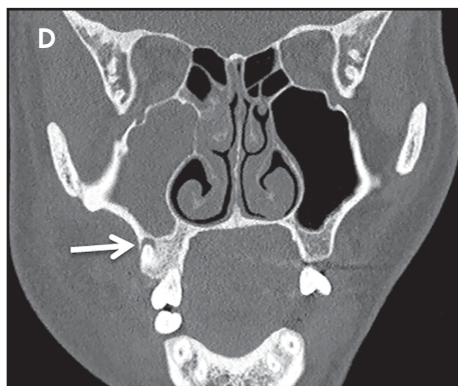
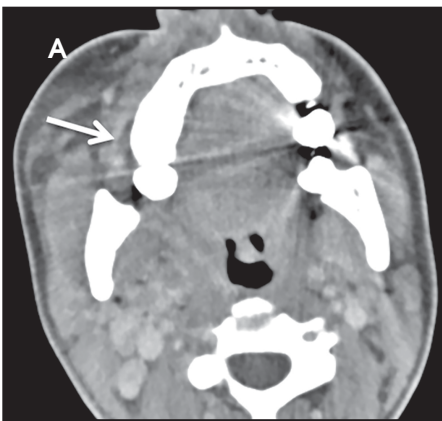
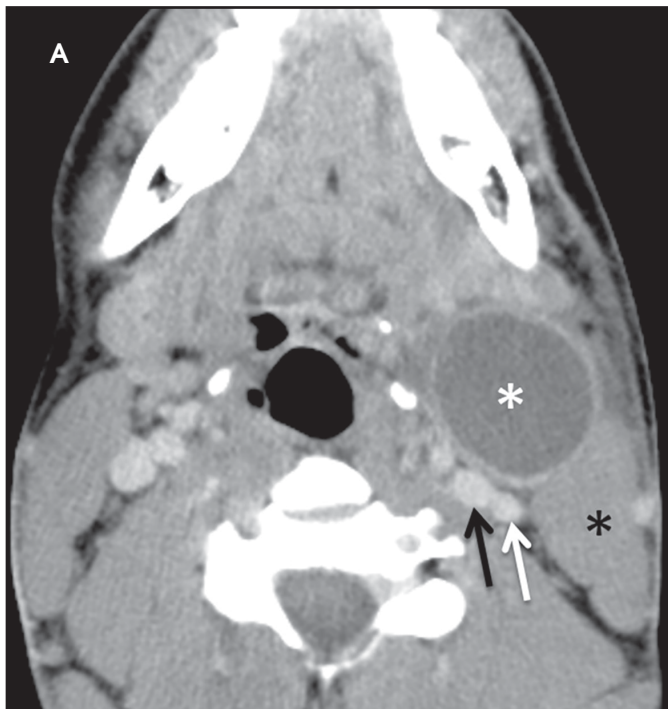


FIGURE 8. An odontogenic abscess in a 28-year-old with facial swelling. Axial (A) and coronal (B) images from a CECT demonstrate a rim-enhancing cystic lesion tracking along the right maxillary alveolar ridge and posterior wall of the maxillary sinus (white arrows). Bone window/algorithm (C) reveals a periapical lucency and adjacent focal dehiscence of the buccal cortex of the alveolar ridge (white arrow), consistent with the extension of periodontal infection to the masticator space. Opacification of the ipsilateral maxillary sinus may represent odontogenic paranasal sinus disease.



FIGURE 9. An axial image from a CECT demonstrating normal landmarks around the mandibular angle, including the submandibular gland (SMG), tail of the parotid gland (ToP), sternocleidomastoid muscle (SCM), jugulodigastric lymph node (asterisk), internal carotid artery (black arrow), and internal jugular vein (white arrow).



in adults.⁸ These lesions are classified as low-flow and high-flow lesions;¹³ the low-flow lesions — venous and lymphatic malformations — are most likely to appear cystic on imaging. When a low-flow vascular malformation is suspected, MRI is the preferred modality for evaluating the extent of the lesion. A typical MRI appearance is a trans-spatial, multilocular mass with fluid-fluid levels (Figure 5).^{14,15} In a venous malformation, portions may appear more solid or microcystic, and phleboliths may be present.

Lesions of the Pharynx

The pharynx is divided into the nasopharynx (posterior to the nasal cavity), oropharynx (posterior to the oral cavity), and hypopharynx (posterior to the larynx). The pharynx is lined by the pharyngeal mucosal space, which includes the mucosal surface, lymphatic tissue (adenoidal, lingual, and palatine tonsils), and submucosal minor salivary glands.¹ Many cystic lesions seen in the pharyngeal mucosal space are almost always incidental and asymptomatic.

A Tornwaldt cyst is a notochordal remnant located in the nasopharynx at the midline. Retention cysts of the pharyngeal mucosal space are seen in the nasopharynx (off midline) and in the oropharynx. Both cysts are well circumscribed and thin walled, with the standard imaging features of a simple cyst. The fluid may demonstrate high T1 signal if it is proteinaceous.

A more serious cystic lesion in the pharyngeal mucosal space is the peritonsillar abscess (PTA). The typical appearance on CT is a rim-enhancing fluid collection just deep to an

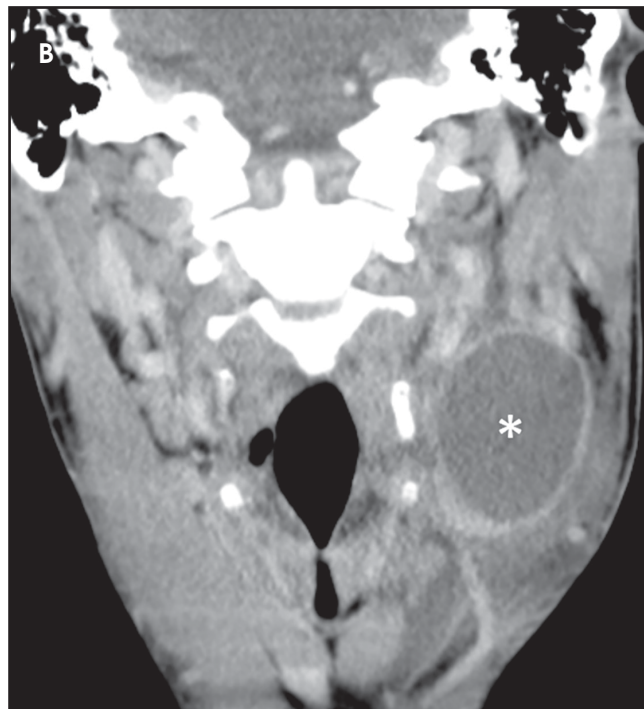


FIGURE 10. An infected second branchial cleft cyst in a 23-year-old with a rapidly enlarging neck lump. Axial (A) and coronal (B) images from a CECT demonstrate a rounded rim-enhancing cystic lesion (white asterisk) just anterior to the sternocleidomastoid muscle (black asterisk), inferior to the angle of the mandible with associated fat stranding. The cyst displaces the internal carotid artery (black arrow) and internal jugular vein (white arrow) posteriorly.

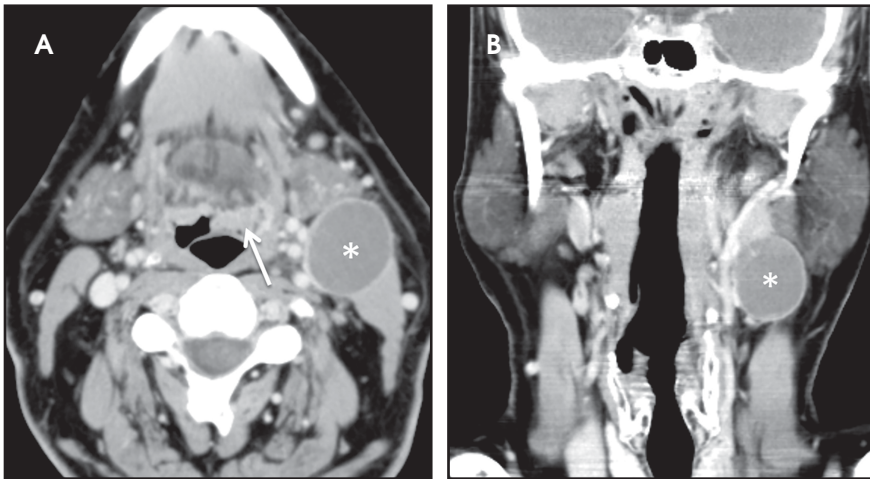


FIGURE 11. A necrotic, metastatic lymph node in a 51-year-old with a neck lump. An axial image from a CECT demonstrates a rounded rim-enhancing cystic lesion (white asterisk) just anterior to the sternocleidomastoid muscle, inferior to the angle of the mandible, mimicking a second branchial cleft cyst. Mild enlargement of the left base of tongue (white arrow) suggests the primary site of malignancy, which turned out to be squamous cell carcinoma.

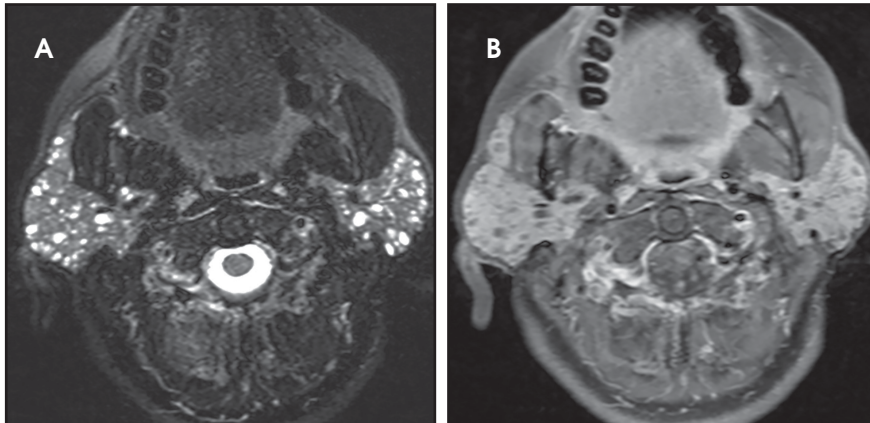


FIGURE 12. Multicystic parotid glands in a 51-year-old with Sjögren syndrome. MRI with axial T2 (A) and T1 images with contrast and fat saturation (B) demonstrates mildly enlarged parotid glands with numerous small T2-hyperintense non-enhancing cysts. Benign lymphoepithelial lesions in a patient with human immunodeficiency virus (HIV) could also have this appearance.

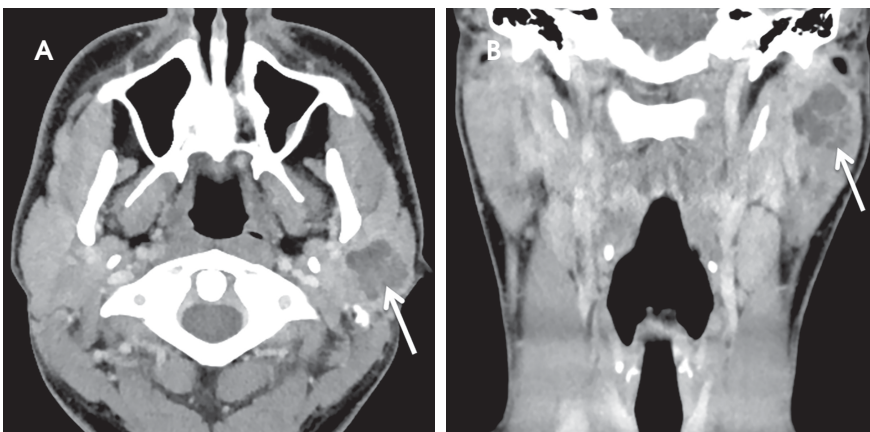


FIGURE 13. A cystic benign mixed tumor (pleomorphic adenoma) in a 24-year-old with a preauricular lump. Axial (A) and coronal (B) images from a CECT demonstrate a lobulated, multilocular, cystic lesion in the left parotid gland (white arrow). A sialocele or hematoma could have a similar appearance.

enlarged palatine tonsil (Figure 6).¹⁶ In severe cases, pus can extend into adjacent spaces, notably the parapharyngeal, masticator, and submandibular spaces. Rarely, an abscess may form within the parenchyma of the tonsil, referred to as an intratonsillar (or tonsillar) abscess (ITA). On imaging, an ITA is surrounded by tonsillar tissue, distinguishing it from a PTA. Although the distinction between a PTA and ITA is not always clear, it may be helpful for optimizing treatment.¹⁷ In any case, the radiologist should provide a precise description of the size and extent of the abscess, including the involved spaces and structures.

Lesions of the Masticator Space and Mandibular Angle

The masticator space is a large paired space containing primarily the muscles of mastication and associated nerves and blood vessels (Figure 7). By far the most common cystic lesion encountered in this space is the odontogenic abscess.¹ The source of the infection is usually a mandibular molar or recent dental procedure. Small fluid collections adjacent to the alveolar ridge may be difficult to see on CT, especially if there is streak artifact from dental amalgam, so clinical suspicion is helpful (Figure 8).

Larger abscesses can track along the mandible or maxilla into deeper, more posterior portions of the masticator space, and even extend into adjacent spaces, such as the parapharyngeal or retropharyngeal space. On the bone window/algorithm (Figure 8), CT often shows signs of associated periodontal disease (periapical lucency) and osteomyelitis (cortical dehiscence, permeative/destructive bone changes, periosteal reaction).¹⁶

The mandibular angle is a convenient landmark for an important differential diagnosis (Figure 9). In adults, a round cystic lesion at the angle of mandible, just anterior to the sternocleidomastoid, may be a second branchial cleft cyst (2nd BCC; Figure 10) or a level II necrotic lymph node (Figure 11).

The wall of the lesion may be thin (typical for BCCs but also seen in necrotic

nodes) or thick and enhancing (more typical for a necrotic node but also seen in infected BCCs). The distinction is important: a 2nd BCC is a benign congenital lesion, whereas a necrotic lymph node may be the first manifestation of oropharyngeal squamous cell carcinoma (SCCa). One clue may be the patient's age: a 2nd BCC usually presents in early adulthood (age 20-40 years), and oropharyngeal SCCa — even HPV-associated cancer — usually presents after age 40.¹⁸

Nevertheless, there is some age overlap, and any new cystic lesion near the mandibular angle in an adult should be viewed with suspicion.¹⁹ Although the primary tumor is often small and difficult to see on CT, careful inspection of the palatine tonsils and base of tongue may be fruitful. It is also essential to confirm that the cystic lesion near the mandibular angle does not, in fact, belong to the parotid tail.

Lesions of the Parotid Space

The parotid space contains the parotid gland, the branches of the facial nerve, and the external carotid artery, as well as the retromandibular vein and lymph nodes (Figure 7). The parotid gland wraps around the posterior margin of the mandibular ramus and is often described on cross-sectional imaging as having a deep lobe and a superficial lobe, separated by the retromandibular vein.

The most inferior part of the superficial lobe is referred to as the parotid tail, which can extend to or below the angle of the mandible (Figure 9). The parotid duct courses anterior to the gland superficial to the masseter muscle and terminates near the second maxillary molar.¹

A wide variety of benign and malignant cystic lesions can arise in the parotid space, most with overlapping imaging features. Often the differential diagnosis can be narrowed by the clinical history and by whether the lesions are solitary or multifocal.²⁰ A solitary rim-enhancing cystic lesion likely represents an abscess if the parotid gland is enlarged (parotitis) with adjacent fat stranding (cellulitis),

and infection is suspected clinically. A large parotid duct with an intraluminal stone suggest the abscess is a complication of sialolithiasis.

A recurrent parotid abscess raises the possibility of an infected first branchial cleft cyst (1st BCC).⁵ In the setting of prior trauma, a simple parotid cyst could represent a sialocele. Multiple small, bilateral cysts (Figure 12) represent only two possibilities: Sjögren syndrome (usually a known clinical diagnosis) or benign lymphoepithelial lesions (which can also be solid or mixed cystic and solid) in a patient with human immunodeficiency virus (HIV).²¹

A cystic mass without associated inflammatory changes in an asymptomatic smoker is suggestive of a papillary cystadenoma lymphomatosum (Warthin tumor), especially if accompanied by multiple or bilateral masses, or if the lesion is located in the parotid tail (the classic “earring lesion”²²). However, almost any parotid mass can appear cystic or necrotic, including benign mixed tumor (Figure 13), various carcinomas, and metastatic nodal disease.²³

An exact diagnosis is often impossible when evaluating a cystic parotid mass; the more important role of the radiologist is to identify any suspicious features, such as invasive margins, perineural tumor spread, and T2 hypointensity of the solid component (suggestive of highly cellular tumors).²⁴ Because parotid malignancy often mimics benign tumors, the usual management of a parotid mass is surgical.²⁵

REFERENCES

1. Koch BL, Hamilton BE, Hudgins PA, Harnsberger HR. *Diagnostic imaging. Head and neck*. Third edition. ed. Philadelphia, PA: Elsevier; 2017.
2. Fang WS, Wiggins RH, Illner A, et al. Primary lesions of the root of the tongue. *Radiographics*. 2011;31(7):1907-1922.
3. Ozturk M, Mavili E, Erdogan N, Cagli S, Guney E. Tongue abscesses: MR imaging findings. *AJNR Am J Neuroradiol*. 2006;27(6):1300-1303.
4. Srivanthapoom C, Yata K. Lingual Abscess: Predisposing Factors, Pathophysiology, Clinical Manifestations, Diagnosis, and Management. *Int J Otolaryngol*. 2018;2018:4504270.
5. Wong KT, Lee YY, King AD, Ahuja AT. Imaging of cystic or cyst-like neck masses. *Clin Radiol*. 2008;63(6):613-622.

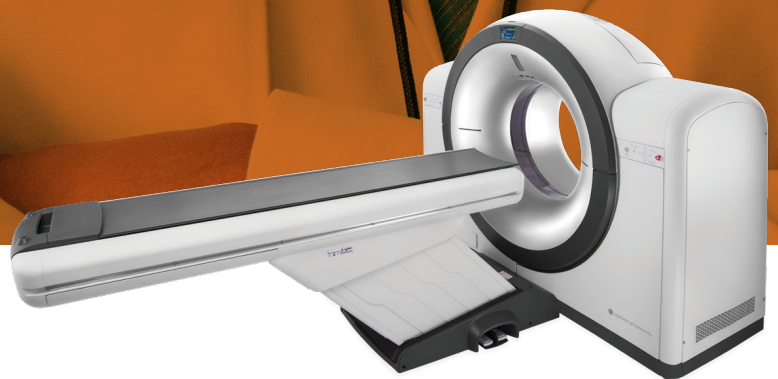
6. Patel S, Bhatt AA. Imaging of the sublingual and submandibular spaces. *Insights Imaging*. 2018;9(3):391-401.
7. Dillon JR, Avillo AJ, Nelson BL. Dermoid Cyst of the Floor of the Mouth. *Head Neck Pathol*. 2015;9(3):376-378.
8. La'porte SJ, Juttla JK, Lingam RK. Imaging the floor of the mouth and the sublingual space. *Radiographics*. 2011;31(5):1215-1230.
9. Koontz N, Kralik S, Fritsch M, Mosier K. MR sialography: a pictorial review. *Neurographics*. 2014;4(3):142-157.
10. Lee JY, Lee HY, Kim HJ, et al. Plunging Ranulas Revisited: A CT Study with Emphasis on a Defect of the Mylohyoid Muscle as the Primary Route of Lesion Propagation. *Korean J Radiol*. 2016;17(2):264-270.
11. Kurabayashi T, Ida M, Yasumoto M, et al. MRI of ranulas. *Neuroradiology*. 2000;42(12):917-922.
12. Coit WE, Harnsberger HR, Osborn AG, Smoker WR, Stevens MH, Lufkin RB. Ranulas and their mimics: CT evaluation. *Radiology*. 1987;163(1):211-216.
13. Wassef M, Blei F, Adams D, et al. Vascular Anomalies Classification: Recommendations From the International Society for the Study of Vascular Anomalies. *Pediatrics*. 2015;136(1):e203-214.
14. Meesa IR, Srinivasan A. Imaging of the oral cavity. *Radiol Clin North Am*. 2015;53(1):99-114.
15. Gaddikeri S, Vattoth S, Gaddikeri RS, et al. Congenital cystic neck masses: embryology and imaging appearances, with clinicopathological correlation. *Curr Probl Diagn Radiol*. 2014;43(2):55-67.
16. Capps EF, Kinsella JJ, Gupta M, Bhatki AM, Opatowsky MJ. Emergency imaging assessment of acute, nontraumatic conditions of the head and neck. *Radiographics*. 2010;30(5):1335-1352.
17. Ali SA, Kovatch KJ, Smith J, et al. Predictors of intratonsillar versus peritonsillar abscess: A case-control series. *Laryngoscope*. 2019;129(6):1354-1359.
18. Viens LJ, Henley SJ, Watson M, et al. Human Papillomavirus-Associated Cancers - United States, 2008-2012. *MMWR Morb Mortal Wkly Rep*. 2016;65(26):661-666.
19. Hudgins PA, Gillison M. Second branchial cleft cyst: not!! *AJNR Am J Neuroradiol*. 2009;30(9):1628-1629.
20. Kuan EC, Mallen-St Clair J, St John MA. Evaluation of Parotid Lesions. *Otolaryngol Clin North Am*. 2016;49(2):313-325.
21. Yousem DM, Kraut MA, Chalian AA. Major salivary gland imaging. *Radiology*. 2000;216(1):19-29.
22. Hamilton BE, Salzman KL, Wiggins RH, Harnsberger HR. Earring lesions of the parotid tail. *AJNR Am J Neuroradiol*. 2003;24(9):1757-1764.
23. Kessler AT, Bhatt AA. Review of the Major and Minor Salivary Glands, Part 2: Neoplasms and Tumor-like Lesions. *J Clin Imaging Sci*. 2018;8:48.
24. Christe A, Waldherr C, Hallett R, Zbaeren P, Thoeny H. MR imaging of parotid tumors: typical lesion characteristics in MR imaging improve discrimination between benign and malignant disease. *AJNR Am J Neuroradiol*. 2011;32(7):1202-1207.
25. Carlson ER, Webb DE. The diagnosis and management of parotid disease. *Oral Maxillofac Surg Clin North Am*. 2013;25(1):31-48.

Visionary Performance.

For the Radiologist,
a quick, confident
diagnosis means
everything to
your patient.

Persona CT delivers
fast, sharp images
to facilitate confident
decision-making.

Be visionary.



#VisionaryCT

Persona CT

Pediatric Cephaloceles: A Multimodality Review

Marijan Pejic, MD; Kyle Luecke, MD; Avner Meoded, MD; Jerry Tuite, MD; Javier Quintana, MD; Jennifer Neville Kucera, MD, MS

Cephaloceles are complex brain malformations that can be further characterized by the content of the herniated tissue. They can be classified by location, which is important for family counseling and surgical planning. Although imaging is vital for characterizing cephaloceles, and fetal MRI is becoming more commonly utilized for prenatal characterization, little appears in the radiology literature on this complex topic. This review illustrates the four major types of cephaloceles using a multimodality approach with prenatal and postnatal correlation. A brief overview of epidemiology and embryology is provided, and associated anomalies and distinguishing features of associated syndromes are discussed. By utilizing the location-based system and understanding the commonly associated features, the radiologist may provide a more comprehensive description of cephaloceles to better facilitate clinical management.

Cephaloceles are one of the most common forms of neural tube defects, ranking only behind myelomeningocele and anencephaly. *Cephalocele* is a generic term defined as a protrusion of the meninges with or without brain tissue through a defect in the skull.¹⁻² A *meningocele* is a protrusion of only meninges and cerebrospinal fluid (CSF). An *encephalocele* is a protrusion of meninges, CSF, and brain tissue. An *encephalocystocele* contains meninges, CSF, brain tissue and ventricle. The term *atretic cephalocele* (also called meningocele manqué) describes a small, midline subscalp nodule that contains meninges, fibrous tissue, and dysplastic brain tissue.³ The term *fronto-ethmoidal* denotes the involvement of the upper anterior cranium and is synonymous with the less commonly used *sincipital* (Table 1).

The incidence of cephaloceles is 0.8-4 of 10,000 live births.⁴ Cephaloceles account for 10-20% of all craniospinal

dysraphisms.⁴ Geographical variation exists, with occipital subtypes representing 66-89% of all cephaloceles in the Caucasian populations of North America and Western Europe.⁵⁻⁷ Anterior subtypes are more common in Southeast Asia.⁶ Most cases of isolated cephaloceles (not associated with other congenital anomalies) are sporadic, with genetic and non-genetic factors involved in the pathogenesis.⁸ Cephaloceles may be associated with myriad genetic syndromes, most commonly Meckel-Gruber, as well as the Chiari III malformation, holoprosencephaly, and Dandy-Walker malformation.^{2,9-10} A cephalocele detected prenatally warrants a detailed diagnostic assessment and characterization for an underlying syndrome.¹¹

Embryology

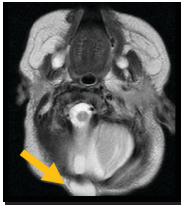
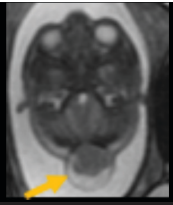
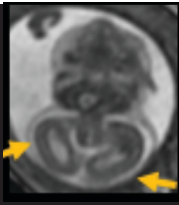
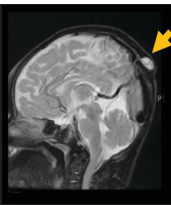
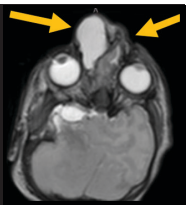
The central nervous system begins forming in the third week of embryonic life as thickened ectoderm called the neural plate. Elevation of the lateral edges of the neural plate forms the neural folds, which fuse to form the neural tube. Fusion begins in the cervical region, proceeding in both the rostral and caudal directions until closure between days 25-27 postconception. The mechanism resulting in cephaloceles is uncertain but presumably involves defective closure of the anterior neural tube. Anterior

Affiliations: University of South Florida Morsani College of Medicine, Tampa, FL (Drs Pejic, Luecke, Meoded, Quintana, Kucera). Johns Hopkins All Children's Hospital, St. Petersburg, FL (Drs Meoded, Tuite, Quintana, Kucera). The authors have no conflicts of interests to declare.

Prior publication/presentation:

Luecke K, Meoded A, Jallo, G, Gonzalez-Gomez I, Tuite J, Carey C, Quintana J, Kucera JN. Pediatric cephaloceles: A pictorial review with radiologic, surgical and pathologic correlation. Paper presented at: Radiological Society of North America 2017 Annual Meeting; November 26 to December 1; Chicago, IL. PD126-ED-WEB6.

Table 1. Definitions of Terms Characterizing Herniated Tissue in Cephaloceles with Imaging Correlates

| Term | Meningocele | Encephalocele | Encephalocystocele | Atretic cephalocele | Fronto-ethmoidal cephalocele |
|---------|---|---|---|--|---|
| Content | Only meninges and CSF | Meninges, CSF, and brain tissue | Meninges, CSF, brain tissue and ventricle | Small midline sub-scalp nodule containing meninges, fibrous tissue, and dysplastic | Involving the upper anterior cranium; also referred to as sincipital cephalocele |
| Example |  |  |  |  |  |

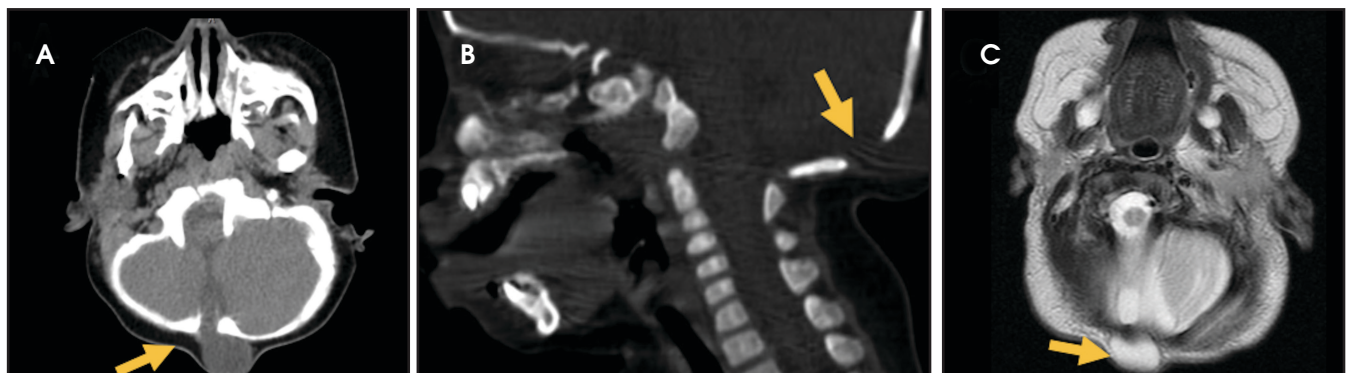


FIGURE 1. Occipital meningocele. Axial (A) and sagittal (B) CT images demonstrate an occipital bone defect (arrow) with protrusion of tissue. Axial (C) T2 images depict a small, CSF-intensity sac (arrows) representing the meningocele protruding through the defect. No brain tissue is identified in the sac.

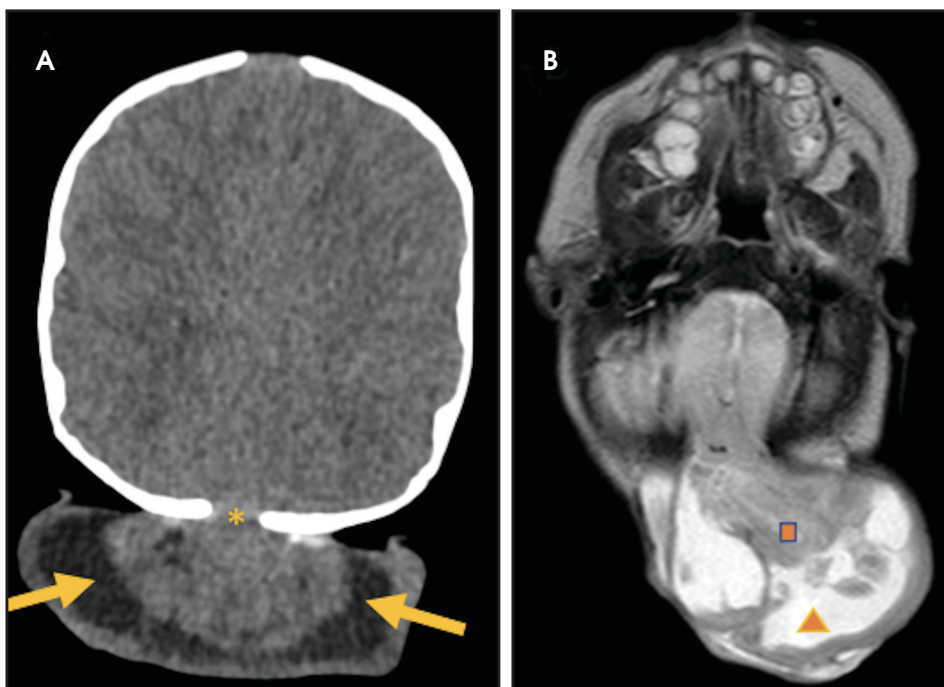


FIGURE 2. Occipital encephalocele. Axial CT image through the supratentorial brain parenchyma (A) shows a fluid- and soft-tissue attenuation sac (arrows) herniating through a midline occipital skull defect (*), consistent with an occipital encephalocele. Axial T2 MRI through the cerebellum (B) demonstrates that the hernia sac contains CSF (triangle) and dysplastic neural tissue (square). Irregular margins of the neural tissue and lack of definite connection to the ventricles argues against encephalocystocele in this case.

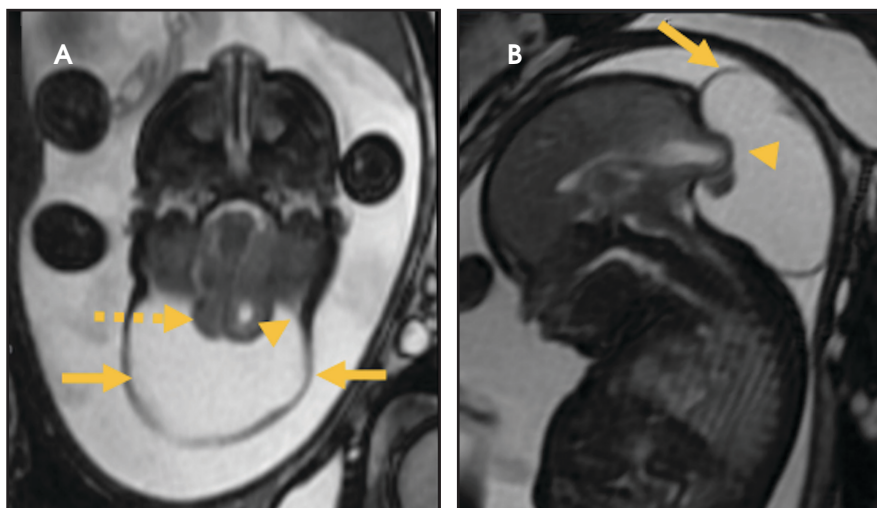


FIGURE 3. Occipital encephalocystocele. Axial (A) and sagittal (B) fetal MRI images demonstrate an occipital cranial defect with a large hernia sac (solid arrows) consisting of meninges and supratentorial neural tissue (dashed arrow) containing a portion of the occipital horns of the lateral ventricles (arrowhead) consistent with an encephalocystocele.

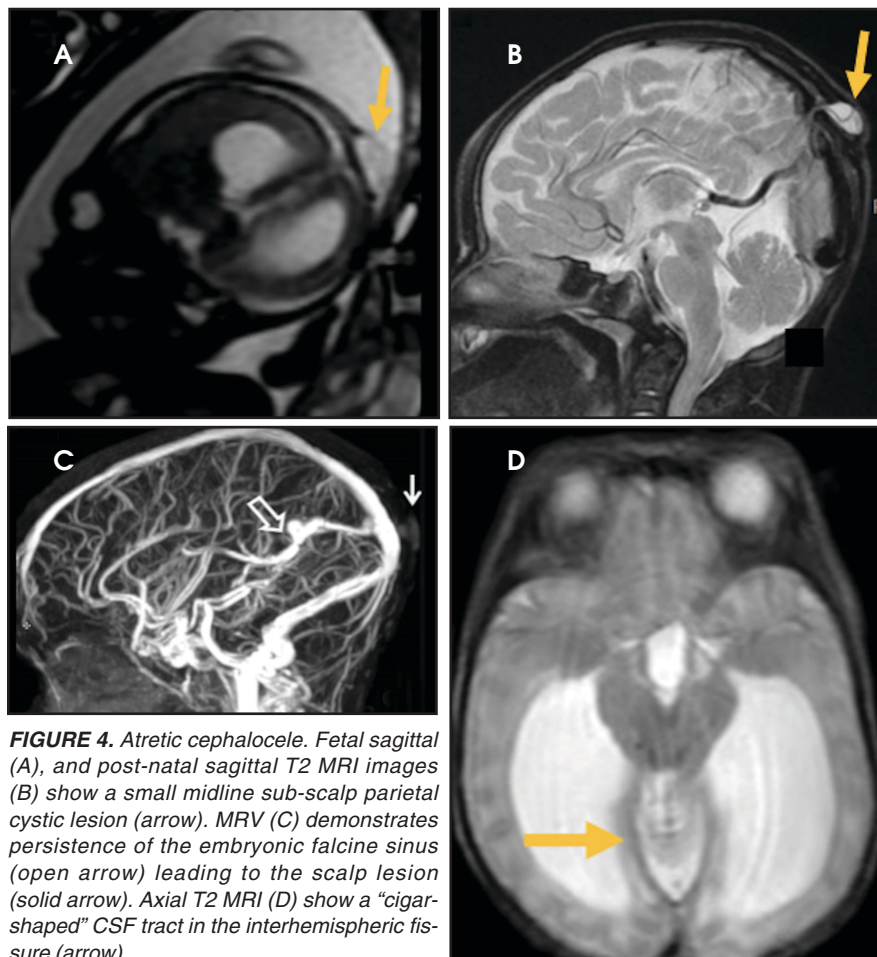


FIGURE 4. Atretic cephalocele. Fetal sagittal (A), and post-natal sagittal T2 MRI images (B) show a small midline sub-scalp parietal cystic lesion (arrow). MRV (C) demonstrates persistence of the embryonic falcine sinus (open arrow) leading to the scalp lesion (solid arrow). Axial T2 MRI (D) show a "cigar-shaped" CSF tract in the interhemispheric fissure (arrow).

cephaloceles (fronto-ethmoidal and basal) are thought to arise from defective development of the prosencephalic neural crest tissue.¹² In contrast, oc-

cipital cephalocele may relate to defective segmentation of the posterior cranial bones.¹³ Some authors believe the etiology of congenital cephalocele

centers on a postneurulation event in which brain tissue herniates through a defect in the mesenchyme that eventually becomes the cranium and dura.¹⁴

Diagnosis and Classification

Most cephalocele can be detected prenatally by ultrasound. Alpha fetoprotein levels may be unreliable given that both maternal serum and amniotic fluid alpha fetoprotein levels may be normal if the cephalocele is covered by skin.¹⁵ On ultrasound these lesions may appear as cystic (meningocele) and/or solid (encephalocele) structures protruding through a calvarial defect. Further evaluation with computed tomography (CT) and magnetic resonance imaging (MRI, including fetal MRI) is useful to determine the extent of herniation as well as the presence of associated anomalies. CT is useful for identifying osseous defects while MRI is superior for defining the portions of herniated tissue, detecting abnormal signal in dysplastic brain tissue, and evaluating the cartilaginous nasofrontal region. An MR or CT angiogram or venogram may provide more detailed evaluation of vascular anatomy and its relation to the cephalocele.

Several classification systems exist. The system proposed by Suwanwela and Suwanwela provides a comprehensive, location-based classification that characterizes cephalocele as 1) occipital, 2) cranial vault, 3) fronto-ethmoidal, and 4) basal. This system has also been found useful for selecting the operative approach.⁶ More extensive cephalocele, however, may encompass more than one type. Clinical features and prognoses of cephalocele depend on location, severity, and presence of dysplastic brain tissue and associated abnormalities.¹⁶⁻¹⁷

Occipital Cephalocele

Occipital cephalocele demonstrate defects involving the occipital bones, with the cephalocele extending posteriorly (Figures 1-3). The herniated tissue may include the supra- and/or infratentorial brain, tentorium, and dural

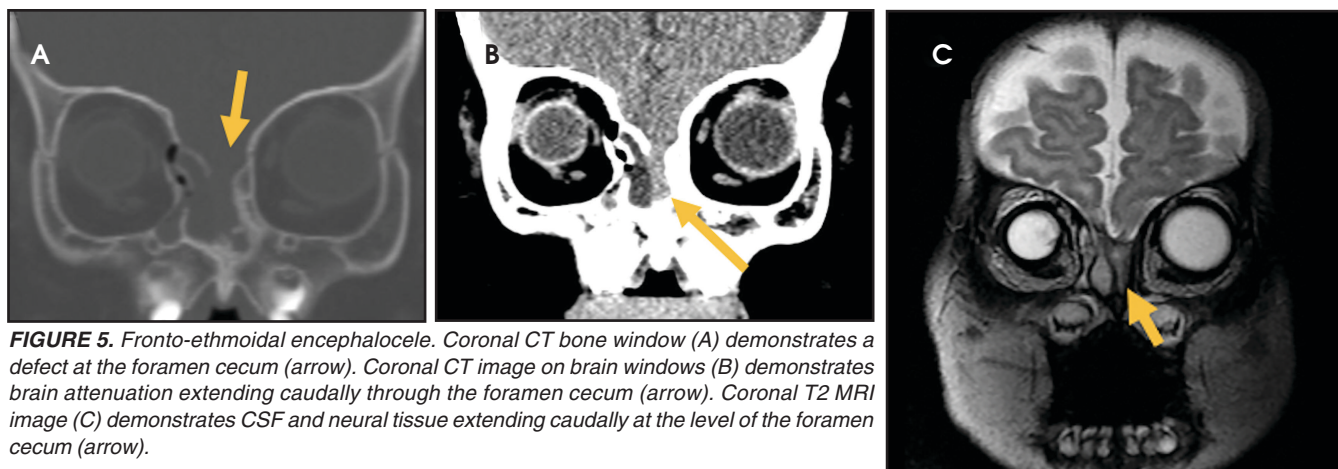


FIGURE 5. Fronto-ethmoidal encephalocele. Coronal CT bone window (A) demonstrates a defect at the foramen cecum (arrow). Coronal CT image on brain windows (B) demonstrates brain attenuation extending caudally through the foramen cecum (arrow). Coronal T2 MRI image (C) demonstrates CSF and neural tissue extending caudally at the level of the foramen cecum (arrow).

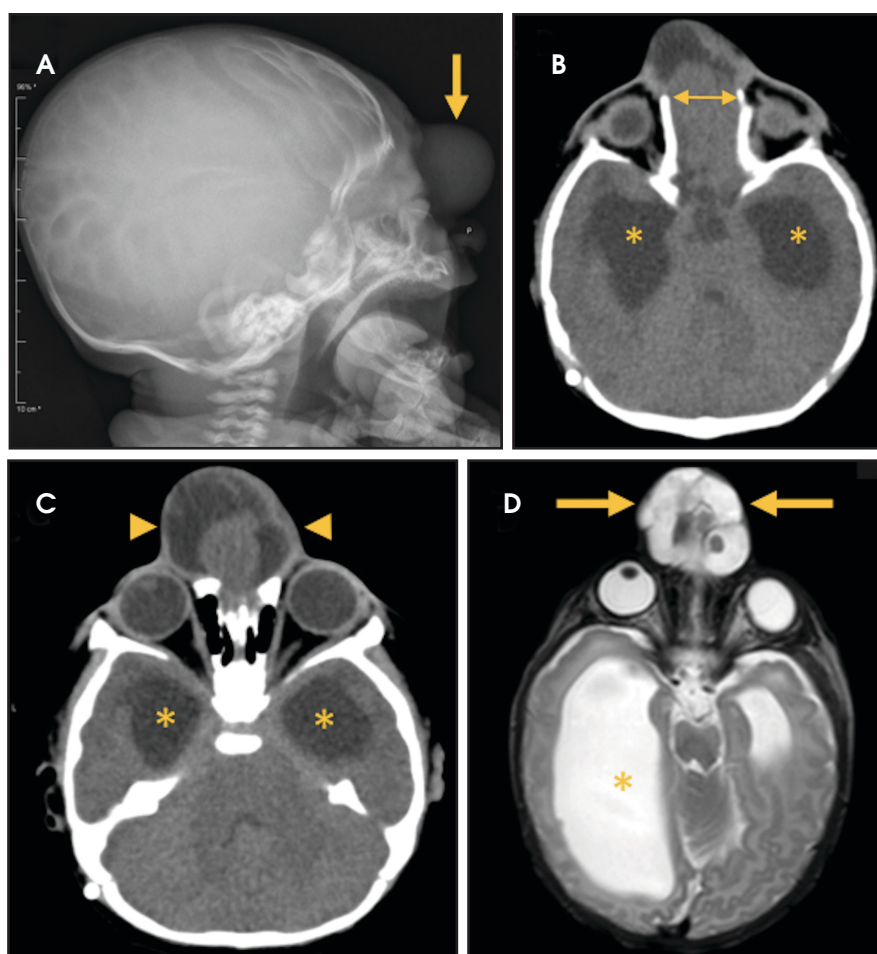


FIGURE 6. Fronto-nasal encephalocele with hydrocephalus. Lateral skull radiograph (A) shows a frontal soft tissue mass (arrows). (B, C) Axial CT images through the glabella demonstrate a frontal bone defect (arrows) and encephalocele (arrowhead). Hydrocephalus is also noted (*). Axial T2 MRI (D) show a midline encephalocele (arrows) at the level of the lower frontal bone. Marked hydrocephalus is also seen (*).

is observed in the majority of cases. Prognostic factors include size of herniation, degree of hydrocephalus, and presence of associated anomalies.¹⁶⁻¹⁷ Large occipital encephaloceles may be associated with developmental delay, blindness, poor feeding, cranial nerve deficits, and seizures.¹⁸

Cranial Vault Cephaloceles

Cranial vault cephaloceles occur along the superior cranium within the fontanelles or defects in the parietal, frontal, or temporal bones. They present as a midline posterior scalp mass. The patient often is otherwise clinically normal unless associated anomalies are present.¹⁹ Atretic cephaloceles, the most common form, are small midline subcutaneous scalp masses consisting of dura and dysplastic meninges connected to the intracranial meninges by a fibrous stalk. They are usually located in the parietal lobe; MRI typically demonstrates a fibrous tract and vertical falxine vein, which extend to a subcutaneous scalp mass (Figure 4). Atretic cephalocele may arise through a bone defect or fenestration, or the bone may be closed with completely separated intra- and extracranial contents.²⁰

The embryonic falxine sinus is often positioned vertically, with a cigar-shaped CSF tract in the interhemispheric fissure.^{19,21} Cranial vault cephaloceles are considered abortive or involuted true cephaloceles²⁰; they have a more favorable prognosis than other true cephaloceles.²²

venous sinuses. These cephaloceles are the most common type overall and account for a higher proportion of cephaloceles in Caucasian populations of

Europe and North America.⁵⁻⁷ Occipital cephaloceles are typically apparent on physical exam at birth, and the size of the herniation varies. Ventriculomegaly

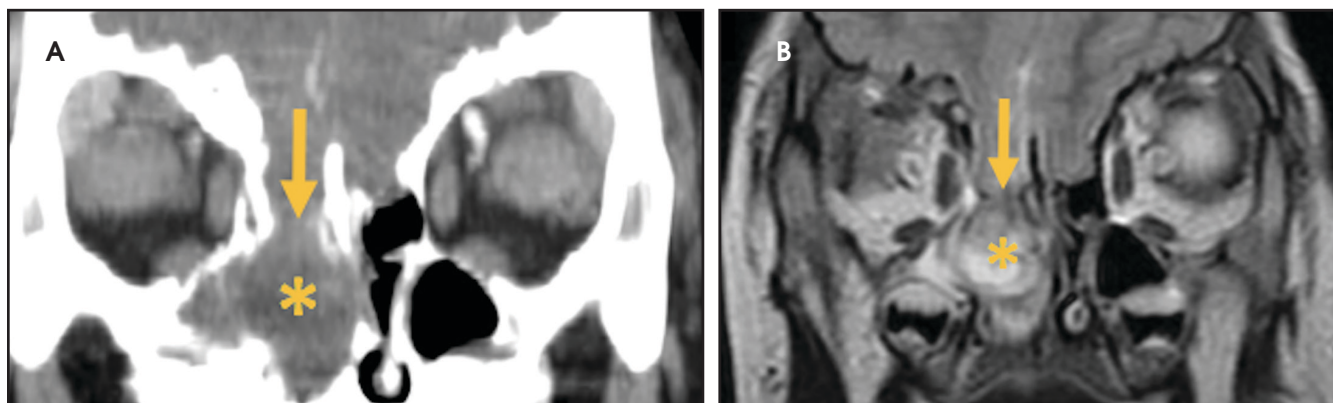


FIGURE 7. Basal encephalocele (A) and T2 MRI images (B). A defect of the cribriform plate (arrow) is seen. There is protrusion of CSF and brain tissue into the nasal cavity and right maxillary sinus (*).

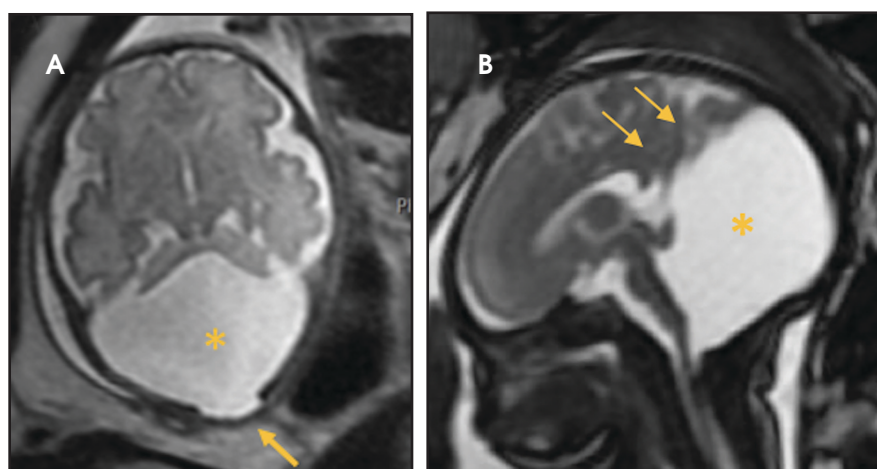


FIGURE 8. Occipital meningocele with Dandy-Walker malformation. Fetal axial T2 image (A) shows a small midline occipital meningocele (arrow) and cystic replacement of an enlarged posterior fossa (*). A fetal sagittal T2 image (B) demonstrates the large posterior fossa cyst (*) and an elevated tentorium (arrows).

Fronto-ethmoidal Cephaloceles

Fronto-ethmoidal cephaloceles (FECs) range from occult lesions to marked craniofacial abnormalities, including microcephaly, telecanthus, hypertelorism, orbital dystopia, or micro/anophthalmos. There is an increased incidence in Southeast Asian populations.⁶ Sagittal and coronal images may be the most helpful in demonstrating contiguity between intracranial contents and the mass.²³ Prior to surgical repair, CT scanning helps to characterize the bone defect. FECs can be classified according to the osseous defect's location.

Naso-ethmoidal cephaloceles are characterized by herniation into the superomedial nasal cavity, with the defect

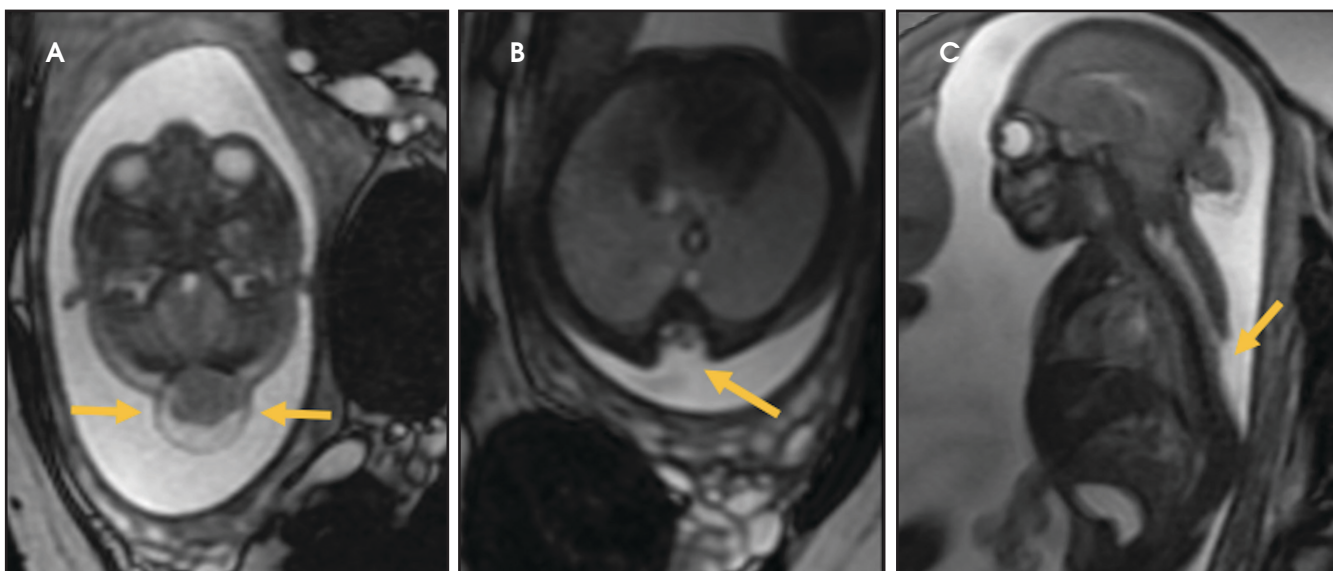


FIGURE 9. Chiari III with thoracic myeloschisis. Axial T2 (A) demonstrates an occipital encephalocele (arrows) with cerebellar crowding and tonsillar herniation. Axial T2 (B) demonstrates open the thoracic dysraphism (arrow). Sagittal T2 (C) demonstrates the open thoracic dysraphism beginning in mid-thoracic spine extending caudally (arrow).

Table 2. Conditions Associated with Cephaloceles

| Site | Condition | Distinguishing Features |
|-----------------------------------|--|---|
| Frontal | Amniotic Band Syndrome | Ring constrictions and amputations of digits and/or limbs, irregular/asymmetric cephalocele, microcephaly, microphthalmia, distal syndactyly, orofacial clefts |
| | Frontonasal Dysplasia/ Median Cleft Face Syndrome | Ocular hypertelorism, widow's peak, anterior cranium bifidum occultum, notching of nostrils, widely set nostrils with lack of elevation of the nasal tip |
| Occipital or high cervical | Chiari III Malformation | Syringomyelia, hydrocephalus, tethered cord, abnormal neuroectodermal tissues |
| Occipital | Cryptophthalmos/Fraser Syndrome | Ear anomalies, notching of nasal wings, extension of forehead skin to cover one or both eyes, unusual hairline, soft-tissue syndactyly of hands and/or feet, genital anomalies including cryptorchidism, micropenis, and clitoromegaly |
| | Dandy Walker Formation | Triad of cystic dilation of the fourth ventricle, complete or partial agenesis of the cerebellum and an enlarged posterior fossa with torcular-lamboid inversion |
| | Dyssegmental Dwarfism | Lethal dwarfism, short broad pelvis with widely flared iliac wings, short broad tubular bones with metaphyseal widening, accelerated carpal bone maturation, bowing of legs, thighs and forearms, vertebral anomalies, small thorax, cleft palate, micrognathia |
| | Fetal Warfarin Syndrome | Nasal hypoplasia, limb shortening, bone stippling, low birth weight, seizures, hydrocephaly, optic atrophy, intellectual disability |
| | Knobloch Syndrome | Myopia, vitreoretinal degeneration, retinal detachment, meningocele, normal intelligence |
| | Meckel-Gruber Syndrome | Classically triad of renal cystic dysplasia, cephalocele or holoprosencephaly, and postaxial polydactyly; microphthalmia, retinal dysplasia, cardiac anomalies, orofacial clefting, ambiguous external genitalia |
| | Pseudo-Meckel Syndrome | Arhinencephaly, agenesis of corpus callosum, Arnold-Chiari defect, cleft palate, congenital heart defects, accessory spleen, clubfoot, hallucal hammertoes; retinal dysplasia is not a feature |
| | von Voss-Cherstvoy Syndrome | Corpus callosum dysplasia, hypoplastic olives and pyramids of medulla oblongata, phocomelia, urogenital anomalies, thrombocytopenia |
| | Walker-Warburg Syndrome | Muscle weakness and atrophy early in life, developmental delay, hydrocephalus, microphthalmia, buphthalmos, cataracts |

centered at the foramen cecum (Figure 5).⁶ They protrude through the foramen cecum into the prenasal space. They are positioned inferior to the nasal bones.

Naso-frontal cephaloceles have a midline frontal defect, often with mass at the glabella (root of the nose) (Figure 6).⁶ They protrude through an unobliterated fonticulus frontalis.

Naso-orbital cephaloceles are characterized by an inferomedial orbital defect. They protrude into the inferomedial orbit through a defect in the

maxillary bones at the lacrimal/frontal process. They can induce proptosis and globe displacement.

FECs are more commonly associated with craniofacial clefts.⁶ FECs also generally have a better prognosis than occipital cephaloceles because the protruding mass in the FEC tends to contain scarred, nonfunctional neural tissue.¹⁸

Basal Cephaloceles

Basal cephaloceles occur when there is a defect in skull base (Figure 7). They

are rare and may present even later in the first decade of life with recurrent meningitis.²⁴ Basal cephaloceles may be occult or present with midface anomalies such as cleft lip/palate, hypertelorism, or a nasal epipharyngeal mass. Immediate surgical repair is indicated because of the elevated risk of meningitis.¹⁸

Associated Anomalies and Neurologic Manifestations

Many cases of cephalocele are associated with additional congenital

anomalies, which are important to identify for prognostic purposes (Table 2). In one of the largest studies on cephaloceles, the following associated anomalies and neurologic manifestations were identified in order of decreasing frequency: hydrocephalus, seizure disorder, corpus callosum abnormalities, cerebral dysgenesis, and migrational disorders, including gray matter heterotopia, microcephaly, and myelomeningocele.⁴

In this study, 52% of patients experienced at least mild developmental delay, with hydrocephalus and other associated intracranial abnormalities identified as predictors of developmental delay.⁴ Lesion location notably was not found to be a significant predictor of outcome. Myriad genetic syndromes and conditions are associated with cephaloceles, including Meckel-Gruber syndrome, the middle interhemispheric variant of holoprosencephaly, Dandy-Walker malformation (Figure 8) and Chiari III malformation (Figure 9).^{2,9-10} Meckel Gruber is the most commonly associated syndrome.²⁵ With the presence of associated malformations affecting cognitive outcome, imaging is a critical component of the workup of patients with cephaloceles and often serves as the primary basis for prenatal counseling.⁴

Conclusion

Cephaloceles are complex cranial malformations that can be classified by

location, each with differing clinical presentation and associated anomalies. Prenatal and postnatal imaging is important to delineate the relevant anatomy. By describing cephaloceles via a location-based classification system, the radiologist may facilitate more accurate presurgical planning and prenatal counseling.

REFERENCES

1. Diebler C, Dulac O. Cephaloceles: Clinical and neuroradiological appearance. *Neuroradiology*. 1983; 25:199-216.
2. Naidich TP, Altman NR, Braffman BH, et al. Cephaloceles and related malformations. *AJNR Am J Neuroradiol*. 1992;13: 655-690.
3. Yokota A, Kajiwara H, Kohchi M. Parietal cephalocele: Clinical importance of its atretic form and associated malformations. *J Neurosurg*. 1988; 69:545-551.
4. Lo BW, Kulkarni AV, Rutka JT, et al. Clinical predictors of developmental outcome in patients with cephaloceles. *J Neurosurg Pediatr*. 2008; 2(4):254-257.
5. Simpson DA, David DJ, White J. Cephaloceles: Treatment, outcome and antenatal diagnosis. *Neurosurgery*. 1984; 15:14-21.
6. Suwanwela C, Suwanwela N. A morphological classification of sincipital encephalomeningoceles. *J Neurosurg*. 1972;36(2):201-211.
7. Chapman PH, Swearingen B, Caviness VS. Subtorcular occipital encephaloceles: Anatomical considerations relevant to operative management. *J Neurosurg*. 1989; 71:375-381.
8. Copp AJ, Stanier P, Greene ND. Neural tube defects: Recent advances, unsolved questions, and controversies. *Lancet Neurol*. 2013; 12(8):799-810.
9. Cohen MM. Mutations affecting craniofacial cartilage. *Biomedical aspects*. New York: Academic Press 1983(53):191-228.
10. Cohen MM, Lemire RM. Syndromes with cephaloceles. *Teratology*. 1982; 25:161-172.
11. Thompson DN. Postnatal management and outcome for neural tube defects including spina bifida and encephaloceles. *Prenat Diagn*. 2009; 29:412-419.
12. Hoving EW, Vermeij-Keers C. Frontoethmoidal encephaloceles, a study of their pathogenesis. *Pediatr Neurosurg*. 1997; 27(5): 246-256.
13. Tavella S, Bobola N. Expressing Hoxa2 across the entire endochondral skeleton alters the shape of the skeletal template in a spatially restricted fashion. *Differentiation*. 2010; 79(3):194-202.
14. Gluckman TJ, George TM, McLone DG. Post-neurulation rapid brain growth represents a critical time for encephalocele formation: a chick model. *Pediatr Neurosurg*. 1996; 25:130-136.
15. Sabbagha RE, Tamura RK, Dal Compo S, et al. *Am J Obstet Gynecol*. 1980; 138(5): 511-517.
16. Raja RA, Qureshi AA, Memon AR, et al. Pattern of encephaloceles: a case series. *J Ayub Med Coll Abbottabad*. 2008; 20:125-128.
17. Kiyamaz N, Yilmaz N, Demir I, et al. Prognostic factors in patients with occipital encephalocele. *Pediatr Neurosurg*. 2010; 46:6-11.
18. Chern JJ, Bollo RJ, Governale LS, et al. *Operative Neurosurg*. 2019; 17(1) Supplement: S182-S208.
19. Patterson RJ, Egelhoff JC, Crone KR, et al. Atretic parietal cephaloceles revisited: An enlarging clinical and imaging spectrum? *AJNR Am J Neuroradiol*. 1998;19(4):791-795.
20. Favoreel N, Devooght M, Devlies F, et al. Atretic cephalocele. *J Belgian Soc. Radiol*. 2015; 98(3):119-120.
21. Murakami N, Morioka T, Kawamura N, et al. Venous anomaly analogous to vertical embryonic positioning of the straight sinus associated with atretic cephalocele at the suboccipital region. *Childs Nerv Syst*. 2017;33(1):179-182.
22. Martinez-Lage JF, Sola J, Casas C. Atretic cephalocele: The top of the iceberg. *J Neurosurg*. 1992;77:230-235.
23. Hedlung G. Congenital frontonasal masses: Developmental anatomy, malformations, and MR imaging. *Pediatr Radiol*. 2006;36(7):647-662.
24. Mealey J Jr, Dzenitis AJ, Hockey AA. The prognosis of encephaloceles. *J Neurosurg*. 1970;32:209-218.
25. Volpe JJ. Intracranial hemorrhage: Neural tube formation and prosencephalic development. *Neurology of the Newborn*. 4th Ed. Philadelphia, PA: WB Saunders; 2001.

Improving Body Imaging Throughput in the Midst of COVID-19

John V Thomas, MD; Kristin K Porter, MD, PhD; Stefanie A Woodard, DO; Aparna Singhal, MD; Mason B Frazier, MD; Desiree E Morgan, MD; Cheri L Canon, MD, FACR, FAAWR

At the onset of the COVID-19 pandemic in the United States, many elective procedures and non-urgent ambulatory visits were re-scheduled to comply with stay-at-home orders and to ensure patient and staff safety. This has created a significant backlog of patients who need service at many clinics and outpatient centers in the coming months. Hospital ambulatory clinics and radiology waiting rooms are typically crowded and not set up to facilitate physical distancing; limiting schedules severely hampers patient throughput and adversely affects ability to provide timely care and address these backlogs. In addition, many patients currently avoid hospitals for fear of contracting the virus. With COVID-19 cases not yet significantly abating in many areas, the question arises whether radiologists can safely and efficiently care for patients until a vaccine for COVID-19 is widely available.

Here we will discuss our experience using fast MRI body imaging protocols in combination with strategic use of free-standing facilities to safely reduce our patient backlog and manage our MR imaging load.

Fast MR Imaging: Rationale for Use

In the setting of the COVID-19 pandemic and significant patient backlogs, shortening MRI protocols to relieve backlogs and minimize potential

Affiliations: University of Alabama at Birmingham, Birmingham, AL. Acknowledgements: The authors would like to acknowledge the essential work of Kecia L. Turner, Verlon Salley, Jeff McGough, Kayla Freeman, and Randy Wells

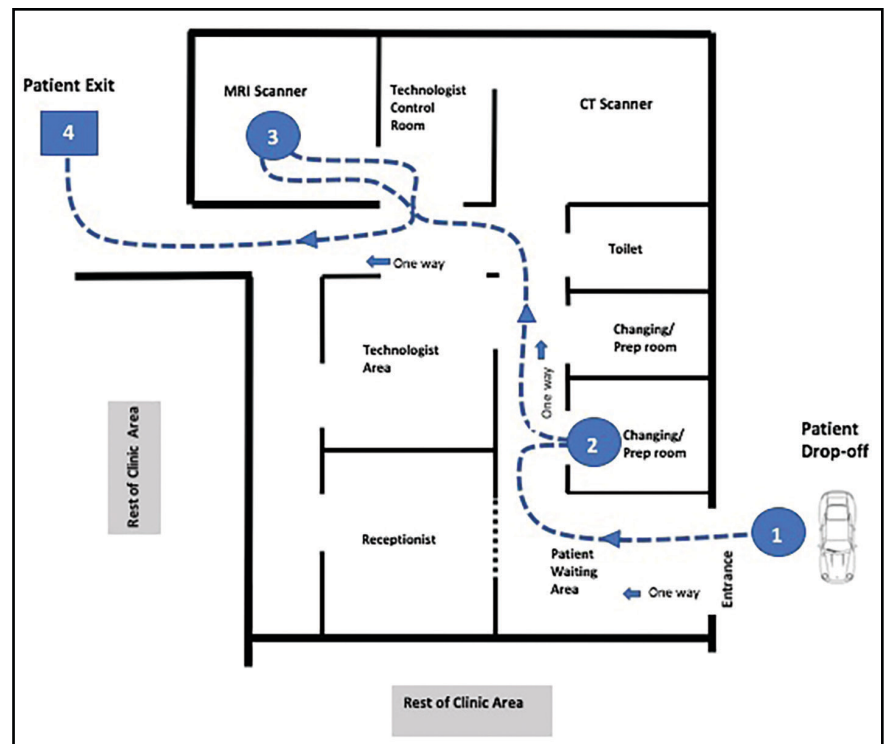


FIGURE 1. Schematic diagram of a radiology out-patient imaging facility (not to scale). (1) Patient drop-off. Patients can wait in car until called. All financial transactions made contactless and curbside, when possible (arrow head). Patient enters facility and directly to 'prep area' (2). Once ready, patient proceeds directly to scanner (3). Once scanned, patient changes in a designated room or scanner room and exits via an alternate exit (4), thus limiting contact with others.

COVID-19 exposure to patients and staff seems logical, particularly with respect to vulnerable populations. However, faster patient turnaround risks undesirable overcrowding of MRI and hospital outpatient waiting areas.

Many hospital systems have affiliated free-standing outpatient imaging centers in proximity to residential areas, thus providing easy access for patients. Parking tends to be more common at ground level and readily accessible to the facility entrance. Patients may also feel more comfortable at smaller facilities, which

can provide a friendlier, "non-hospital" environment, decrease the stress on large hospital outpatient waiting areas, and allay any fears patients might have with regard to satisfactory physical distancing measures. Free-standing imaging centers often have a smaller footprint, allowing for nimble operational changes and facilitating physical distancing. It is also faster to test fast scanning protocols in a small number of scanners at free-standing imaging centers instead of attempting to implement them across an entire hospital system. Several of our

suggested solutions allow for safer, more expeditious patient throughput, which is key for the effective application of fast MRI protocols to help reduce patient backlog.

Fast MRI Effectiveness

The growing trend toward more patient-centered health care has challenged radiologists to assess MRI protocols more critically, with an emphasis on efficient and fast protocols.¹ Fast (also called rapid, focused, or abbreviated) MRI protocols offer an alternative to standard protocols for answering specific clinical questions, potentially improving workflows, addressing imaging demand, and reducing costs, all without sacrificing patient safety.

Several retrospective studies have shown the effectiveness of fast MRI for HCC screening.²⁻⁷ Nougaret, et al, for example, reported that contrast-enhanced scans did not provide additional information over unenhanced scans of pancreatic cystic lesions.⁸ Short protocols have also been proposed for other procedures, such as screening the adrenal glands, kidneys, and female pelvis.¹ Seo, et al proposed using MR enterography to evaluate small-bowel inflammation in Crohn disease with non-enhanced diffusion weighted imaging (DWI).⁹ Kang, et al evaluated 10 studies and found no significant differences in specificity or sensitivity between bi-parametric and multi-parametric MRI scans for prostate cancer evaluation.¹⁰ Short, specific protocols have been proposed for breast MRI screening and assessment of breast lesion size.¹¹⁻¹³ Ross, et al showed high sensitivity and specificity for hip and pelvic fractures using an abbreviated MRI protocol.¹⁴ Khurana, et al showed similar results with a short MRI protocol to evaluate hip pain in the emergency room setting.¹⁵

Planning Fast MRI Implementation

Our healthcare system consists of hospital, outpatient, and free-standing clinics, with imaging equipment acquired from three MRI vendors. There-

fore, a free-standing imaging center and a limited number of scanners of similar generation and vendor were key to effective and efficient rollout of fast body MR imaging.

To begin, we created an ad hoc group to rapidly conceive and implement a fast MR scanning program. An experienced radiologist from each imaging section reviewed the literature and proposed feasible protocols. Whenever possible, more frequently used comprehensive MRI protocols were converted to fast MRI protocols. Each of these protocols was then vetted by each section and the MRI imaging modality group (Table 1, online at <http://appliedradiology.com/articles/improving-body-imaging-throughput-in-the-midst-of-covid-19>). We established the following inclusion and exclusion criteria for fast body MRI protocols:

Inclusion Criteria

- Prior good quality baseline MRI scan in the PACS as a reference scan;
- As a follow up scan of a pre-existing medical condition; and
- Scan indication is a focused clinical question; eg, is the tumor bigger or smaller, was locoregional therapy effective, or was there tumor recurrence or new metastasis?

Exclusion criteria

- Request for lesion characterization;
- Work-up of findings seen on other imaging modalities;
- Specific request for standard MRI study.

Fast MRI Practices

Patient Access

All patients were asked to comply with masking and were screened for signs/symptoms of illness in advance of and upon arrival for their appointment (Figure 1). Waiting room seating was configured to maintain a distance of 6 feet between patients. To minimize use of waiting areas, patients who arrived by automobile were asked to wait in their car until called for scanning. Our health system is implementing a patient texting

platform, which is expected to further expedite this process. If necessary for an exam, oral contrast was delivered to the patient's vehicle. Cashless co-payment procedures and devices prevented contact with registration staff.

Facility Changes

Physical barriers created a six-foot perimeter around the MRI console; no one was allowed within that zone while it was occupied by a technologist. An MRI technologist oversaw and maintained a clean and safe environment in all work areas. The scanner room was cleaned with hospital-grade germicidal wipes between each procedure. High-contact surfaces (eg, doorknobs, locker handles) were also cleaned with these wipes. All used linens were removed and disposed of appropriately. Restroom signs indicated occupancy. Patients were prepped in designated areas, further limiting contact with other patients and staff. Entry and exit of patients were regulated as much as possible through a "one-way-only" system. Arrow markers on the floors and walls helped facilitate this system.

Personal Protective Equipment and Other Protection Measures

All staff were provided with personal protective equipment (PPE). Owing to resource limitations, more extensive PPE was used for COVID-19-positive patients or patients under investigation for the disease, while standard universal protection measures were implemented for other patients. Staffing of these sites was important to manage the increase in patient volume and to provide safety for patients and staff. Whenever possible, two teams of technologists alternated scanning patients, thus providing continuity of care. At least two prep rooms were also used to help patients prepare patients expeditiously.

Scanning Checklist

Protocols were tested and approved for use. An additional torso coil was also acquired to help speed patient

throughput and case turnaround. Once completed, scans were automatically sent to the PACS system, without providing radiologists with the opportunity to check them or to add sequences. Hence, it was important that the scanning technologist closely adhere to the imaging parameters and review all images for screening and diagnostic quality. To facilitate this process, technologists were provided with a checklist (Appendix 1) to complete and scan into the PACS at the conclusion of each study.

Teamwork Is Vital

Since success in this endeavor required the support of our clinical colleagues, we consistently kept channels of communication open. For example, we established a list of patients whose tests were rescheduled because of stay-at-home orders. We designated radiologists in each imaging section to consult with referring physicians for approval of fast MRI protocols on a patient-by-patient basis. At every stage we made sure to involve all stakeholders, including MRI staff, imaging supervisors, administrators, and local technical applications support personnel. Including technologists on our task force facilitated their buy-in during the operational change process.

Implementation Challenges

Change often raises questions and challenges, especially with regard to implementing unconventional approaches to long-standing procedures. For example, some radiologists expressed their fear of missing findings and the accompanying medico-legal ramifications. We addressed this issue by having any patient who required more detailed imaging to return for a more comprehensive scan. Using a smaller facility, located apart from our main hospital, is not always ideal for patients with clinic visits at a different location on the same day. Working with the patient's clinical team to coordinate appointment times helped us to prevent delays in patient care.

Scan Reimbursement

Institution-specific guidelines were created for assessing a limited charge modifier (CPT modifier 52) for billing of the fast MR protocols. For example, limited-charge modifiers may be appropriate for scanning procedures or room use lasting less than 10 minutes. Similarly, a limited-charge modifier may be considered if the protocol sequences do not fulfill the study recommendations put forth by the appropriate accrediting body (eg, The American College of Radiology). The application of the limited-charge modifier is largely at an institution's discretion; many fast protocols will not require it, as they meet recommended guidelines. Indeed, the majority of fast protocols at our institution did not require the modifier. Billing can be nuanced, however, with regional and institutional variations based on payer mix, standard of care and, ultimately, the clinical question being answered.

Fast MRI Improves Throughput

At the start of this fast MRI protocol implementation, nearly half of our body imaging backlog studies were deemed eligible for fast protocols. By utilizing the resources of our free-standing imaging centers, the fast protocols enabled our facility to return to 90% of our average pre-COVID-19 MRI scans per day within one month of implementation. By comparison, our hospital-based outpatient facility MR imaging volume returned to only 57% of the pre-COVID-19 average.

Based on our experience, a thoughtful, well-planned execution of fast MRI protocols in smaller and more easily modified imaging facilities can potentially provide more efficient patient care and reduce scanning backlogs during the continuing COVID-19 pandemic. Indeed, these protocols may continue to be utilized beyond cessation of these conditions, pending assessment of radiologist, technologist, patient, and clinician satisfaction.

REFERENCES

1. Canellas R, Rosenkrantz AB, Taouli B, et al. Abbreviated MRI protocols for the abdomen. *RadioGraphics* 2019;39(3):744-758.
2. Marks RM, Ryan A, Heba ER, et al. Diagnostic per-patient accuracy of an abbreviated hepatobiliary phase gadoteric acid-enhanced MRI for hepatocellular carcinoma surveillance. *AJR* 2015;204(3):527-535.
3. Besa C, Lewis S, Pandharipande PV, et al. Hepatocellular carcinoma detection: diagnostic performance of a simulated abbreviated MRI protocol combining diffusion-weighted and T1-weighted imaging at the delayed phase post gadoteric acid. *Abdom Radiol (NY)* 2017;42(1):179-190.
4. Lee JY, Huo EJ, Weinstein S, et al. Evaluation of an abbreviated MRI screening protocol for patients at risk for hepatocellular carcinoma. *Abdom Radiol (NY)* 2018;43(7):1627-1633.
5. Tillman BG, Gorman JD, Hru JM, et al. Diagnostic per-lesion performance of a simulated gadoterate disodium-enhanced abbreviated MRI protocol for hepatocellular carcinoma screening. *Clinical Radiology* 2018 May;73(5):485-493.
6. Khatri G, Pedrosa I, Ananthakrishnan L, et al. Abbreviated-protocol screening MRI vs. complete-protocol diagnostic MRI for detection of hepatocellular carcinoma in patients with cirrhosis: an equivalence study using LI-RADS v2018. *J Magn Reson Imaging* 2020 Feb;51(2):415-425.
7. Vilgrain V, Esvan M, Ronot M, et al. A meta-analysis of diffusion-weighted and gadoteric acid-enhanced MRI imaging for the detection of liver metastases. *Euro Radiol* 2016;26(12):4595-4615.
8. Nougaret S, Reinhold C, Chong J, et al. Incidental pancreatic cysts: natural history and diagnostic accuracy of a limited serial pancreatic cyst MRI protocol. *Eur Radiol* 2014;24(5):1020-1029.
9. Seo N, Park SH, Kim K, et al. MR enterography for the evaluation of small-bowel inflammation in Crohn disease by using diffusion-weighted imaging without intravenous contrast material: a prospective noninferiority study. *Radiology* 2016;278(3):762-772.
10. Kang Z, Min X, Weinreb J, Li Q, Feng Z, Wang L. Abbreviated biparametric versus standard multiparametric MRI for diagnosis of prostate cancer: a systematic review and meta-analysis. *AJR* 2019;212(2):357-365. doi: 10.2214/AJR.18.20103.
11. Harvey SC, Di Carlo PA, Lee B, Obadina E, Sippon D, Mullen L. An abbreviated protocol for high-risk screening breast MRI saves time and resources. *JACR* 2016 Nov;13(11):R74-R80.
12. Ko ES, Morris EA. Abbreviated magnetic resonance imaging for breast cancer screening: concept, early results, and considerations. *Korean J Radiol* 2019;20(4):533-541. Published online 2019 Mar 11.
13. Kim SY, Cho N, Choi Y, et al. Ultrafast dynamic contrast-enhanced breast MRI: lesion conspicuity and size assessment according to background parenchymal enhancement. *Korean J Radiol* 2020;21(5):561-571. Published online 2020 Mar 31.
14. Ross AB, Chan BY, Yi PH, Repplinger MD, Vanness DJ, Lee KS. Diagnostic accuracy of an abbreviated MRI protocol for detecting radiographically occult hip and pelvis fractures in the elderly. *Skeletal Radiol* 2019;48(1):103-108.
15. Khurana B, Okanobo H, Ossiani M, Ledbetter S, Dulaimy KA, Sodickson A. Abbreviated MRI for patients presenting to the emergency department with hip pain. *AJR* 2012;198(6):W581-W588.

The Power of Triage (CADt) in Breast Imaging

Lisa Watanabe, MD

Artificial intelligence (AI) has already made—and continues to make—significant impacts on radiology.

One area of clinical practice, in particular, is in triage, also known as CADt. Indeed, CAD triage already is playing an active role in some clinical practices, where a deep learning-based algorithm acts as the “first reader” of medical images and highlights cases based on suspicion level of pathology, thus providing a prioritized worklist to the radiologist as the “second reader.”

Longstanding research on error-reduction practices in aviation and surgery underscores the usefulness of prioritization to minimize human error and improve efficiencies. One study found that prioritizing urgent exams in a worklist helped improve reporting turnaround times.¹ Radiologists typically read exams either in a random fashion or on a sequential “first in, first out” basis. This means suspicious cases may not be interpreted promptly, depending on practice backlogs. This inefficiency can impact practices, outcomes, and patient care.

Triage software for worklist prioritization or physician notification has been successfully deployed for medical imaging studies such as stroke imaging and other emergency indications.

Dr Watanabe is a clinical associate professor at the USC Keck School of Medicine, Los Angeles, CA, and Chief Medical Officer, CureMetrix Inc, San Diego, CA.

Diagnostic Desktop - 8.1.2 SPI - ahe07.demo.agfa.net - AGFA_PACS

File Tools List area Help

Start reading

Open

Start List

More

User: Doe, John

Started tasks (1)

Activities overviews

Mammo-CureMetrix

To Do's0 total

Details

Follow-up

MG-CureMetrix74

Study list - 'MG-CureMetrix'

74 studies

| | | Patient name and ID | Procedure name | Study Date | Accession number | CureMetrix |
|--|--|---------------------|----------------|-----------------|------------------|----------------------|
| | | Q METRIX NINA | MAMMOGRAPH | 16/07/19, 11:21 | CMA000008 | cmTriage: Suspicious |
| | | Q METRIX ANDREA | MAMMOGRAPH | 19/07/19, 10:32 | CMA000013 | cmTriage: Suspicious |
| | | Q METRIX WENDY | MAMMOGRAPH | 17/07/19, 09:02 | CMA000002 | cmTriage: Suspicious |
| | | Q METRIX MARY | MAMMOGRAPH | 16/07/19, 12:30 | CMA000022 | cmTriage: Suspicious |
| | | Q METRIX GENEVIEVE | MAMMOGRAPH | 16/07/19, 09:28 | CMA000023 | cmTriage: Suspicious |
| | | Q METRIX JESSICA | MAMMOGRAPH | 15/07/19, 16:05 | CMA000017 | cmTriage: Suspicious |
| | | Q METRIX JOEY | MG UNKNOWN | 18/07/19, 15:14 | CMA000014 | cmTriage: Suspicious |
| | | Q METRIX VIVIAN | MAMMOGRAPH | 19/07/19, 13:55 | CMA000003 | cmTriage: Suspicious |
| | | Q METRIX SANDY | MAMMOGRAPH | 15/07/19, 12:09 | CMA000018 | cmTriage: |
| | | Q METRIX JOAN | MAMMOGRAPH | 17/07/19, 14:36 | CMA000027 | cmTriage: |
| | | Q METRIX SALLY | MAMMOGRAPH | 17/07/19, 11:07 | CMA000024 | cmTriage: |
| | | Q METRIX JENNIFER | MAMMOGRAPH | 16/07/19, 08:12 | CMA000004 | cmTriage: |
| | | Q METRIX ERIKA | MAMMOGRAPH | 19/07/19, 13:42 | CMA000007 | cmTriage: |
| | | Q METRIX JOANNA | MAMMOGRAPH | 15/07/19, 11:22 | CMA000015 | cmTriage: |
| | | Q METRIX MIRANDA | MAMMOGRAPH | 19/07/19, 09:17 | CMA000016 | cmTriage: |
| | | Q METRIX SANDRA | MAMMOGRAPH | 17/07/19, 13:33 | CMA000029 | cmTriage: |
| | | Q METRIX JEANETTE | MAMMOGRAPH | 16/07/19, 14:01 | CMA000016 | cmTriage: |
| | | Q METRIX FELICIA | MAMMOGRAPH | 16/07/19, 12:52 | CMA000025 | cmTriage: |
| | | Q METRIX ALEX | MAMMOGRAPH | 18/07/19, 11:41 | CMA000001 | cmTriage: |
| | | Q METRIX ANALYNN | MAMMOGRAPH | 18/07/19, 14:25 | CMA000031 | cmTriage: |

FIGURE 1. CureMetrix cmTriage on an anonymized PACS Worklist. Triage functions as the first reader and sorts mammograms based on case-based scoring. cmTriage can also be displayed on a RIS worklist such as Nuance.

FDA-cleared software for stroke triage includes solutions from Avicenna, RapidAI, and Viz.ai. The benefits of these programs include direct notification of stroke teams to expedite decision making and treatment. Vendors like Aidoc also offer software that prioritizes such critical cases as intracranial hemorrhage, pneumothorax, cervical spine fracture, and pulmonary embolus.

CAD triage also holds significant benefits for mammography, where it has been shown to outperform traditional CAD. As stated in an editorial recently appearing in *Radiology*, “Ultimately, this innovative application [CADt] of artificial intelligence may prove more effective and reliable than conventional computer aided detection in advancing a so-called lean approach to mammographic screening.”²

CureMetrix brought the first FDA-cleared AI-based triage product for mammography to market. The company’s cmTriage automatically moves suspicious studies to the top of a worklist and expedites recall of suspicious mammogram cases. Triage can also be used to strategically distribute mammograms to multiple readers in a large practice. In addition, triage sensitivity can be set high to facilitate segregation of most-likely normal mammograms for reading.

The positive reader bias from triage can result in up to 30% faster reading times. A study presented at the Society of Breast Imaging’s 2020 annual meeting showed that an academic practice could realize up to a 55% reduction in false-positive recalls, a 12% reduction in benign biopsies, and a 17% improvement in cancer detection rates using triage.

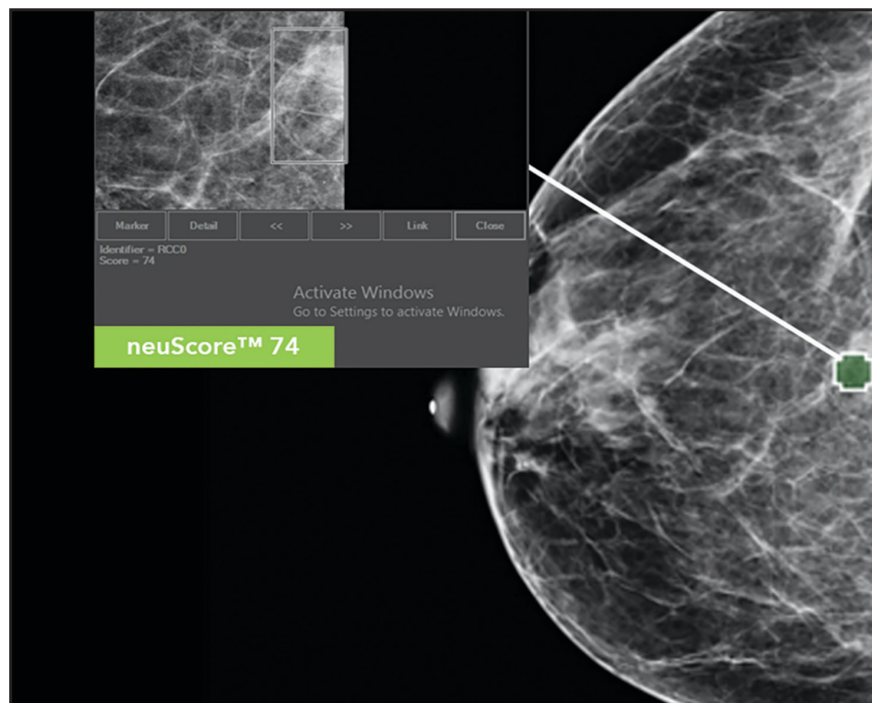


FIGURE 2. In this case, a clinically missed cancer was sorted as suspicious through cmTriage and the lesion was flagged by cmAssist with a high neuScore = 74.

workflow as compared to clinical workflows without triage.³

Case-based triage software works hand in hand with lesion-based CAD. Once a suspicious case is opened for viewing, lesion-based CAD flags areas of concern. Traditional CAD (CADE) was intended to be used as a second reader. While initial publications suggested improved reader accuracy with CADE, subsequent research in a large, multi-reader study showed an overall decrease in radiologist performance in the clinical setting, dampening enthusiasm for CADE.⁴ AI-based quantitative CAD, based on deep learning, is also known as CADx. CADx tools such as CureMetrix's cmAssist can enhance sensitivity and specificity.

A recently published MD Anderson Cancer Center study demonstrated a 69% reduction in false-positive markings per image with cmAssist AI-based CAD.⁵ Multiple-reader studies have shown that AI-based CAD improves cancer detection rates in mammography. In one published study, cancer detection

rates averaged a 27% improvement for readers of varying experience and training levels using AI-based CAD, without an increase in recall rates.⁵

Hologic and iCAD offer AI-based solutions designed to increase reader efficiency for 3D mammography, or digital breast tomosynthesis (DBT). Hologic's 3DQuorum technology reconstructs 3D imaging data from the company's DBT solution into 6mm slices that identify clinically relevant features and regions of interest. According to Hologic, 3DQuorum can reduce tomosynthesis image volume by up to 66%, or an average of 1 hour per 8 hours of image interpretation without compromising image quality, sensitivity, or reader accuracy.⁶

iCAD's ProFound AI analyzes DBT images to provide information on the Certainty of Finding lesion and Case Scores to assist reader efficiency. A recent study reported the solution reduced radiologist reading times by 52.7%, reduced unnecessary patient recall rates by 7.2%, and improved

radiologist sensitivity by 8%.⁷ iCAD also reports its solution reduces reading times by up to 57.4% in women with dense breasts.⁸

In summary, applications of AI, particularly in triage, have become a clinical reality and are well suited to mammography, offering numerous benefits that include cost savings⁹ and increased efficiency, accuracy, overall practice value, and job satisfaction. It behooves all breast imagers to investigate and consider implementing AI solutions in clinical practice.

REFERENCES

- Ekram T, Halabi S, Ciarelli J. Prioritizing work list to improving reporting turn-around times.. Conference: Radiological Society of North America 2011 Scientific Assembly and Annual Meeting. December 2011.
- Kontos D, Conant EF. Reviews and commentary editorial: Can AI help make screening mammography "Lean"? *Radiology*. 2019; 293: 47–48. <https://doi.org/10.1148/radiol.2019191542>
- Watanabe AT, Lim V. Workflow reduction using artificial intelligence-based mammography triage. Society of Breast Imaging Annual Meeting 2020. https://www.youtube.com/watch?v=_OVJTpb14U&feature=youtu.be
- Lehman CD, et al. Diagnostic accuracy of digital screening mammography with and without computer-aided detection. *JAMA Intern Med*. 2015; 175(11).
- Mayo RC, Kent D, Sen LC, Kapoor M, Leung JWT, Watanabe AT. Reduction of false-positive markings on mammograms: A retrospective comparison study using an artificial intelligence-based CAD. *J Digit Imaging*. 2019; 32(4): 618–624. DOI: 10.1007/s10278-018-0168-6 PMID: 30963339 PMCID: PMC6646646
- Hologic announces FDA approval of 3DQuorum imaging technology, powered by Genius AI. Press release. November 12, 2019. Available at: <https://investors.hologic.com/press-releases/press-release-details/2019/Hologic-Announces-FDA-Approval-of-3DQuorum-Imaging-Technology-Powered-by-Genius-AI/default.aspx>.
- Conant EF, Toledano AY, Periaswamy S, et al. Improving accuracy and efficiency with concurrent use of artificial intelligence for digital breast tomosynthesis. *Radiol Artif Intell*. 2019;1(4): e180096. doi:10.1148/ryai.2019180096
- iCAD to showcase leading breast health solutions suite including expanded ProFound AI Platform at RSNA Annual Meeting. Press release. December 2, 2019. Available at: <https://www.icadmed.com/newsroom.html#!/posts/iCAD-to-Showcase-Leading-Breast-Health-Solutions-Suite-Including-Expanded-ProFound-AI-Platform-at-RSNA-Annual-Meeting/187>.
- Watanabe AT, Lim V, Vu HX, et al. Improved cancer detection using artificial intelligence: A retrospective evaluation of missed cancers on mammography. *J Digit Imaging*. 2019; 32: 625. <https://doi.org/10.1007/s10278-019-00192-5>

DOTAREM[®]

(gadoterate meglumine) Injection

REAL-WORLD TESTED.
**REAL-WORLD
PROVEN.**

The Dotarem[®] safety profile has been tested and proven in both studies and 30 years of global clinical use.*



0.007% Spontaneously Reported
Worldwide Adverse Events.
(>50 million doses)³⁻¹⁰

1 Dotarem[®]
The first macrocyclic
and ionic GBCA molecule.¹

Dotarem remains an industry standard for contrast imaging with a low incidence of immediate adverse events for patients of all ages.²⁻¹⁰

A low incidence of adverse events can help your patient focus on what matters most in their life.

Guerbet | 

COMMITTED



IMPORTANT SAFETY INFORMATION¹

WARNING: NEPHROGENIC SYSTEMIC FIBROSIS (NSF)

Gadolinium-based contrast agents (GBCAs) increase the risk for NSF among patients with impaired elimination of the drugs. Avoid use of GBCAs in these patients unless the diagnostic information is essential and not available with non-contrast MRI or other modalities. NSF may result in fatal or debilitating fibrosis affecting the skin, muscle and internal organs.

- The risk for NSF appears highest among patients with:
 - Chronic, severe kidney disease (GFR < 30 mL/min/1.73m²), or
 - Acute kidney injury.
- Screen patients for acute kidney injury and other conditions that may reduce renal function. For patients at risk for chronically reduced renal function (e.g. age > 60 years, hypertension, diabetes), estimate the glomerular filtration rate (GFR) through laboratory testing.
- For patients at highest risk for NSF, do not exceed the recommended DOTAREM dose and allow a sufficient period of time for elimination of the drug from the body prior to any re-administration.



Indications and Usage

DOTAREM[®] (gadoterate meglumine) injection is a prescription gadolinium-based contrast agent indicated for intravenous use with magnetic resonance imaging (MRI) in brain (intracranial), spine and associated tissues in adult and pediatric patients (including term neonates) to detect and visualize areas with disruption of the blood brain barrier (BBB) and/or abnormal vascularity.

Contraindications

History of clinically important hypersensitivity reactions to DOTAREM.

Warnings and Precautions

- **Hypersensitivity Reactions:** Anaphylactic and anaphylactoid reactions have been reported with DOTAREM, involving cardiovascular, respiratory, and/or cutaneous manifestations. Some patients experienced circulatory collapse and died. In most cases, initial symptoms occurred within minutes of DOTAREM administration and resolved with prompt emergency treatment.
- Before DOTAREM administration, assess all patients for any history of a reaction to contrast media, bronchial asthma and/or allergic disorders. These patients may have an increased risk for a hypersensitivity reaction to DOTAREM.
- Administer DOTAREM only in situations where trained personnel and therapies are promptly available for the treatment of hypersensitivity reactions, including personnel trained in resuscitation.
- **Gadolinium Retention:** Gadolinium is retained for months or years in several organs. The highest concentrations have been identified in the bone, followed by brain, skin, kidney, liver and spleen. The duration of retention also varies by tissue, and is longest in bone. Linear GBCAs cause more retention than macrocyclic GBCAs.
- Consequences of gadolinium retention in the brain have not been established. Adverse events involving multiple organ systems have been reported in patients with normal renal function without an established causal link to gadolinium retention.
- **Acute Kidney Injury:** In patients with chronically reduced renal function, acute kidney injury requiring dialysis has occurred with the use of GBCAs. The risk of acute kidney injury may increase with increasing dose of the contrast agent; administer the lowest dose necessary for adequate imaging.
- **Extravasation and Injection Site Reactions:** Ensure catheter and venous patency before the injection of DOTAREM. Extravasation into tissues during DOTAREM administration may result in tissue irritation.

Adverse Reactions

- The most common adverse reactions associated with DOTAREM in clinical trials were nausea, headache, injection site pain, injection site coldness and rash.
- Serious adverse reactions in the Postmarketing experience have been reported with DOTAREM. These serious adverse reactions include but are not limited to: arrhythmia, cardiac arrest, respiratory arrest, pharyngeal edema, laryngospasm, bronchospasm, coma and convulsion.

Use in Specific Populations

- **Pregnancy:** GBCAs cross the human placenta and result in fetal exposure and gadolinium retention. Use only if imaging is essential during pregnancy and cannot be delayed.
- **Lactation:** There are no data on the presence of gadoterate in human milk, the effects on the breastfed infant, or the effects on milk production. However, published lactation data on other GBCAs indicate that 0.01 to 0.04% of the maternal gadolinium dose is present in breast milk.
- **Pediatric Use:** The safety and efficacy of DOTAREM at a single dose of 0.1 mmol/kg has been established in pediatric patients from birth (term neonates ≥ 37 weeks gestational age) to 17 years of age based on clinical data. The safety of DOTAREM has not been established in preterm neonates. No cases of NSF associated with DOTAREM or any other GBCA have been identified in pediatric patients age 6 years and younger.

You are encouraged to report negative side effects of prescription drugs to the FDA. Visit www.fda.gov/medwatch or call 1-800-FDA-1088.

Please see the full Prescribing Information, including the patient Medication Guide, for additional important safety information.

¹Dotarem was launched globally in 1989 and approved by the FDA for use in the US in 2013.

References:

1. Dotarem [package insert]. Princeton, NJ: Guerbet LLC; July 2019.
2. Internal data as of May 2019.
3. de Kerviler E et al. Adverse reactions to gadoterate meglumine: review of over 25 years of clinical use and more than 50 million doses. *Invest Radiol.* 2016 Sep;51(9):544-51.
4. Briand et al. Efficacy and safety of the macrocyclic complex Gd-DOTA in Children: Results of a Multi-Centre Study. *Proceedings of the 29th Congress of the European Society of Pediatric Radiology.* 1992; 128.
5. Briand Y. Daily Paediatric Use of MRI Contrast Agents: Results of a Multi-Centre Survey. *Proceedings of the 29th Congress of the European Society of Pediatric Radiology.* 1992.
6. Ishiguchi T & Takahashi S. Safety of gadoterate meglumine (Gd-DOTA) as a contrast agent for magnetic resonance imaging: results of a post-marketing surveillance study in Japan. *Drugs R D.* 2010;10(3):133-45.
7. Emond S & Brunelle F. Gd-DOTA administration at MRI in children younger than 18 months of age: immediate adverse reactions. *Pediatr Radiol.* 2011 Nov;41(11):1401-6.
8. Maurer M et al. Tolerability and diagnostic value of gadoteric acid in the general population and in patients with risk factors: results in more than 84,000 patients. *Eur J Radiol.* 2012 May;81(5):885-90.
9. Soyer et al. Observational Study on the Safety Profile of Gadoterate Meglumine in 35,499 Patients: The SECURE Study. *J. Magn. Reson. Imag.* 2017; 45, 988-997.
10. Radbruch A et al. Gadolinium retention in the dentate nucleus and globus pallidus is dependent on the class of contrast agent. *Radiology.* 2015 Jun;275(3):783-97.

The Future is Bright for Collaboration Between AI and Breast Imagers

Mary Beth Massat



AI is well suited
to breast
imaging
due to the
nature of
what we do.

Michael Linver,
MD, FACR, FSBI
X-Ray Associates
of New Mexico

Artificial intelligence (AI) is gaining credibility in breast imaging.

Whether it is a study showing that AI outperforms human readers¹ or one showing that a combination of AI and radiologist assessment improves diagnostic accuracy,² AI is being recognized for its potential to help address a wide range of challenges in breast imaging.

"In radiology, we have challenges with access to quality care, human error, and radiologist burnout," says Constance Lehman, MD, PhD, director of Breast Imaging and co-Director of the Avon Comprehensive Breast Evaluation Center at Massachusetts General Hospital.

"Although X-ray technology has been around for a very long time, a minority of humans in the world have access to quality radiology technology," Dr Lehman says. "And we need to fix that."

AI may help address these disparities by providing access to specialists and helping to raise the overall quality of care, says Dr Lehman, lead author of a 2016 study by the Breast Cancer Surveillance Consortium (BCSC) that assessed screening digital mammography trends in the US.

According to the study, sensitivity and cancer detection rates have increased since BCSC's 2005 and 2008 reports, likely reflecting digital mammography's improved performance over screen-film mammography, as well as access to

pathology data. However, abnormal interpretation rates have also increased.

The authors found these increases "particularly concerning, given that recall rates have continually failed to meet the recommendations of the ACR and other expert panels going back to the initial report in 2005, despite calls for attention to this matter."³

"We found that 40 percent of certified specialized breast imagers operated outside of the recommended guidelines associated with false-positive exams," Dr Lehman says. "That's ... something that we really need to address. AI can help reduce the variation in the human ability to perform consistent and accurate interpretations."

Michael Linver, MD, FACR, FSBI, emeritus director of Mammography at X-Ray Associates of New Mexico, agrees, and he expects the potential for AI to aid breast cancer screening and diagnosis to continue growing.

"AI is well suited to breast imaging due to the nature of what we do. We are only looking for one basic disease," says Dr Linver, who is also Program Co-Director of the annual "Mammography in Santa Fe" course. Breast imaging, he says, is unlike chest or abdominal imaging, which can be used to identify multiple possible diagnoses and targets.

"What's problematic as a breast imager is that more mammograms are read by non-specialists than by specialists. [The non-specialists] don't have the same level of expertise, and that means they need a little help," he adds. "That's where CAD (computer aided detection) and AI are

Mary Beth Massat is a freelance writer based in Crystal Lake, IL.



AI tools may help provide a more targeted, specific, and higher-quality image for every patient, every time. We can be more precise in how we acquire the images targeted specifically to that patient's body habitus to answer the clinical question at hand. -

Constance Lehman, MD, PhD
Avon Comprehensive Breast Evaluation Center
Massachusetts General Hospital

particularly useful to help them achieve the next level of expertise, where they can perform a lot closer to specialists.”

Serving as an assistant to help radiologists interpret breast imaging studies more accurately is likely to come soon, says Christopher Comstock, MD, FACR, attending radiologist and director of breast imaging clinical trials at Memorial Sloan-Kettering Cancer Center.

“We will need a physician’s involvement for oversight and to interpret the complexities of each patient,” Dr Comstock says. “There is a saying that computers won’t replace radiologists, but radiologists with computers will replace radiologists.” He analogizes the relationship to that of a pilot and the plane’s autopilot capabilities. While technology may often “land” the plane, the pilot must still oversee the landing process.

“We can really benefit from more quantitative analysis of findings,” Dr Comstock says. “Humans can take into consideration several features and put together components of the image for the interpretation. Computers can recognize and analyze more information, such as patterns and associations, faster than a radiologist.”

Artificial intelligence may also help streamline workflow by previewing and prioritizing mammograms based on suspicious findings.

“There are several studies showing there is a subset of mammograms that could be triaged by AI. [However,] I think it is premature to do that,” says Linda Moy, MD, FSBI, Fellowship Director for Breast Imaging at New York University (NYU) Langone Medical Center. Dr

Moy was involved in a study finding that the combination of AI and radiologists could more significantly improve breast cancer detection than either one alone.⁴

Another issue is whether patients and referring physicians will accept a diagnosis based only on algorithms or AI, Dr Moy notes, adding that external validation by clinicians and scientists is required to continue pushing the field forward. While screening mammography demonstrates a great need for AI assistance, Moy says, AI can help clinicians read digital breast tomography (DBT) and breast MRI studies containing a large number of images.

AI in Image Capture

Some experts predict a growing role for AI in image capture.

“AI tools may help provide a more targeted, specific, and higher-quality image for every patient, every time,” says Dr Lehman. “We can be more precise in how we acquire the images targeted specifically to that patient’s body habitus to answer the clinical question at hand.”

Dr Moy explains that AI may also help decrease radiation dose in DBT by creating so-called “synthetic images.” Generated by a DBT 3D data set, these images can be used to replace standard 2D images. Synthetic CT images are also being created from MRI data, potentially obviating the need for additional imaging. There are also technologies that create synthetic MR images from an MRI dataset, such as diffusion weighted images, which can shorten the MRI scan time.



Computers can recognize and analyze more information, such as patterns and associations, faster than a radiologist.

Christopher Comstock, MD, FACR, Memorial Sloan-Kettering Cancer Center

With an estimated 75% of U.S. breast imaging centers now using DBT, the need for AI to help specialists read more efficiently is growing, says Dr Linver, adding that a screening tomosynthesis exam typically takes him two to three times longer to read than a screening mammogram.

“If we can use AI to decrease the pool of images, where only the valuable potential pathology information is presented to the radiologist, then that would be a huge step forward and make a difference in our efficiency,” he says.

The picture is less clear with respect to AI’s value in breast MRI. Although AI may be able to help radiologists read through voluminous MRI data, Dr Moy believes multi-center validation studies are more difficult to perform because comparatively fewer imaging centers perform breast MRI, resulting in less data to train an AI-based breast MRI algorithm.

However, with abbreviated breast MRI protocols becoming more widespread, Dr Comstock foresees an opportunity for AI to help quantify the data from breast MRI, which also delivers kinetic and compositional information; different MR sequences provide different information for interpretation.

“Since there is so much more information, I think it’s only natural that CAD and AI are needed more,” Dr Comstock says, noting that AI has the potential to offer more robust analyses of multiple sets of data at one time through a trained network that has looked at thousands of cases on a level that is not easily achieved on a case-by-case basis.

“I think it can only improve the accuracy of the interpretation,” he says.

Risk Analysis

Beyond imaging, AI may also garner a role in radiomics and radio-genomics, where Drs Comstock and Moy believe AI could help breast specialists go beyond diagnosing and treating breast cancer to predicting breast cancer risk and treatment response.

“There is another layer where we can analyze treatment effect,” Dr Comstock says. “There is a whole other realm of AI in terms of analyzing the entire environment, including patient history, genetic testing, pathology, therapy, and how

they navigate through the healthcare system to potentially improve outcomes.”

“Radiomics and radiogenomics can broaden the scope of how we can interpret images beyond the (traditional) normal or abnormal finding on any imaging test we perform,” agrees Dr Moy. “The whole concept of precision medicine is not just treatment of cancer but the treatment of a particular person and what works best for them.”

Indeed, Dr Moy points to a growing body of research showing a relationship between a patient’s genetic profile and their response to treatment. Precision medicine, she asserts, can encompass lifestyle changes to improve overall health and potentially reduce the likelihood of developing cancer or enhancing treatment response.

Through a collaborative effort of MGH and the Massachusetts Institute of Technology, Dr Lehman has led efforts to develop and evaluate AI algorithms to improve breast cancer risk prediction. For example, the team has used an algorithm to evaluate breast density on mammograms and predict risk of developing breast cancer. The model performed well at MGH and has since been validated at other centers. The most recent findings will soon be published, Dr Lehman says.

“Commercially available risk models to predict future risk of breast cancer for an individual woman just don’t work that well,” Dr Lehman says. “It’s an uncomfortable truth, but most ... women diagnosed with breast cancer have no currently known risk factors, other than being female. Second, there are patients who were identified as high risk who never developed breast cancer. Third, what was really shocking to us is how poorly the commercial models performed in racial and ethnic subgroups.”

Most models, she says, were developed in Caucasian women but are also being applied to Hispanic, Black, and Asian women.

“So poor sensitivity, poor specificity, and racial and ethnic biases of existing risk models plague us,” Dr Lehman says.

Despite Some Challenges, AI’s Future Is Bright

One hurdle still standing in the way of widespread adoption of AI in breast imaging, says Dr

Comstock, is that many such developing technologies may not be applicable across different practices and population groups.

“The challenge is wide validation of these different systems so that the radiologist has a clear understanding of what that information, or score, means,” he says. “How does the information impact the decision to biopsy or not? How will it change actual patient care and practice decisions? It needs to be clear for the users who adopt the technology how to use the specific tool.”

AI will also need to be seamlessly incorporated into reading environments. Dr Comstock indicated historically many centers have needed separate workstations in addition to their PACS workstation to interpret DBT and MRI CAD studies. He believes most radiologists, like himself, don’t want yet another workstation for AI-assisted interpretations.

Data sharing issues also need to be addressed, says Dr Moy, who was recently involved in the RSNA’s AI COVID-19 Task Force to identify institutions interested in sharing data. Many institutions in China had already signed contracts with vendors for chest X-ray or chest CT data to develop AI solutions.

“We need to share our data anonymously and safely, and from multiple areas of research,” Dr. Moy says. “That requires buy-in from multiple centers.”

Fourth, AI algorithms developed on modern digital systems may not deliver the same or similar results on older technology.

“Some AI tools have been developed on very high quality images from select specialized centers, and the results didn’t translate into general practice where the quality of the images was not as high,” Dr. Lehman says.

Finally, quality assurance is vital, Dr. Lehman says. Whether the “reader” is a computer or a human, “In the end, it’s an answer given to

a patient or referring physician. We still need to have that quality oversight,” she says.

Dr Linver agrees. “Anytime we rely on a machine, we had better be sure it is basing a decision on valid, good data, otherwise it is potentially dangerous. Breast imagers want to be more efficient in the ability to get through the cases but not sacrifice accuracy.”

Despite these challenges, the experts consulted for this article believe the future of collaboration between AI and radiologists is bright.

“It’s an exciting time as we enter a new era in breast imaging,” Dr Linver says. “While we’ve decreased the death rate from breast cancer by 40 percent in the US in the last three decades, some countries in Europe have decreased it by as much as 60 percent because more specialists read mammograms. This is the greatest potential for AI, to bring us all to the level of experts in breast imaging and make breast cancer a less lethal disease.”

“We can imagine a day when we have more time to provide higher-quality care to our patients,” Dr Lehman says, and “when we’re using these tools to free up more of our time to focus on those things that require human intervention and allow the AI tools to do what they do best.”

REFERENCES

1. McKinney, S.M., Sieniek, M., Godbole, V. *et al.* International evaluation of an AI system for breast cancer screening. *Nature* 577, 89–94 (2020). <https://doi.org/10.1038/s41586-019-1799-6>
2. Schaffter T, Buist DSM, Lee CI, *et al.* Evaluation of Combined Artificial Intelligence and Radiologist Assessment to Interpret Screening Mammograms. *JAMA Netw Open*. 2020;3(3):e200265. doi:10.1001/jamanetworkopen.2020.0265.
3. Lehman CD, Arao RF, Sprague BL, *et al.* National Performance Benchmarks for Modern Screening Digital Mammography: Update from the Breast Cancer Surveillance Consortium. *Radiology*. 2017;283(1):49-58. doi:10.1148/radiol.2016161174.
4. Wu N, Phang J, Park J, *et al.* Deep Neural Networks Improve Radiologists’ Performance in Breast Cancer Screening. *IEEE Trans Med Imaging*. 2020;39(4):1184-1194. doi:10.1109/TMI.2019.2945514.



The whole concept of precision medicine is not just treatment of cancer but the treatment of a particular person and what works best for them.

Linda Moy, MD, FSBI
New York University
Langone Medical
Center

Cystic Fibrosis Liver Disease

David Chung, MD; Joseph J Palermo, MD; Richard Towbin, MD; Alexander J Towbin, MD

CASE SUMMARY

A 13-year-old diagnosed with cystic fibrosis (CF) and pancreatic insufficiency was seen for gastroenterology consultation after being found to have new onset of mild transaminase elevation during an admission for CF pulmonary exacerbation. They showed no jaundice or manifestations of liver disease and denied abdominal complaints, hematemesis, diarrhea, constipation, easy bleeding or bruising, or symptoms of encephalopathy. After an initial work-up, no other causes of liver disease were identified.

IMAGING FINDINGS

Two years following initial consultation, abdominal ultrasound (Figure 1) showed the liver to have a coarsened, heterogeneous echotexture with a nodular surface. Subsequent MRI (Figure 2), performed 2 years after the initial ultrasound, showed the liver to have a cirrhotic morphology with an irregular, macronodular contour and diffuse periportal edema. There were associated findings of portal hypertension with borderline enlargement

of the main portal vein, splenomegaly, and enlarged tortuous splenic vein.

DIAGNOSIS

Cystic fibrosis liver disease (CFLD)

DISCUSSION

Cystic fibrosis is a systemic, autosomal recessive disease that can give rise to complications involving multiple organ systems. As patient life expectancies increase, liver disease has increasingly become recognized as a major consequence of CF. CFLD often arises in children prior to puberty and is believed to be the third-most common cause of death in CF patients.^{1,2} Reported prevalence rates have ranged from 2 to 37 percent;³ however, owing to its lack of widely agreed-upon diagnostic criteria, its variable imaging and clinical presentations, and slowly progressive nature, CFLD's true prevalence is unknown.

In the hepatobiliary system, the CF transmembrane conductance regulator (CFTR) protein is expressed in the apical membranes of cholangiocytes and the gallbladder epithelium, where

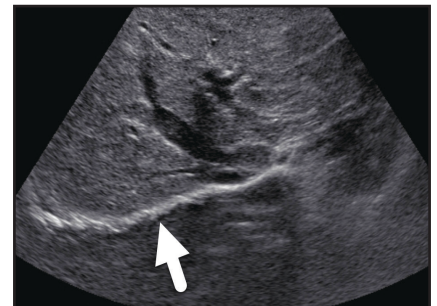


FIGURE 1. Transverse ultrasound of the liver shows a diffuse coarsened echotexture of the hepatic parenchyma. In addition, the surface of the liver (arrow) has a micronodular contour.

it regulates the water and electrolyte contents and alkalization of bile. Impaired function of CFTR results in abnormally viscous bile with reduced alkalinity that accumulates in the biliary tree and obstructs the small bile ducts. Abnormal bile composition and reduced flow leads to injury of cholangiocytes and collateral hepatocytes, stimulating the release of inflammatory cytokines and growth factors and inducing hepatic stellate cells to secrete collagen.³ This fibrotic process results in the focal, then multilobular cirrhotic, patterns seen in patients with

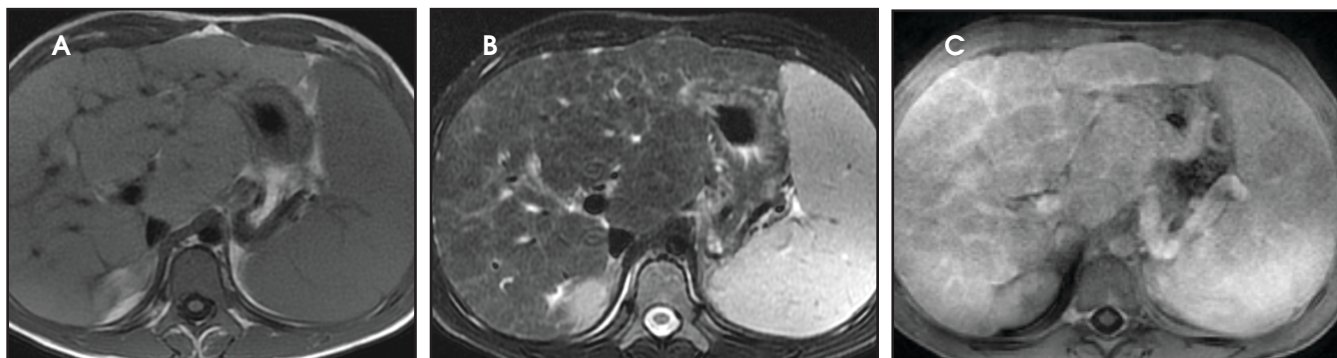


FIGURE 2. (A) Axial T1 FSE, (B) axial T2 with fat saturation, and (C) axial T1 GRE sequence performed in the portal venous phase of contrast enhancement show hepatic fibrosis and splenomegaly. On all sequences, the liver has a macronodular appearance. On the T1 FSE sequence, hypointense bands of hepatic fibrosis are present within the liver. On the T2 image, the fibrosis appears as diffuse, wispy increased signal throughout the liver.

CFLD. Hepatobiliary complications are believed to occur exclusively in those with severe CFTR gene mutations.² An important observation that correlates with severe CFTR mutations is that CFLD rarely occurs with pancreatic sufficiency. However, no specific risk factors for liver disease have been identified, and why only certain patients with severe mutations present with CFLD remains unclear.³

CFLD is characterized by three different hepatic parenchymal imaging patterns.³ The first pattern is presumed to represent hepatic steatosis with or without hepatitis. On ultrasound, the liver is enlarged and hyperechoic compared to the right kidney. As fat content increases, the through-transmission of the hepatic parenchyma and visualization of portal triads and the right hemidiaphragm decrease.⁴ The second imaging pattern is thought to be caused by focal biliary cirrhosis. In this pattern, the liver has a heterogeneous appearance with focal areas of increased periportal echogenicity.⁴ Finally, the nodular pattern is thought to represent changes related to hepatic fibrosis; it is present in approximately 10% of CFLD patients.³ Left untreated, continued fibrotic changes can lead to multilobular cirrhosis. On ultrasound, the liver appears heterogeneous with a

coarsened echotexture and an irregular, nodular margin. As fibrosis progresses, cirrhosis can develop, leading to other complications of hepatic dysfunction, including jaundice, coagulation disorders, portal hypertension, esophageal varices and, as seen in this patient, ascites and splenomegaly.³

Clinically diagnosing CFLD is challenging for two reasons. First, laboratory markers are neither sensitive nor specific for CFLD. While the condition is commonly associated with normal-to-moderate elevations in liver enzymes, these values are similar to the liver enzyme levels found in CF patients without liver disease. Second, most patients are asymptomatic. The most common form of CFLD is hepatic steatosis, which occurs in 20 to 60% of CF patients.⁴

Ultrasound has been proposed as a screening tool for CFLD. In one study of 719 patients, 18% had abnormal ultrasound liver patterns, with some showing a nodular cirrhotic ultrasound pattern prior to any clinical evidence of liver damage.⁵ Another study showed a strong correlation between surface nodularity on ultrasound and fibrotic histologic findings on liver biopsy. However, the same study highlighted other patients with histological signs of fibrosis who had normal-appearing

ultrasounds. The authors concluded that a negative ultrasound does not preclude diagnosis of CFLD and should be used in concert with other markers of liver disease.⁶ Based on these findings and the imaging findings previously described, an ultrasound scoring system has been proposed.⁷ Three points are allotted to findings of liver parenchymal coarseness, liver edge nodularity, and periportal echogenicity, each based on severity, for a potential total of 9 points. Scores of 4 and above correlated with significant elevations of liver enzymes and serum bilirubin and decreased levels of serum albumin and platelet counts.

MRI is also useful in detecting and quantifying liver disease, as it may detect cirrhotic changes with fibrosis, regenerative nodules, portal hypertension, and fatty changes.⁸ One study identified three MRI findings that reliably distinguished CFLD patients from a control group. These were altered gallbladder morphology, periportal tracking on diffusion weighted imaging, and periportal fat deposition in chemical-shift imaging.⁹ More recent MR imaging techniques allow for quantification of the different patterns of liver disease. Objective measures such as liver stiffness, liver fat fraction, liver volume and spleen volume can be used

to quantitatively evaluate the liver.

Currently, ursodeoxycholic acid (UDCA) is the main pharmacologic treatment for CFLD. Originally used to treat gallstones, UDCA is believed to improve bile acid flow. However, there are few longitudinal randomized controlled trials studying UDCA therapy for CFLD. In a systematic review of randomized controlled trials comparing the efficacy of UDCA to placebo, there was no difference in rate of portal hypertension or improvement in abnormal biliary excretion.¹⁰ Treatment also includes nutritional therapy with optimizing caloric intake, pancreatic enzyme replacement, and fat-soluble vitamin supplementation. For patients with severe portal hypertension, a surgical portosystemic shunt may be used to reduce the risk of life-threatening variceal bleeding. As with other decompensated liver diseases, the only curative treatment for advanced CFLD is liver transplant.

Our patient has remained asymptomatic despite evidence of more advanced liver disease.

CONCLUSION

Hepatobiliary complications have become increasingly relevant in CF as

treatments and patient life expectancy continue to improve. Hepatic US and MRI remain the least-invasive methods of CFLD screening. However, CFLD remains difficult to diagnose, as clinical signs often manifest well after liver disease has advanced. As this disease arises largely in the pediatric population, the need remains for improved screening measures. Medical management is currently limited to proper nutrition, fat-soluble vitamin supplementation, and UDCA, although there is little evidence for its efficacy.

REFERENCES

1. Stonebraker JR, Ooi CY, Pace RG, et al. Features of Severe Liver Disease with Portal Hypertension in Patients With Cystic Fibrosis. *Clinical Gastroenterology and Hepatology*. 2016;14(8). doi:10.1016/j.cgh.2016.03.041.
2. Colombo C. Liver disease in cystic fibrosis: A prospective study on incidence, risk factors, and outcome. *Hepatology*. 2002;36(6):1374-1382. doi:10.1053/jhep.2002.37136.
3. Kobelska-Dubiel N, Klincewicz B, Cichy W. Liver disease in cystic fibrosis. *Gastroenterology Review*. 2014; 3:136-141. doi:10.5114/pg.2014.43574.
4. Diwakar V, Pearson L, Beath S. Liver disease in children with cystic fibrosis. *Paediatric Respiratory Reviews*. 2001;2(4):340-349. doi:10.1053/prrv.2001.0170.
5. Leung DH, Ye W, Molleston JP, Weymann A, Ling S, Paranjape SM, Romero R, Schwarzenberg SJ, Palermo J, Alonso EM, et al. Baseline ultrasound and clinical correlates in children with cystic fibrosis. *J Pediatr*. 2015; 167:862-868.e2.
6. Mueller-Abt PR, Frawley KJ, Greer RM, Lewindon PJ. Comparison of ultrasound and biopsy findings in children with cystic fibrosis related liver disease. *J Cystic Fibrosis*. 2008;7(3):215-221. doi:10.1016/j.jcf.2007.08.001.
7. Williams SGJ, Evanson JE, Barrett N, Hodson ME, Boulton JE, Westaby D. An ultrasound scoring system for the diagnosis of liver disease in cystic fibrosis. *J Hepatol*. 1995; 22:513-521.
8. King LJ, Scurr ED, Murugan N, Williams SGJ, Westaby D, Healy JC. Hepatobiliary and Pancreatic Manifestations of Cystic Fibrosis: MR Imaging Appearances. *RadioGraphics*. 2000;20(3):767-777. doi:10.1148/radiographics.20.3.g00ma08767.
9. Poetter-Lang S, Stauder K, Baltzer P, et al. The Efficacy of MRI in the diagnostic workup of cystic fibrosis-associated liver disease: A clinical observational cohort study. *Euro Radiol*. 2018;29(2):1048-1058. doi:10.1007/s00330-018-5650-5.
10. Cheng K, Ashby D, Smyth RL. Ursodeoxycholic acid for cystic fibrosis-related liver disease. *Cochrane Database Syst Rev* 2017;9:CD000222.

Affiliations: University of Cincinnati College of Medicine, Cincinnati, OH (Dr Chung); Cincinnati Children's Hospital (Dr Palermo, Dr Alexander Towbin); Phoenix Children's Hospital (Dr Richard Towbin)

Hemangiopericytoma of the Third Ventricle

Shreeja Kadakia, BS; Khuram Kazmi, MD

CASE SUMMARY

A 70-year-old with a history of atrial fibrillation and prostate cancer, and thalassemia had a third ventricular mass incidentally detected on a brain MRI.

IMAGING FINDINGS

A contrast-enhanced T1 image showed an enhancing mass located in the anterior third ventricle near the foramen of Monro (Figure 1). Endoscopic biopsy of the mass demonstrated histologic findings consistent with hemangiopericytoma. CT 5 months later demonstrated that the mass had grown (Figure 2).

DIAGNOSIS

Hemangiopericytoma of the third ventricle

DISCUSSION

Hemangiopericytoma (HPC) is a central nervous system tumor that arises from the pericytes of meningeal capillaries.¹ These tumors are more likely to occur in males, most com-

monly in the fourth or fifth decade.¹ Signs and symptoms at presentation may include headache, blurred vision, nausea, vomiting, and photophobia.⁴ Intraventricular HPC is rare and most often found in the lateral ventricles. HPC in the third ventricle are exceedingly rare, with only one previous case found in our literature search.²

Intraventricular HPC may arise from pericytes within the tela choroidea or choroid plexus.³ There are many pathological and imaging similarities between HPC and angioblastic/anaplastic meningioma. Histologically, HPC shows a staghorn vascular pattern of spindly cells and are reactive to vimentin, but not to epithelial membrane antigen, unlike meningioma, which is positive for both substances.⁵ One of the most characteristic features of HPC is a dense reticulin network composed of individual cells.⁴

On imaging, intracranial HPC tends to occur supratentorially along meningeal surfaces, with most occurring in parasagittally. They are usually oval,

have lobulated margins, are dense on CT, and have avid contrast enhancement on CT and MRI.⁵ They may show vascular flow voids, as in our case, and cystic areas. Peripheral HPC lacks the “dural tail” sign typical of meningioma.^{5,6} Differential diagnostic considerations for intraventricular masses include include colloid cyst, central neurocytoma, ependymoma, subependymal giant cell astrocytoma and intraventricular meningioma.

Although third ventricular HPC is extremely rare, their consideration can be important. Their noncontrast appearance and location can mimic those of a colloid cyst.⁷ Colloid cyst, however, is a non-neoplastic lesion. Biopsy of an HPC may be more likely to hemorrhage than other third ventricular lesions, given its hypervascularity.⁵ In our case, the patient developed postoperative intraventricular and subarachnoid hemorrhage (Figure 2). HPC also has a propensity to recur and metastasize through the CNS and beyond. Therefore, gross total surgical resection is the goal.⁵ Postoperative

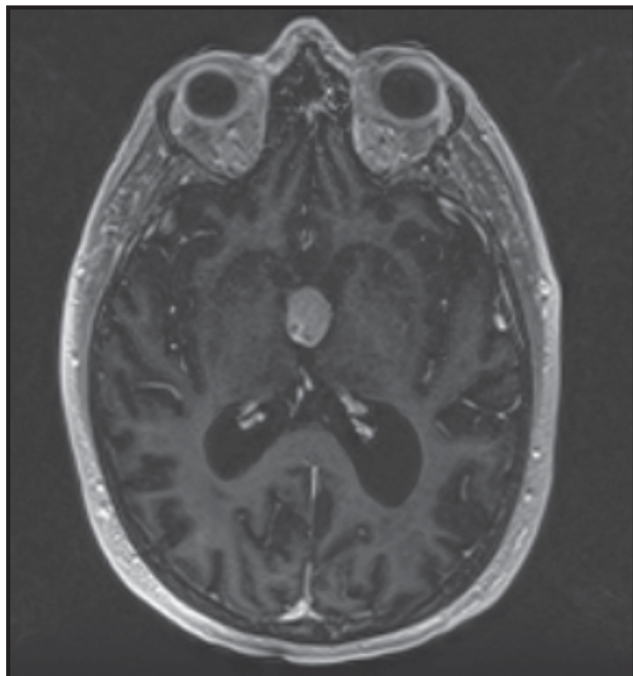


FIGURE 1. Contrast-enhanced T1 MRI shows an enhancing mass in the third ventricle near the foramen of Monro.



FIGURE 2. Noncontrast CT 5 months later demonstrates interval enlargement growth of the mass. Postoperative subarachnoid hemorrhage resulted in hydrocephalus and need for shunt placement.

adjuvant radiotherapy can lower risk of recurrence.⁷

CONCLUSION

This case demonstrates an extremely rare intraventricular hemangiopericytoma of the third ventricle. While the imaging features of these lesions can be similar to those of other intraventricular masses, consideration of HPC is important, given their vascularity and risk of hemorrhage, as well as their similar noncontrast appearance to the colloid cyst.

REFERENCES

1. Thakur P, Sharma M, Gupta M, Chatterjee D, Fotedar V. Anaplastic cerebral hemangiopericytoma: Rare variant of a rare disease. *Clin Cancer Invest. J.* 2015; 4: 277-279.
2. Abrahams JM, Forman MS, Lavi E, Goldberg H, Flamm ES. Hemangiopericytoma of the third ventricle. Case report. *J Neurosurg.* 1999;90 (2): 359-362.
3. Towner, JE, Johnson MD, Li YM. Intraventricular Hemangiopericytoma: A Case Report and Literature Review. *World Neurosurg.* 89: 728-728.
4. Abdollahi A, Abdollahpour R, Tavangar S-M. Meningeal Hemangiopericytoma in 33-Year-Old Female; a Case Report. *Iranian J Pathol.* 2016;11(3): 281-285.
5. Pang H, Yao Z, Ren Y, Liu G, Zhang J, Feng X. Morphologic patterns and imaging features of

- intracranial hemangiopericytomas: a retrospective analysis. *OncoTargets and Therapy.* 2015; 8: 2169-2178.
6. Sotoudeh H, Yazdi HR. A review on dural tail sign. *World Journal of Radiology.* 2010;2(5): 188-192.
 7. O'Neill AH, Gagnaniello C, Lai LT. Natural history of incidental colloid cysts of the third ventricle: A systematic review. *J Clin Neuroscience.* 2018; 53: 122-126.

Affiliations: Drexel University College of Medicine, Philadelphia, PA (Ms Kadakia); Cooper University Hospital, Camden, NJ (Dr Kazmi).

GIST of the Duodenum and Proximal Jejunum with an Ampullary Neuroendocrine Tumor

Mohammed Mirza, MD; Joshua Boulter; Alula Tesfay, MD

CASE SUMMARY

A 58-year-old with a history of neurofibromatosis type 1 (NF-1) and recurrent nephrolithiasis presented to the emergency department with right flank pain.

IMAGING FINDINGS

Abdominal radiographs were unremarkable. Contrast-enhanced CT (CECT) of the abdomen revealed a right renal subcapsular hematoma and multiple masses in the duodenum. The largest of these being a 2cm mass in the second portion of the duodenum, along with numerous subcutaneous soft-tissue nodules (Figure 1).

The same patient presented 3.5 years later with diffuse abdominal pain. Repeat CECT of the abdomen revealed pancreaticobiliary obstruction along with findings suggestive of gallbladder hydrops secondary to a 2cm duodenal mass and an obstructing left nephrolith (Figure 2). Surgery revealed a neuroendocrine neoplasm of the ampulla of Vater and five tumors in the duodenum and proximal jejunum, the largest measuring 3.7cm.

DIAGNOSIS

Gastrointestinal stromal tumors (GISTs) of the duodenum and proximal jejunum with an ampullary neuroendocrine tumor (NET).

DISCUSSION

The coexistence of a periampullary/ampullary NETs and multifocal GIST is nearly pathognomonic of NF-1.¹ Although intra-abdominal tumors are common in the setting of NF-1, the concurrence of these two entities is rare. A majority of NETs in NF-1 are nonfunctional, even in cases of histologically confirmed somatostatinomas, the most common being periampullary/ampullary NET.²

In most cases, NETs and GISTs are asymptomatic and found incidentally on imaging. Uncommonly, they present with abdominal pain, upper GI bleed, palpable abdominal mass, bowel obstruction, perforation and/or biliary obstruction.^{3,4} Extremely rare cases of ampullary insulinoma, gastrinoma, gangliocytic paragangliomas, and adenocarcinomas associated with multifocal GISTs have been reported.² Peripheral nerve sheath tumors commonly occur in NF-1, and 1-3% of patients develop pheochromocytomas.³

These cases must be differentiated from other hereditary and nonhereditary tumor syndromes, such as multiple endocrine neoplasias, Carney triad, and Carney-Stratakis syndrome, all of which have a propensity to coexist with GIST. In this case, the ampul-

lary tumor was well differentiated and stained positive for synaptophysin and chromogranin confirming the diagnosis of a NET (Figures 3,4). The five additional tumors had spindle cell histology and were positive for c-kit immunohistochemistry, confirming the diagnosis of multifocal GIST.

GISTs are the most common gastrointestinal manifestation of NF-1, with one third of patients found to have GISTs at autopsy.⁵ While cutaneous manifestations of NF-1 are generally reported earlier, GISTs present with a mean age of 53 years, 8 years earlier than the average presentation of sporadic GIST. In addition, compared to sporadic GIST associated with NF-1 are more commonly occur in the small bowel rather than the stomach, and have a smaller mean diameter, 3.8 cm vs. 7.4 cm.⁴ Radiographically, the appearance of GIST varies based on size and location. Nonetheless, they appear as homogeneous soft-tissue masses with or without signs of central necrosis.

CONCLUSION

This case illustrates the importance of radiographically recognizing the intra-abdominal manifestations of NF-1. Particularly, NF-1 predisposes to ampullary/periampullary neoplasia

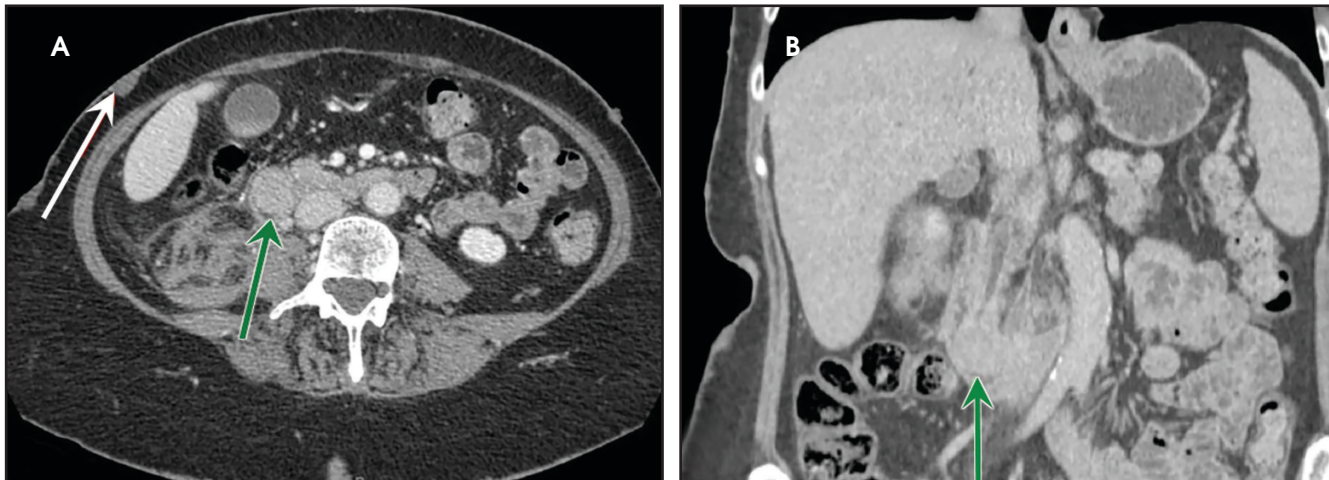


FIGURE 1. Axial (A) and coronal (B) contrast-enhanced CT of the abdomen demonstrates periaampullary duodenal mass (green arrow) and multiple subcutaneous nodules overlying the anterior abdominal wall (white arrow).

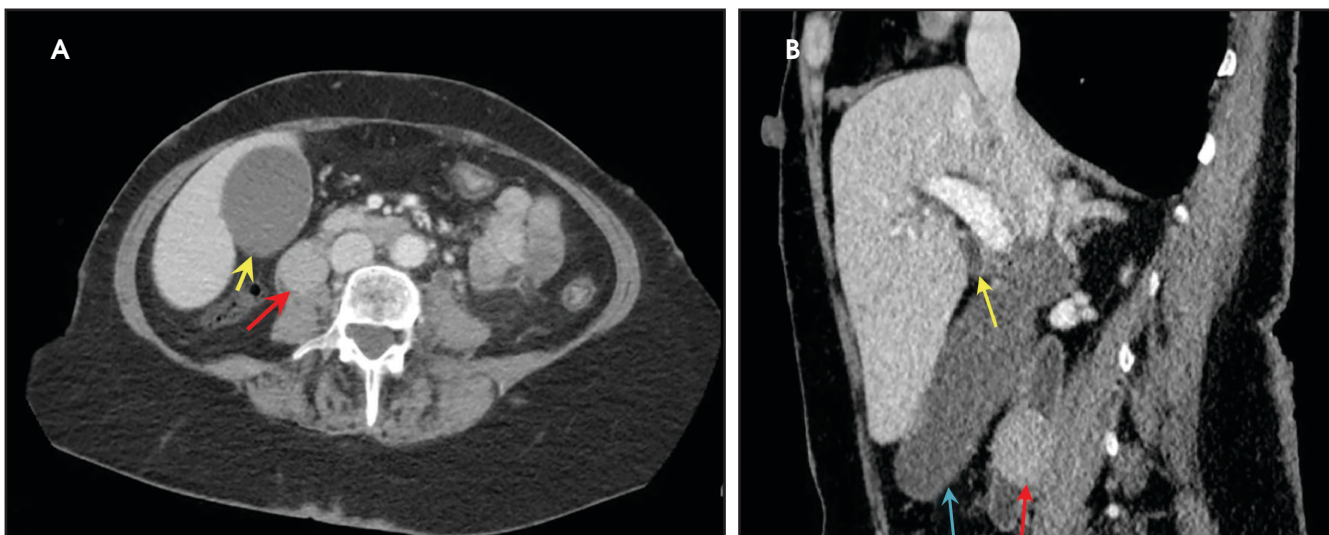


FIGURE 2. Axial (A) and sagittal (B) contrast-enhanced CT of the abdomen demonstrates obstructing periaampullary duodenal mass (red arrow) with gallbladder hydrops (blue arrow).

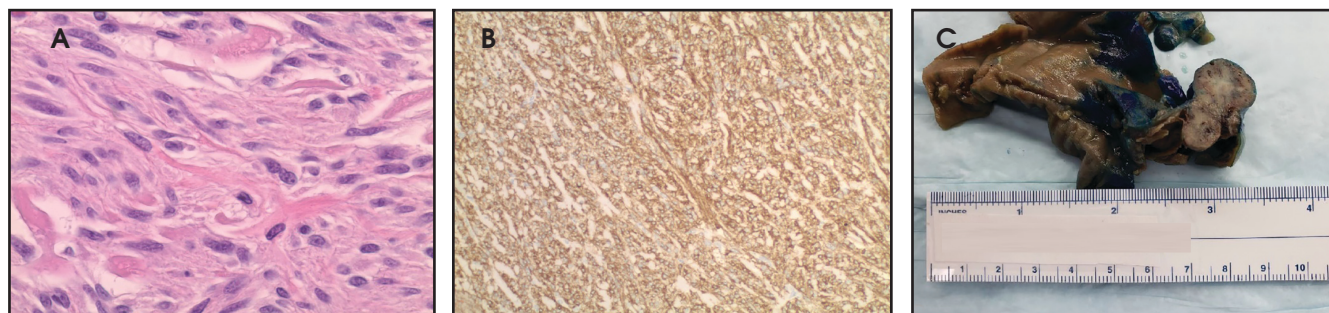


FIGURE 3. H&E stains at 400x (A), CD117 immunostain (B) and gross specimen (C) of spindle cell type of gastrointestinal stromal tumor in the duodenum and proximal jejunum.

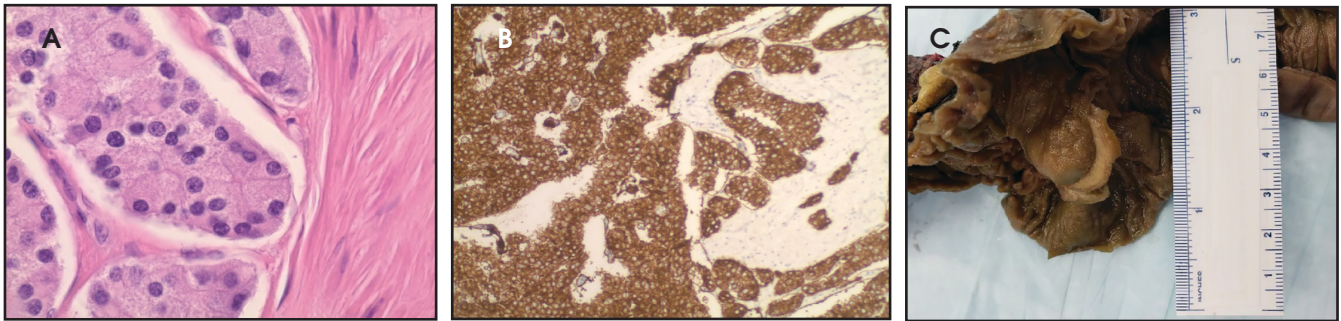


FIGURE 4. H&E stains at 400x (A), synaptophysin immunostain (B) at 100x, and gross specimen of well-differentiated grade I neuroendocrine neoplasm of the ampulla of Vater (C).

and small-bowel GIST formation. In the undiagnosed patient, the coexistence of these two entities is highly suggestive of NF-1. Over time, periampullary tumors can lead to complications such as pancreaticobiliary obstruction, as this case. GI tumors in patients with NF-1 often present earlier than sporadic tumors and imaging studies should be evaluated with this in mind.

REFERENCES

1. Agaimy A, Vassos N, Croner RS. Gastrointestinal manifestations of neurofibromatosis type 1 (Recklinghausen's disease): clinicopathological spectrum with pathogenetic considerations. *International Journal of Clinical and Experimental Pathology*. 2012;5(9):852-862.
2. Costi R, Caruana P, Sarli L, Violi V, Roncoroni L, Bordi C. Ampullary adenocarcinoma in neurofibromatosis type 1. Case report and literature review. *Mod Pathol*. 2001;14:1169-74.
3. Kramer K, Hasel C, Aschoff AJ, Henne-Bruns D, Wuerl P. Multiple gastrointestinal stromal tumors and bilateral pheochromocytoma in neurofibromatosis. *World J Gastroenterol*.; *WJG*. 2007;13(24):3384-3387. doi:10.3748/wjg.v13.i24.3384.
4. Salvi PF, Lorenzon L, Caterino S, Antolino L, Antonelli MS, Balducci G. Gastrointestinal Stromal Tumors Associated with Neurofibromatosis 1: A Single Centre Experience and Systematic Review of the Literature Including 252 Cases. *International Journal of Surgical Oncology*. 2013; 2013:398570. doi:10.1155/2013/398570.
5. Zoller ME, Rembeck B, Oden A, Samuelsson M, Angervall L. Malignant and benign tumors in patients with neurofibromatosis type 1 in a defined Swedish population. *Cancer*. 1997;79:2125-2131.

Affiliations: Michigan State University and St John Providence Hospital, Southfield, MI (Mirza and Tesfay); Michigan State University-CHM, Lansing, MI (Boulter)

Dorsal Thoracic Arachnoid Web and Spinal Cord Compression

Tiffany Y So, MBBS, BMedSci, MMed (Radiology), FRANZCR; Kateryna Burlak, MBBS; William A Maclaurin, MBBS, FRANZCR

CASE SUMMARY

A 64-year-old presented with a 3-year history of progressive back pain, lower limb weakness, and unstable gait. They experienced no bowel or bladder difficulty and denied any history of prior trauma, spinal surgery, or spinal inflammation. Physical examination revealed lower limb weakness with spasticity.

IMAGING FINDINGS

Magnetic resonance imaging (MRI) demonstrated a focal dorsal indentation of the thoracic spinal cord at the T6 level, with associated compression and deformity of the cord, which was displaced anteriorly (Figure 1). Extensive spinal cord signal abnormality was present below the level of the indentation, extending to the T8 level. No abnormal contrast enhancement was present (Figure 2). CT myelography showed the “upside down scalpel sign,” with the characteristic focal indentation of the dorsal thoracic spinal cord, widening of the dorsal cerebrospinal fluid

(CSF) space, and spinal cord expansion below the level of the dorsal indentation. No filling defects were demonstrated on the myelogram to indicate the alternative diagnoses of arachnoid cyst or ventral cord herniation. Myelography through the level of the dorsal indentation demonstrated a remaining thin CSF space between the anterior cord and the ventral thecal sac.

DIAGNOSIS

Dorsal thoracic arachnoid web with spinal cord compression. Differential diagnosis includes ventral spinal cord herniation and dorsal arachnoid cyst.

DISCUSSION

Spinal arachnoid webs represent intradural, extramedullary bands of arachnoid tissue that extend to the pial surface of the spinal cord. They are an uncommon entity that typically occurs in the upper thoracic spine, producing a focal indentation on the dorsal spinal cord.¹

There is lack of consensus on the terminology describing arachnoid webs, and their differentiation from other forms of arachnopathies, such as arachnoid adhesions, arachnoid scarring, and arachnoiditis.¹ Arachnoid webs have been known to develop after focal inflammation or trauma in the spine.¹ However, there have also been reports of non-traumatic arachnoid webs of unknown etiology, leading to consideration of congenital arachnoid webs, associated with a thickened ligamentum flavum.² It has been proposed that arachnoid webs arise from the process of formation or collapse of arachnoid cysts.^{1,3} Arachnoid webs can disrupt the normal craniocaudal flow of CSF, leading to focal compression of the spinal cord and/or syringomyelia.^{4,5}

Owing to their thin structure, spinal arachnoid webs are not readily visualized on routine imaging.⁶ Instead, they produce a characteristic dorsal indentation of the cord on MRI and CT myelography, described as the

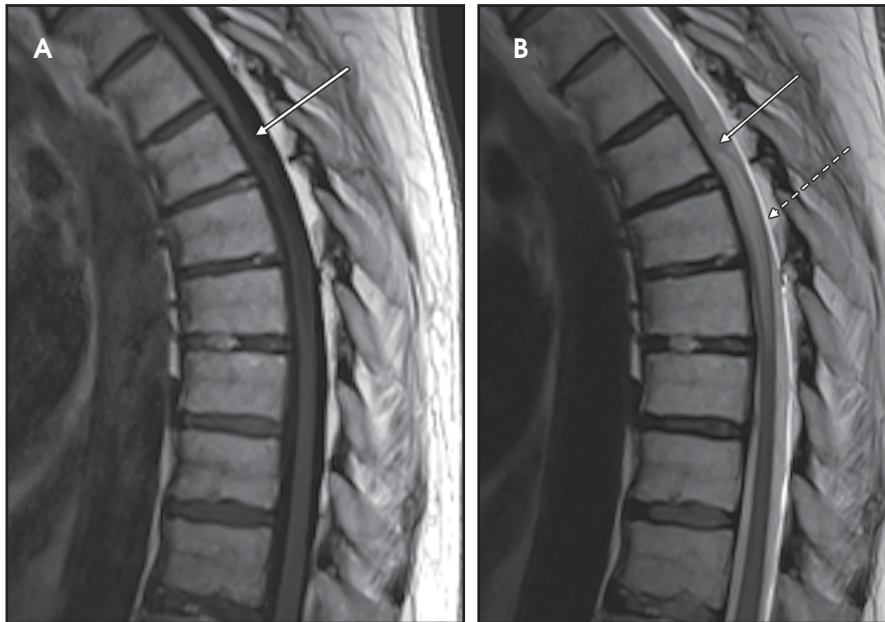


FIGURE 1. Sagittal T1 (A) and sagittal T2 (B) show a focal dorsal indentation of the thoracic spinal cord at the T6 level, with associated compression and deformity of the spinal cord (white arrows). Extensive abnormal spinal cord signal was present below the level of the indentation extending to the T8 level (dashed white arrow).

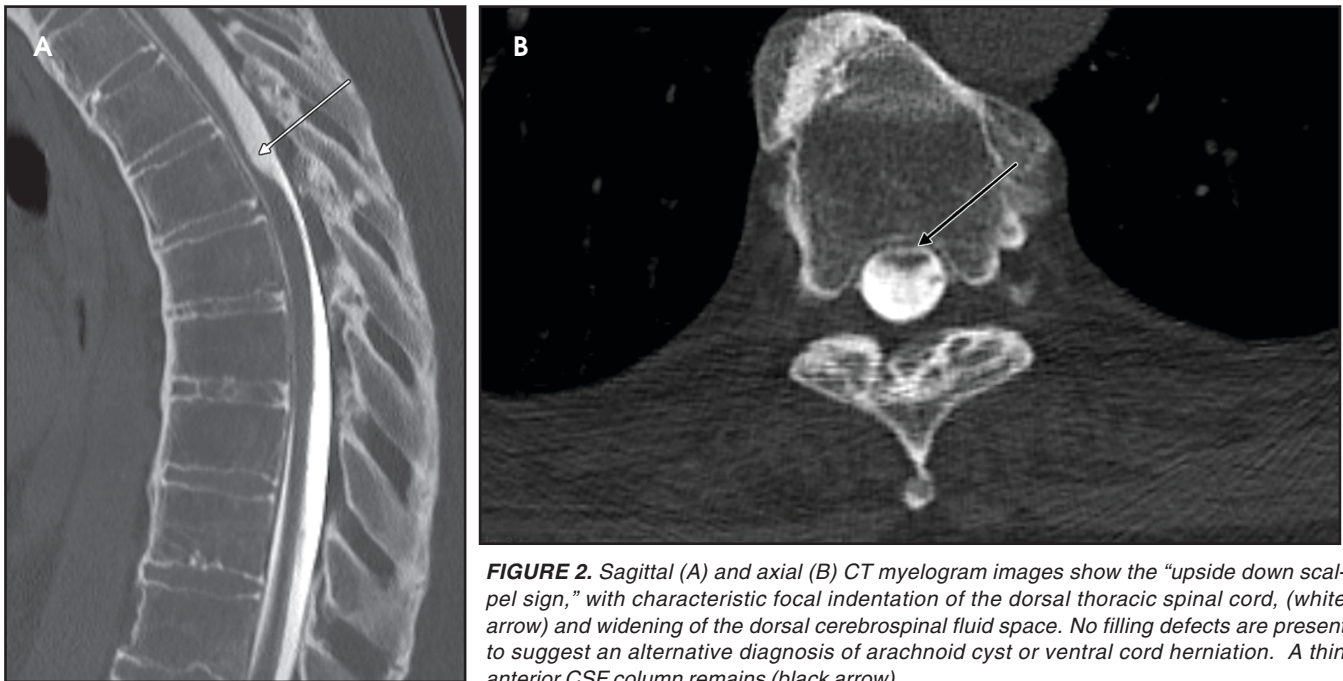


FIGURE 2. Sagittal (A) and axial (B) CT myelogram images show the “upside down scalpel sign,” with characteristic focal indentation of the dorsal thoracic spinal cord, (white arrow) and widening of the dorsal cerebrospinal fluid space. No filling defects are present to suggest an alternative diagnosis of arachnoid cyst or ventral cord herniation. A thin anterior CSF column remains (black arrow).

“scalpel sign,” with the “blade” pointing posteriorly.^{4,7}

Anterior displacement of the spinal cord, an abrupt change in spinal cord caliber, or evidence of adjacent syringomyelia are other important secondary imaging signs.⁴ The topological relationship of the arachnoid

web to the syrinx is variable. Klekamp reported a rostrally located syrinx in 47% of cases, caudally located syrinx in 24% of cases, and bilocalized syrinx in 29% of cases.⁸

MRI CSF flow studies have also been advantageous in providing an early diagnosis of arachnoid webs by

demonstrating disrupted CSF flow dynamics.^{2,9} Arachnoid webs can be accurately localized by assessing the site of CSF flow blockage.²

Spinal arachnoid webs can be definitively diagnosed with intraoperative ultrasound, where they resemble membrane-like structures in the dorsal

subarachnoid space, moving in sync with the cardiac cycle.^{1,2}

Surgical opening of the dura allows direct visualization of the arachnoid webs and provides an opportunity to restore the normal CSF pathway. Options for management of a symptomatic arachnoid web include marsupialization, fenestration, or laminectomy with exploration of the intradural space and subsequent resection of the arachnoid web.^{1,10,11} Postoperative MRI CSF flow study should demonstrate improved flow dynamics.

Failure to consider arachnoid web as a diagnosis preoperatively increases the risk of future myelopathy, and diagnosis prior to development of spinal cord signal abnormality and syringomyelia reduces morbidity.^{6,9}

Differential diagnoses are ventral spinal cord herniation and dorsal arachnoid cyst. In ventral spinal cord herniation, there is deformity of the ventral surface of the spinal cord as it protrudes through a ventral dural defect, and no space between the spinal cord and ventral thecal sac. Arachnoid cysts can be identified, particularly on thin-section volumetric MR by their marginated walls, and they produce a relatively smooth scalloping

on the spinal cord surface.^{1,12} An intraspinal filling defect with delayed filling of the arachnoid cyst are also present on myelography. In our case, the patient underwent surgical decompression with symptomatic improvement.

CONCLUSION

Spinal arachnoid webs demonstrate relatively typical imaging features, with characteristic focal indentation of the dorsal spinal cord and widening of the dorsal CSF space on MR and CT myelography. Their association with syringomyelia and spinal cord compression can result in significant patient morbidity, and identification of the described imaging features facilitates early diagnosis and prompt surgical treatment to prevent progressive myelopathy.

REFERENCES

1. Zhang D, Papavassiliou E. Spinal intradural arachnoid webs causing spinal cord compression with inconclusive preoperative imaging: A Report of 3 cases and a review of the literature. *World Neurosurgery*. 2017 Mar; 99: 251–8.
2. Chang HS, Nagai A, Oya S, et al. Dorsal spinal arachnoid web diagnosed with the quantitative measurement of cerebrospinal fluid flow on magnetic resonance imaging. *J Neurosurg Spine*. 2014; 20: 227–33.
3. Paramore CG. Dorsal arachnoid web with spinal cord compression: variant of an arachnoid cyst? Report of two cases. *J Neurosurg*. 2000; 93: 287–290.

4. Reardon MA, Raghavan P, Carpenter-Bailey K, Mukherjee S, Smith JS, Matsumoto JA, et al. Dorsal thoracic arachnoid web and the “scalpel sign”: a distinct clinical-radiologic entity. *Am J Neuroradiol*. 2013; 34: 1104–1110.
5. Hubbard ME, Hunt MA, Jones KE, Polly DW. Thoracic spinal cord impingement by an arachnoid web at the level of a hemivertebra: case report. *J Neurosurg Spine*. *American Association of Neurological Surgeons*. 2017 Dec; 27(6): 638–42.
6. Sayal PP, Zafar A, Carroll TA. Syringomyelia secondary to “occult” dorsal arachnoid webs: Report of two cases with review of literature. *Journal of Craniovertebral Junction & Spine*. 2016; 7(2): 101–104.
7. Aiyer R, Voutsinas L, El-Sherif Y. An overview of arachnoid webs. *The J Neurol Neuromed*. 2016; 1(6): 66–68.
8. Klekamp J, Batzdorf U, Samii M, Bothe HW. Treatment of syringomyelia associated with arachnoid scarring caused by arachnoiditis or trauma. *J Neurosurg*. 1997; 86: 233–240.
9. Mauer UM, Freude G, Danz B, Kunz U. Cardiac-gated phase—contrast magnetic resonance imaging of cerebrospinal fluid flow in the diagnosis of idiopathic syringomyelia. *Neurosurgery*. 2008; 63 (6): 1139–1144.
10. Gottschalk A, Schmitz B, Mauer UM, Bornstedt A, Steinhoff S, Danz B, et al. Dynamic visualization of arachnoid adhesions in a patient with idiopathic syringomyelia using high-resolution cine magnetic resonance imaging at 3T. *J Magn Reson Imaging*. 2010; 32: 218–222.
11. Petridis AK, Doukas A, Barth H, Mehdorn HM. Spinal cord compression caused by idiopathic intradural arachnoid cysts of the spine: review of the literature and illustrated case. *Eur Spine J*. 2010; 19: S124–S129.
12. Wang MY, Levi AD, Green BA. Intradural spinal arachnoid cysts in adults. *Surg Neurol*. 2003; 60: 49–55.

Affiliations: Alfred Hospital, Melbourne, Australia



THE POWER TO Take workflow and connectivity to a new level

Designed to do the heavy lifting in your practice, EmpowerCTA[®]+ Injector System helps optimize your imaging capabilities, streamline workflow, and enhance patient care when and where you need it.



STREAMLINING WORKFLOW

- **Digital touchscreen technology** to increase user control right beside the patient
- **Saline advance** to evaluate patency and vein integrity at the patient's side
- **Saline jump** allows for immediate advancement or "jump" from contrast delivery to saline delivery, potentially minimizing the contrast volume a patient receives
- **Increased control of contrast** and saline delivery through variable flow rates



SEAMLESS CONNECTIVITY

- **Connects your systems automatically**, giving you the information you need in just a few clicks
- **All documentation and reporting** is standardized, saving you from the need to manually enter information



EFFICIENT PROTOCOL MANAGEMENT

- **Easily access and manage protocols** across multiple sites
- **Monitor contrast dose data** from your desk

EmpowerCTA[®]+
Injector System

NEXO[®]
Contrast Management System

Contact your Bracco representative at
1-877-BRACCO 9 to learn how you can bring
control and data to your fingertips.

eGFR=estimated glomerular filtration rate.

*EDA is designed to aid in the detection of extravasations and is not intended as a substitute for proper patient monitoring and good clinical practice.

IMPORTANT SAFETY INFORMATION

NEXO[®] Contrast Management System Intended Use:

The NEXO Contrast Management System is a server-based application intended to be used as a data-management and visualization system. The NEXO Contrast Management System is able to read, store, share, compare/relate, as well as graphically display data and injection programs coming from RIS, PACS and multiple enabled EmpowerCTA[®] Injector Systems. This device provides users with record-lists, graphics and reports about data and performances.

This device is intended for retrospective and statistical data management and visualization. It is not intended for real time data visualization, diagnostic applications or for any other use for which the device is not indicated. This device is only to be operated by and under quasi-continuous supervision of qualified and trained staff in an appropriate licensed health care facility.

The NEXO Contrast Management System is compatible with the EmpowerCTA Injector System version 8.0, and EmpowerCTA[®]+ Injector System version 9.0 and higher.

Bracco Injengineering S.A. reserves the right at any time and without notice, to change the specifications and features described herein, or to change the production or adjust the product described.

Not all products available in all global markets.

EmpowerCTA[®]+ Injector System INDICATIONS:

The EmpowerCTA[®] Injector System is indicated for the vascular administration of contrast and flushing media in conjunction with computed tomography (CT) scanning of the body with an optional interface to a CT scanner and an optional calculator for glomerular filtration rate (GFR).

The Extravasation Detection Accessory (EDA[™]) is an optional accessory and is indicated for the detection of extravasations of ionic and nonionic contrast during CT procedures using a power injector.

Protocols have been independently developed and are not intended as medical advice. Bracco and Bracco Injengineering S.A. shall not be responsible for any physicians' reliance on these or any other products.

CONTRAINDICATIONS:

The EmpowerCTA[®] Injector System is not intended for use as a long-term infusion pump, nor is it intended to be used to inject any agents other than contrast or flushing media. Do not attempt to use the Injector for any other purpose (such as chemotherapy or drug infusion). The EmpowerCTA[®] Injector System should not be used to inject substances into nonvascular body cavities. Any applications of the EmpowerCTA[®] Injector System other than those described in its Operator Manual are inappropriate and should not be attempted.

Not all products available in all global markets.

About Bracco Injengineering S.A.

Bracco Injengineering S.A., located in Lausanne, Switzerland, is the most recently added Business Unit of Bracco Imaging. Bracco Injengineering is committed to develop the best-in-class integrated injection solutions with a strong heritage in research and innovation. It provides quality solutions for state-of-the-art radiology centers, offering proven injection technology, built on Bracco Imaging's expertise.

Thanks to this strengthened product portfolio, including the CT Exprim[®] 3D Contrast Media Delivery System, EmpowerCTA[®] Injector System, EmpowerMR[®] Injector System, NEXO Contrast Management System and NEXO [DOSE][®] Multi-Modality Radiation Informatics, Bracco Imaging will be able to focus on constant innovation, not only for devices, but also for software development and data management.

CT Exprim[®], EmpowerCTA, EmpowerMR, NEXO and NEXO [DOSE] are registered trademarks of Bracco Injengineering S.A.

EDA is a trademark of Bracco Injengineering S.A.

Customer Service:
1-877-BRACCO 9 (1-877-272-2269)

Professional Services:

1-800-257-5181 (Option 2)

EmpowerCTA[®] email:

empowerinfo@diag.bracco.com.

EmpowerCTA[®] website:

<http://imaging.bracco.com/us-en/products-and-solutions/contrast-injectors/empowercta+>.

NEXO questions: Nexo.Answers@diag.bracco.com

NEXO U.S. Technical Service and Support:

Phone: 888-670-7701; Fax: 609-514-2448;

NEXO email: customer.support@acismedical.com

EmpowerCTA[®] and NEXO are distributed by:

Bracco Diagnostics Inc.

259 Prospect Plains Road, Bldg. H

Monroe Township, NJ 08831 USA

Phone: (800) 631-5245; Fax: (609) 514-2424

EmpowerCTA[®] and NEXO are manufactured by:

Bracco Injengineering S.A.

Avenue de Sevelin 46,

CH - 1004 Lausanne, Switzerland.

<http://imaging.bracco.com>

©2018 Bracco Diagnostics Inc.

All Rights Reserved.

Committed to Science,
Committed to You.™





*“Opportunity
is often difficult
to recognize;
we expect it to
beckon us with
beepers and
billboards.”
— William
Arthur Ward*

An Ode to a Beeper

C Douglas Phillips, MD, FACR

My first portable electronic signaling device!

Fastened to my belt
you looked sleek and modern
and you had an (initially) soothing buzz.
I felt important
and needed.

Almost no one else
had one like it
(except drug dealers).
Many a time you summoned me
to the site of a waiting family
or patient
to be asked questions that as a medical student
I had no earthly idea how to answer.

In residency, you were even cooler.
A digital display
and a clock.
But, you woke me up all the time.
“Check this lateral c-spine.”
I wasn’t very nice to you, often.
Can I ever forgive myself
for slamming you into the wall?
At least the page operator was forgiving.

You followed me for years.
We grew up together, you and I.
Giving me numbers to call
and people’s names to ponder over
before finally calling.
A constant companion
(usually unwanted)
but you’re gone.
Replaced.
I sign out to my cell.
And now, I’m starting to hate it, too.

Mahalo.

Dr Phillips is a Professor of Radiology, Director of Head and Neck Imaging, at Weill Cornell Medical College, New York-Presbyterian Hospital, New York, NY. He is a member of the Applied Radiology Editorial Advisory Board.

Intraosseous Lipoma of the Sacrum

Scott P Patterson, MD; Dina Patterson, MD; Shaka M Walker, MD

CASE SUMMARY

A 29-year-old presented two months postpartum with persistent low back pain and coccydynia. Obstetrical history revealed a normal spontaneous vaginal delivery. After delivery, she reported significant pain in her tailbone. Initially the pain abated with non-steroidal anti-inflammatory therapy; however, the coccydynia worsened over the next month with increased difficulty sitting to the point where breastfeeding was possible only in a standing position. Because of the persistent pain, the patient was referred for orthopedic consultation. Initial imaging workup included radiography and MRI.

IMAGING FINDINGS

Pelvic radiographs were unrevealing, with no osseous or articular abnormalities. Subsequent pelvis MRI revealed intact muscles, ligaments, and tendons. The coccyx and sacroiliac joints appeared normal. In the left inferior sacrum, a 1.7 cm well-circumscribed lesion was hyperintense on T1 and T2 (Figure 1). The lesion had a narrow zone of transition and demonstrated signal dropout on fat-suppressed sequences (Figure 2). It had no associated aggressive features such as surrounding edema or soft tissue invasion.

DIAGNOSIS

Intraosseous lipoma of the sacrum

DISCUSSION

Intraosseous lipomas are rare, accounting for 0.1% to 2.5% of primary bone tumors.¹ No age or sex predilection has been reported. These tumors are often asymptomatic and generally are discovered incidentally. Symptomatic intraosseous lipomas typically present with pain, local swelling, or tenderness.^{1,2} The metaphysis of long bones and the calcaneus are the most common locations. Pelvic involvement is uncommon; only 4 cases of sacral lipoma have been reported in the literature to the best of our knowledge.^{3,4,5,6}

Lipomas are benign with little potential for malignant transformation; familiarity with the imaging characteristics avoids unnecessary work-up and potential biopsy. Intraosseous lipomas that do not affect bone stability may be treated conservatively and require no follow-up.³ Cases with imminent fractures are treated with curettage and bone grafting.⁷

As in our case, radiographs are often falsely negative. If visible on radiographs, intraosseous lipomas are usually well-defined, lucent lesions without aggressive features.^{2,8} On CT

they typically appear as well-defined lytic lesions with a thin, sclerotic rim and with Hounsfield units of fat density.^{3,8} Intraosseous lipomas are hyperintense on T1 and T2 MR sequences.^{2,9} Fat-suppressed images demonstrate signal dropout; the lesions are iso-intense to adipose tissue.⁹

Milgram^{1,7,8,9} outlined a 3-stage classification for intraosseous lipomas combining both histological and radiologic features: 1) Uniformly adipose tumors of viable fat cells; 2) A mixture of viable fat cells, fat necrosis, and calcifications; and 3) Necrotic fat, cystic formation, and reactive woven bone.

In this case, the MR images demonstrated uniformity of fat-signal intensity throughout the lesion, consistent with a Stage 1 lipoma. After reviewing the patient's symptoms and consulting with the orthopedic surgeon, we believed the lesion to be incidental with no further imaging or histopathologic correlation required. The patient returned in 1 month and reported an improvement of symptoms with conservative management as well as a return to normal daily activities.

CONCLUSION

Our case illustrates several points. First, the discovery of incidental findings, including benign bone tumors,

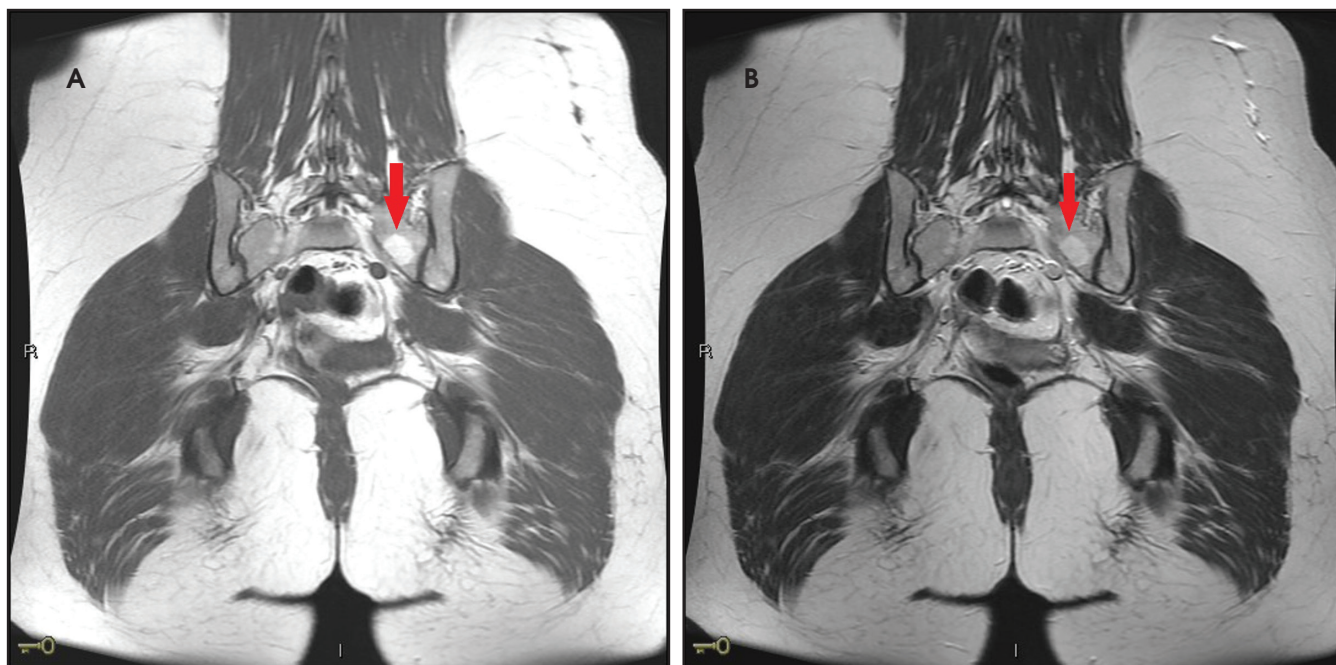


FIGURE 1. (A) coronal T1, and (B) coronal T2 images demonstrate a 1.7cm well-defined lesion in the left sacrum, hyperintense on T1 and T2 images.



FIGURE 2. Axial T2 fat-suppressed images. The lesion demonstrates uniform signal drop-out, confirming the lesion is composed of fat, consistent with an intraosseous lipoma.

has markedly increased with increased utilization of cross-sectional imaging. Second, while rare, intraosseous lipomas are an important consideration in the differential diagnosis of osseous lesions, particularly when asymptomatic and incidentally discovered. Third, familiarity with the imaging characteristics of these “don’t touch” lesions

helps avoid unnecessary imaging workup and biopsy.¹⁰

REFERENCES

1. Yazdi HR, Radouli B, Borhani A, Noorolahli MM. Intraosseous Lipoma of the Femur: Image Findings. *J Ortho Case Reports*. 2014; 4(1) 35-38.
2. Mohapatra NC, Sahoo A, Mishra J, Kumar HV. Intraosseous Lipoma of the Ilium: A rare case report with review of literature. *Oncol J India*. 2017; 1: 10-12.
3. Campbell RS, Grainger AJ, Mangham DC et al. Intraosseous lipoma: report of 35 new cases and a review of the literature. *Skeletal Radiol*. 2003; 32(4): 209-222.
4. Milgram JW. Involved intraosseous lipoma of sacrum. *Spine*. 1991; 16: 243-245.
5. Ehara S, Kattapuram SV, Rosenberg AE. Case report 619. Intraosseous lipoma of the sacrum. *Skeletal Radiol*. 1990;19: 375-376.
6. Kamekura S, Nakamura K, Oda H, Inokuchi K, Iijima T, Ishida T. Involved intraosseous lipoma of the sacrum showing high signal intensity on T1-weighted magnetic resonance imaging (MRI). *J Orthop Sci*. 2002; 7:274-280.
7. Bagatur AE, Raleinkaya M, Dogan A, Gur S, Mumeoglu E, Albayrak M, et al. Surgery is not always necessary in intraosseous lipoma. *Orthopedics* 2010; 33:306.
8. Mannem RR, Mautz AP, Baynes KE, Zambrano EV King DM. AIRP Best Cases in Radiologic-Pathologic Correlation. *RadioGraphics*. 2012; 32: 1523-1528.
9. Blackshin MF Ende N, Bnevenia. Magnetic resonance imaging of intraosseous lipomas: radiologic-pathologic correlation. *Skeletal Radiol*. 1995; 24: 37-41.
10. Helm C. 2014. Chapter 4 in Fundamentals in Skeletal Radiology. 4th ed. Philadelphia (PA): Saunders.

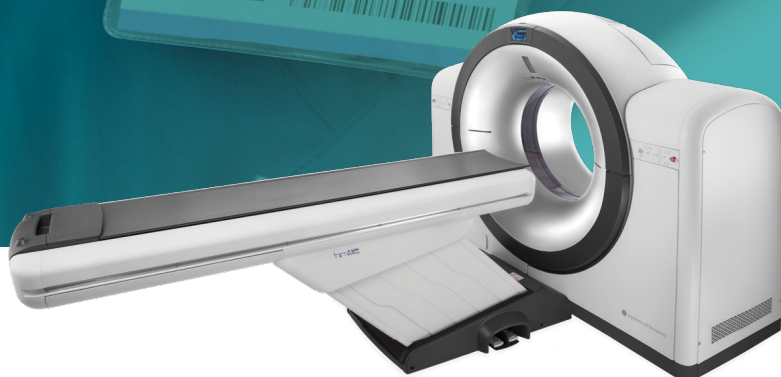
Affiliations: St. Clair Hospital, Pittsburgh, PA (Drs Scott Patterson and Walker); Children's Hospital, Pittsburgh, PA (Dr Dina Patterson).

People-First Design.

For the Technologist,
your patient's positive
experience builds trust
during their treatment.

Persona CT delivers an
intuitive design,
64 slice, 85cm big bore,
for optimized patient
comfort, speed
and accuracy.

Be visionary.



**Focus on patient safety.
Operational efficiency.
Cost savings.**

All included with the MEDRAD® Stellant FLEX.



With the newest MEDRAD® Stellant FLEX CT Injection System from Bayer, you can deliver quality patient care while maintaining healthy business operations, letting you:



Focus on patient safety with added system features



Increase operational efficiency with interoperability and design



Decrease departmental costs with syringe savings



Extend the lifespan of your CT technology with FLEX upgrade packages



To learn more, ask your Bayer representative or explore our CT solutions at StellantFLEX.com

Bayer, the Bayer Cross, MEDRAD Stellant, MEDRAD Stellant FLEX, MEDRAD, Stellant, and Stellant FLEX are trademarks owned by and/or registered to Bayer in the U.S. and/or other countries. Other trademarks and company names mentioned herein are properties of their respective owners and are used herein solely for informational purposes. No relationship or endorsement should be inferred or implied. © 2020 Bayer. PP-M-STE-F-US-0138-1 August 2020

MEDRAD® Stellant FLEX
CT Injection System